AN ABSTRACT OF THE THESIS OF

Moo-young Kim for the degree of Doctor of Philosophy in Chemistry presented on December 13, 2000. Title : Mass Spectrometric Studies on Peptides and Proteins: Conformations of *Escherichia coli* Thioredoxin and Its Alkylated Adducts Studied by Hydrogen/Deuterium Exchange and HPLC-Electrospray Ionization Mass Spectrometry.

Redacted for Privacy

Abstract approved: _____

Max L. Deinzer

E. coli thioredoxin (TRX) was modified by the episulfonium ion derived from *S*-(2-chloroethyl)glutathione (CEG) or *S*-(2-chloroethyl)cysteine (CEC). The alkylation site was located at Cys-32, which was confirmed by tandem mass spectrometry. Two forms of native TRX, Oxi- and Red-TRX, and two modified TRXs, GS- and Cys-TRX, were examined by hydrogen/deuterium (H/D) exchange reactions using electrospray ionization mass spectrometry (ESI-MS) for the analysis.

Conformational dynamics during thermal denaturation were probed by H/D exchange-in experiments. Under conditions in which the folded conformational state is marginally stable, H/D exchange-in experiments resulted in mass spectra differing in the number of incorporated deuteriums which indicates the presence of two distinct populations of molecules. As the exchange-in time increased, the population representing the unfolded state increased and the population for the folded state decreased. The rate of conversion was used to estimate the rate

constant of unfolding. ESI mass spectra were also recorded as a function of temperature without H/D exchange, and the observed bimodal charge state distributions were analyzed in order to estimate melting temperatures. GS-TRX showed increased resistance to hydrogen isotope exchange in comparison with Red-TRX indicating that there were enhanced intramolecular interactions in the former protein.

Pepsin digestion was performed on deuterated TRXs to analyze different structural regions. The amount of deuterium incorporated was monitored with peptic peptides from deuterated TRXs with different exchange-in incubation periods. Deuterium levels of each peptide were plotted versus the exchange time and fitted with a series of first-order rate terms. The regions 59-80 and 81-108 of Oxi- and Red-TRX showed an EX1 mechanism as evidenced by two distinct mass envelopes that appeared after a short incubation time in deuterated solvent.

Tandem mass spectrometry (MS/MS) was carried out to obtain the information on individual amide linkages. MS/MS data showed generally excellent correlations with the exchange rate constants from published NMR data on Oxi- and Red-TRXs. Two residues, Ile-75 and Ala-93 in GS-TRX indicated the most probable sites responsible for induced H-bonding by the attached glutathionyl group, which was consistent with the energy minimized structure predicted by AMBER force field constants.

Mass Spectrometric Studies on Peptides and Proteins: Conformations of *Escherichia coli* Thioredoxin and Its Alkylated Adducts Studied by Hydrogen/Deuterium Exchange and HPLC-Electrospray Ionization Mass Spectrometry

by

Moo-young Kim

A THESIS

submitted to

Oregon State University

in partial fulfillment of

the requirements for the

degree of

Doctor of Philosophy

Completed December 13, 2000

Commencement June 2001

Doctor of Philosophy thesis of Moo-young Kim presented on December 13, 2000

APPROVED:

Redacted for Privacy

Major Professor, Chemistry

Redacted for Privacy

Chair, Department of Chemistry

Redacted for Privacy

Dean of Graduate School

I understand that my thesis will become part of the permanent collection of Oregon State University libraries. My signature below authorizes the release of my thesis to any reader upon request.

Redacted for Privacy

Moo-young Kim, Author

ACKNOWLEDGMENTS

I thank Dr. Max Deinzer for his guidance, support, and example, and for the opportunity to pursue mass spectrometric studies on proteins. I thank Dr. Claudia Maier and Dr. Xuguang Yan for their enthusiasm, advice, and encouragement. I thank my committee members, Dr. Don Reed, Dr. Kevin Gable, Dr. Victor Hsu, Dr. Douglas Barofsky, and Dr. Goran Zovanovic for their willingness and critical evaluation of my thesis. I would especially like to thank Dr P. Shing Ho for his efforts for the energy-minimized protein structure.

I would also like thank Don Griffin and Brian Arbogast for their consistent and patient support in mass spectrometry and HPLC experiments. I also value the friendships of Dr. Susan Chen, Lilo Barofsky, and Alan Taylor. I thank Jeannine Lawrence for the technical advice related to circular dichroism. I thank fellow students Dr. Philip Gafken, Dr. Paul Mazurkiewicz, Heidi Zhang, April Mixon, Sunghwan Kim, Catalin Doneau, and Melissa Shultz for their help and friendship.

I owe very special thanks to my parents for my up-bringing and teaching me to have a Christian faith. I am also thankful to my son, Seokwon, for his radiant smile, my nephew, Myunghoon, for his unexpected questions and my sister, Heeyoung, for her long distance love.

My sincere apologies to the many other people not mentioned here who also deserve my thanks.

TABLE OF CONTENTS

TABLE OF CONTENTS (CONTINUED)

LIST OF FIGURES

LIST OF FIGURES (CONTINUED)

LIST OF FIGURES (CONTINUED)

LIST OF FIGURES (CONTINUED)

LIST OF TABLES

LIST OF TABLES (CONTINUED)

LIST OF TABLES (CONTINUED)

LIST OF EQUATIONS

ABBREVIATIONS

CD, circular dichroism

CEC, *S*-(2-chloroethyl)cysteine

CEG, *S*-(2-chloroethyl)glutathione

CID, collisionally induced dissociation

ESI, electrospray ionization

FTMS, fourier transform mass spectrometry

H/D, hydrogen/deuterium

HPLC, high performance liquid chromatography

MALDI, matrix assisted laser desorption ionization

MS, mass spectrometry

MS/MS, tandem mass spectrometry

NADPH, nicotinamide adenine dinucleotide phosphate, reduced

NMR, nuclear magnetic resonance

SORI, sustained off-resonance irradiation

TR, thioredoxin reductase

TCEP, tris(2-carboxyethyl)phosphine

TRX, *Escherichia coli* thioredoxin

- Oxi-TRX, oxidized *Escherichia coli* thioredoxin
- Red-TRX, reduced *Escherichia coli* thioredoxin
- GS-TRX, glutathionyl *Escherichia coli* thioredoxin
- Cys-TRX, cysteinyl *Escherichia coli* thioredoxin

UV, ultraviolet

DEDICATION

I dedicate this thesis to my wife, Anna. I am eternally grateful for her love, encouragement, friendship, and support.

"You did not choose Me, but I chose you and appointed you that you should go and bear fruit, fruit that shall last." John 15:16

Mass Spectrometric Studies on Peptides and Proteins: Conformations of *Escherichia coli* Thioredoxin and Its Alkylated Adducts Studied by Hydrogen/Deuterium Exchange and HPLC-Electrospray Ionization Mass Spectrometry

CHAPTER 1

BACKGROUND

1.1 Protein folding

Proteins are responsible for many of the chemical and physical processes that support life. These molecules are ubiquitous in all living creatures. Proteins are linear polymers consisting of amino acids. They have four levels of structural organization: primary (sequence), secondary (local folding), tertiary (overall folding), and quaternary (multichain association). To function, it is necessary for polypeptide chains to fold into the unique native three-dimensional structure that is characteristic for each protein. The three-dimensional structures of folded proteins results from a combination of non-covalent interactions including short-range repulsion, electrostatic forces, van der Waals interactions, and hydrogen bonding.

Protein folding problems are among the most fundamental and challenging problems in the life sciences. Localized as well as global structural changes often accompany protein functions such as catalysis and electron or oxygen transport. Characterization of these structural changes in terms of atomic locations, thermodynamics and dynamics is the basis for our understanding of how a protein performs its function. From a practical point of view, a knowledge of how a protein folds may be key to understanding many of

the events involved in cellular regulation, the causes of certain cancers and genetic diseases, and ultimately the information necessary to find corresponding therapeutic treatments.

The folded conformations of proteins are only marginally stable under the best of conditions and can often be disrupted by environmental factors, such as a rise in temperature, variation in pH, increase in pressure, or the addition of denaturants. The protein is then said to be denatured. Denaturation, when it clearly involves protein unfolding, need not involve changes in covalent structure and, therefore, is almost always reversible. In some cases, proteins can be unfolded by (a) breaking disulfide bonds present, (b) removing essential cofactors, (c) mutating certain crucial residues, or (d) deleting residues from the primary structure.

The conformations of proteins are categorized into three different states: native state, unfolded state, and molten globule state. The native states of proteins are well packed, with an optimal reduction in solvent exposed hydrophobic surface areas and all hydrogen bonding groups have either additional protein groups or solvents as partners. The molten globule states are protein conformations that are neither fully folded nor fully unfolded. The general consensus of the condition of this state is that it is compact and has a sizable hydrophobic core; it has a high content of secondary structure and native-like tertiary fold; while at the same time it has significant structural flexibility with mostly nonspecific tertiary interactions.[1] Unlike the structures of native states, the structures of unfolded or denatured states of proteins are much less well understood because so many conformations are possible.

Information about secondary structures of proteins can be obtained by circular dichroism (CD).[2] The proportion of α-helix and β-sheet structures can be determined by this method. However, CD does not reveal the specific

location of α-helical or β-sheet structures within the protein. X-ray crystallography determines the tertiary and quaternary structures of proteins.[3] At the highest resolution, X-ray diffraction can be used to assign the three-dimensional location of every atom in a protein crystal. Spectrophotometry is used to determine the absorption of ultraviolet and visible light by proteins.[4] The amino acids tryptophan, tyrosine, and phenylalanine all have useful absorption spectra, and measuring their absorptions with light at 280 nanometers (nm) wavelength is a simple way of determining protein concentration. Nuclear magnetic resonance (NMR) has been used for determining the tertiary structures of peptides and small proteins.[5]

Mass spectrometry (MS) gives highly accurate determinations of protein molecular mass. Electrospray ionization (ESI)[6] and matrix-assisted laser desorption ionization (MALDI) MS[7] have provided a breakthrough to analyzing macromolecules larger than 100 kDa. Whereas these methods have been successfully applied to determine the molecular weight and primary structure of biopolymers, the recently developed methodology for direct characterization by ESI-MS of complexes containing noncovalent interactions, opens new perspectives for supramolecular chemistry and analytical biochemistry.

Hydrogen/deuterium (H/D) exchange measurements are important in studies of the dynamics of protein molecules and their folding behavior.[8] Amide hydrogen exchange rates appear to depend on whether the hydrogens are participating in intramolecular hydrogen bonding, as well as on the extent to which the hydrogens are shielded from the solvent. Hydrogen exchange has proved useful for studies of proteins for which the structures of two functionally different states are similar, while their stabilities and hydrogen exchange rates are substantially different.[9] Such differences in hydrogen exchange behavior suggest that hydrogen exchange may be an important source of information

about the dynamic processes proteins undergo. Hydrogen exchange has also proved useful for identifying intermediates formed during protein folding and unfolding[10] and in studies of protein-protein complexation.[11]

The principal advantages of hydrogen exchange by MS are the small concentrations of protein required, the lack of a requirement for completely purified proteins, and the ability to perform time resolved studies over a very broad dynamic range. NMR methods retain the advantage of atomic resolution, but MS methods are moving rapidly in that direction. MS is unique in its ability to distinguish populations with differing hydrogen exchange properties, whereas NMR can only yield a population average of proton occupancy. This feature has made it possible to probe the multiplicity of folding pathways and the energy landscape of protein conformations.[10c]

Recent advances have been made to enhance the ability of MS to localize sites of exchange by using proteolysis under conditions where further exchange is minimized.[12] Site-specific information can be obtained by quenching the isotope exchange after a certain time. These experiments are performed by dropping the solution pH and temperature, and digesting the partly H/D exchanged protein with pepsin. Pepsin is used to fragment the protein into peptides because it has maximum activity in the pH range 2-3, where amide hydrogen exchange is slowest. Even at 0 °C, pepsin has substantial proteolytic activity, thereby further allowing the analytical procedure to be carried out under minimal hydrogen exchange condition. In addition, pepsin usually cleaves at many points to give small peptides, which are a convenient size for analysis by ESI-MS. Small peptides consisting of only a few residues are desirable because they more accurately define the regions of the protein that have undergone isotopic exchange. The deuterium content of each peptic fragment can then be measured directly by ESI-MS. One limitation of the

method is the back-exchange that inevitably occurs during purification and subsequent analysis of the fragments. As we have seen, however, back exchange can be minimized by performing work-up experiments at low pH, low temperature and quickly, this method has proved useful for probing the dynamic nature of proteins.

1.2 Hydrogen exchange mechanism

Hydrogen exchange is extremely sensitive to protein conformational changes because exchange is effectively irreversible and cumulative. The hydrogen exchange half times of labile protons in native proteins vary over 8-10 orders of magnitude, from less than a second to more than a year, under physiological conditions. The most rapidly exchanging protons have rates similar to rates of small peptides, and presumably constitute sites freely accessible to solvent on the protein surface.

Isotopic exchange of peptide amide hydrogens is catalyzed by acid and base. Hence, the rate constant for HX, k_{ex} can be expressed as the sum of two terms, as indicated in the equation

$$k_{ex} = k_H [H^+] + k_{OH} [OH^-] \quad (1)$$

where k_H and k_{OH} are the rate constants for acid- and base-catalyzed exchange, respectively. For polyalanine model compounds, it was found that k_H and k_{OH} usually have values of 11.3 and 2.32 x 10^9 $M^{-1}min^{-1}$, respectively, at 278°K and low concentrations of salts.[13] The isotopic exchange rate constants, k_{ex}, for amide hydrogens of polyalanine and side chain hydrogens of some amino acids are given as a function of pH (**Figure 1.1**).

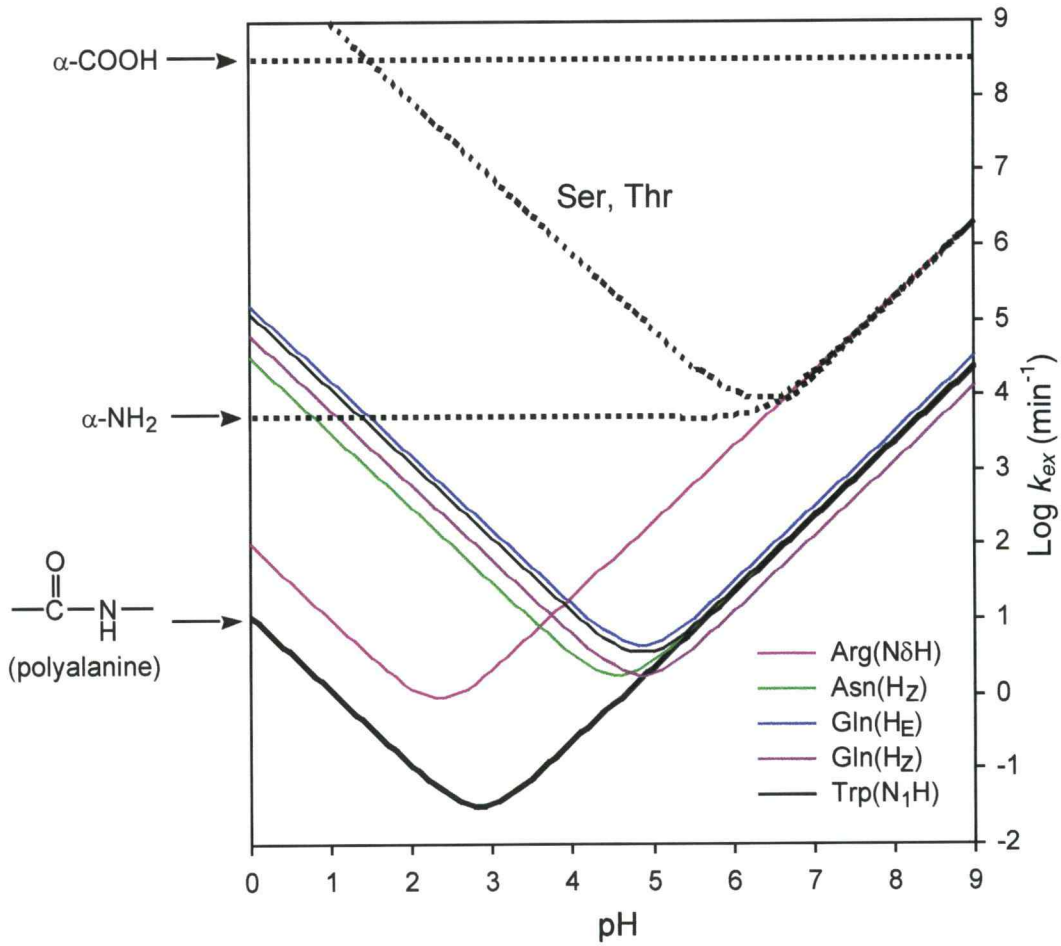

Figure 1.1. Hydrogen exchange rate constants for freely exposed amide hydrogens in polyalanine and in the side chains of dipeptide models for some amino acids. Results for Arg, Asn, Gln, Trp, and polyalanine were calculated using eq (1) and values of k_H and k_{OH} (278°K) given in the text.[13b] Results for α-COOH, α-NH_2, Ser, and Thr were obtained from model groups.[14]

At the minimum exchange rates for amide hydrogens between pH 2 and 3, the exchange rates of side chain hydrogens are much faster than for the amide hydrogens. The high pH sensitivity of isotopic exchange rates dictates careful control of pH in all hydrogen exchange experiments. In addition to their

pH sensitivity, exchange rates of amide hydrogens are affected by adjacent amino acid side-chains. The sensitivity to neighboring side-chains has been quantitatively assessed using model dipeptides of the naturally occurring amino acids. Both inductive and steric effects appear to influence amide hydrogen exchange rates. The effects of neighboring side-chains are generally additive, thereby forming the basis for estimating the amide hydrogen exchange rates in peptides of any amino acid sequence as a function of pH.[13b]

To predict hydrogen exchange rates at other temperatures, each rate constant obtained at 293 °K can be modified according to eq (2) in which the activation energies for k_H and k_{OH} are 14 and 17 kcal/mol, respectively.[13b] For instance, decreasing the temperature from 20 to 0 °C lowers the exchange rate approximately tenfold.

$$k_{ex}(T) = k_{ex}(293)\exp^{-\frac{Ea}{R}(\frac{1}{T}-\frac{1}{293})} \qquad (2)$$

Although side-chain effects in peptides of different amino acid sequences alter the amide hydrogen exchange rates by as much as tenfold, secondary and tertiary structural features of folded proteins may decrease amide hydrogen exchange rates as much as 10^8. It is this large reduction in isotopic exchange rates that facilitates use of amide hydrogen exchange as a sensitive probe for detecting and locating conformational changes in proteins (**Figure 1.2**). Isotopic exchange occurs while the folded protein is incubated in D_2O buffered to the desired pD. Almost all exchangeable hydrogens except those participating in hydrogen bonds or being shielded from solvent are displaced with deuterium. Following the deuterium exchange-in step, isotopic exchange at peptide amide linkages is quenched by decreasing the pD to 2.5

and the temperature to 0 °C. If isotopic exchange was performed using typical conditions of neutral pH at 25 °C, decreasing the pH and temperature for isotopic quench conditions would decrease the amide hydrogen exchange rate in an unfolded polypeptide by ~10^5 (**Figure 1.1** and **eq (2)**).

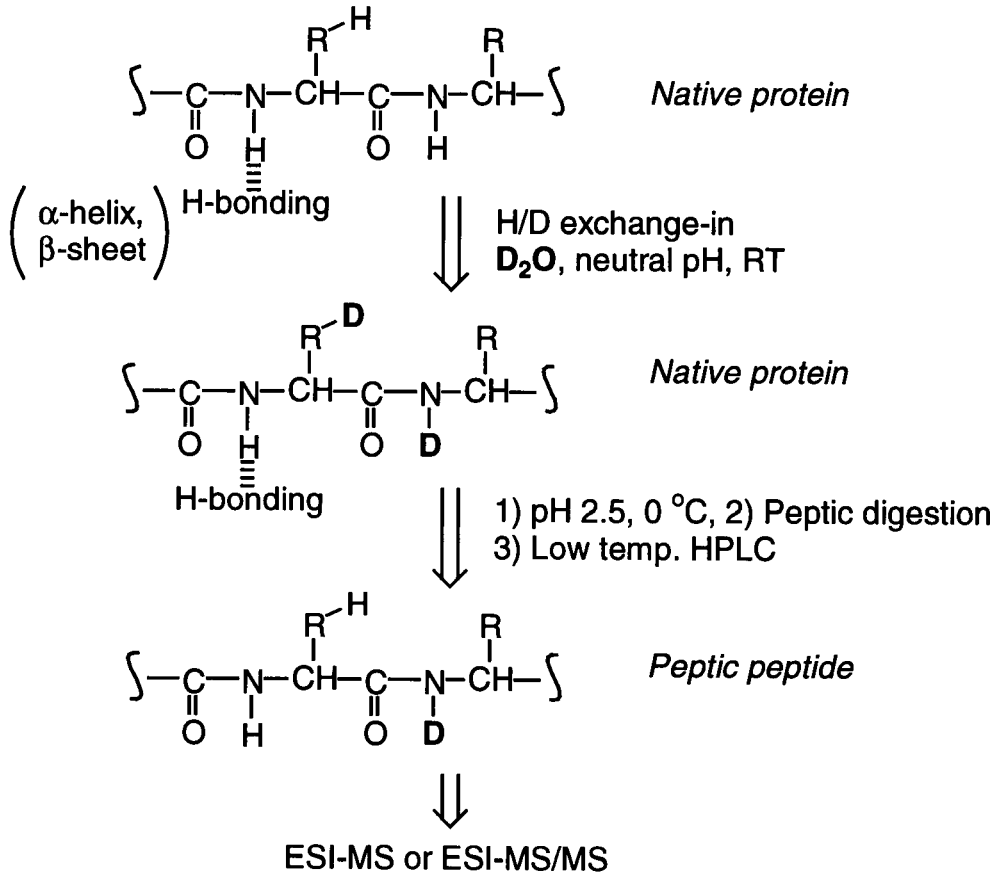

Figure 1.2. Identification of the secondary structures in protein by H/D Exchange and mass spectrometry

To determine isotopic exchange rates within small, defined regions of a protein, the acid protease, pepsin, is used to fragment the protein into peptides. The peptic digest is analyzed by HPLC-MS or HPLC-MS/MS to

determine the deuterium levels of the peptic fragments or the individual peptide amide linkages. Of course, isotopic quench conditions must be maintained during digestion and HPLC separation. Since a protiated mobile phase is used for HPLC, deuterium located at rapidly exchanging sites, such as on the side-chains or on the N- and C-termini of the peptides, are replaced with hydrogens. Hence, the increment in molecular mass is due to deuterium located at peptide amide linkages.

Following incubation of a folded polypeptide in D_2O, one may find an increased level of deuterium at peptide amide linkages. The time dependence of the deuterium level can be translated into a phenomenological isotopic exchange rate constant, k_{ex}. For the simplest interpretation of hydrogen exchange results, finding different exchange rates for different samples or forms of a protein is evidence that the protein is present in different conformations.

Various kinetic models have been developed to describe amide hydrogen exchange in folded proteins. Most of the results for amide hydrogen exchange in folded proteins can be explained through a two-process model (**Figure 1.3**). The rate constant for isotopic exchange from the folded protein is designated as $k_f = \beta\, k_2$ where β is the probability for exchange from folded form (a function of several parameters, including solvent accessibility and intramolecular hydrogen bonding), and k_2 is the rate constant for hydrogen exchange at each amide linkage in an unstructured peptide, a value that can be calculated.[13b] Hydrogen exchange directly from the folded protein is expected to dominate for amide hydrogens located on peptide linkages near the surface or open channels within a folded protein. Amide hydrogens that are involved in intramolecular hydrogen bonding, e.g. in α-helices or β-sheets, are unlikely to undergo isotopic exchange directly from the folded protein.

Hydrogen exchnage in proteins

$$k_{ex} = k_f + k_u$$

Hydrogen exchange from folded proteins

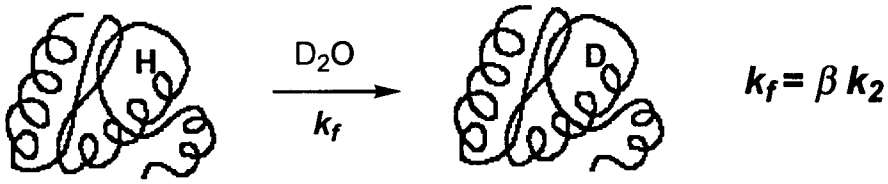

Hydrogen exchange from unfolded proteins

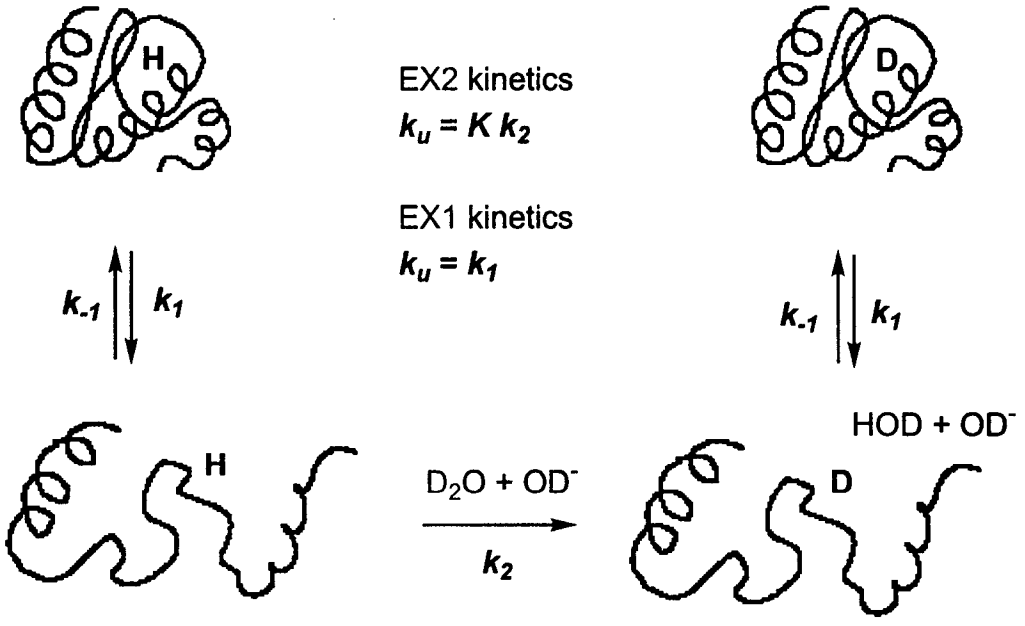

Figure 1.3. Pictorial representation of hydrogen exchange mechanism from folded and unfolded proteins. The hydrogen exchange rate constants from folded and unfolded proteins are described by k_f and k_u. The kinetics of the unfolding and refolding processes are described by rate constants k_1 and k_{-1}, respectively, and exchange from unstructured protein backbone is described by k_2.

A competing process, described by k_u, allows for a rapid unfolding and refolding of small regions (localized unfolding), as well as the entire protein (global unfolding). Rate constants for unfolding and refolding are designated by k_1 and k_{-1}, respectively. According to this model, isotopic exchange can occur only after unfolding, which breaks intramolecular hydrogen bonds, exposing amide hydrogens to the deuterated solvent. Hydrogen exchange involving protein unfolding is especially important because it provides a direct measure of the rates of protein unfolding and refolding (k_1 and k_{-1}), as well as a link to the free energy change accompanying protein folding. From the steady state approximation, the rate constant for the hydrogen exchange can be described by the following eq (3).

$$k_{ex} = \frac{k_1 k_2}{k_{-1} + k_2} \tag{3}$$

For most proteins at neutral pH and in the absence of denaturants, the interconversion between the native and denatured states is rapid compared with the exchange rates of amides in the denatured state, i.e. $k_{-1} >> k_2$. Under these conditions, local refolding can occur in less than a microsecond and even global unfolding reactions may take place within 50 ms.[15] Then, the proton occupancy at each amide linkage is uniform over all the protein populations. The phenomenological rate constant for this second-order reaction mechanism (EX2) is given by

$$k_{ex} = (k_1/k_{-1})k_2 = Kk_2 \tag{4}$$

where K is the equilibrium constant describing the unfolding process and k_2 is the exchange rate constant for the amide hydrogen in an unstructured peptide.

The EX2 mechanism would yield a single peak in the mass spectrum, gradually increasing in mass over time for the exchange of a protiated protein dissolved in D_2O. Measuring k_{ex} and calculating k_2 leads to a direct determination of the equilibrium constant, K, and hence ΔG for the protein unfolding process, which may be localized to a particular element of secondary structure or regional domain, or it may include the entire molecule.

Under some destabilizing conditions, e.g. in the presence of denaturants, at extreme pHs, or high temperature, the interconversion between native and denatured states is slow with respect to the rate of amide hydrogen exchange, i.e. $k_2 >> k_{-1}$. This exchange reaction is first-order (EX1), and the measured isotope exchange rate constant, k_{ex}, may be used to determine the rate of protein unfolding, k_1:

$$k_{ex} = k_1 \tag{5}$$

The EX1 mechanism would produce bimodal isotope patterns, i.e. two separated peaks in the mass spectrum corresponding to the fully exchanged and fully protected forms, respectively.[15b] In this case, the intensity of the two peaks would change with time. Mass spectometric approaches to monitor exchange reactions can be used to distinguish between these exchange mechanisms, EX1 and EX2. The presence of bimodal mass to charge ratio (m/z) patterns indicates 'correlated exchange' of all amide hydrogens within the peptide. The 'correlated exchange' refers to conditions for which all of the amide hydrogens in a region undergo isotopic exchange during one unfolding event in this region. The ability to detect correlated exchange is especially important, as it provides the basis for a more detailed description of the folding and exchange processes.

The rate constant for isotope exchange at each individual amide linkage in a normally folded protein, k_{ex}, can be described by eq (6)

$$k_{ex} = k_f + k_u = (\beta + K)\, k_2 \qquad (6)$$

where k_{ex} is indicated as the sum of the contributions of exchange from folded (k_f) and unfolded forms (k_u, EX2 kinetics) of the protein. Recent NMR studies have used denaturants to distinguish between β and K.[16] Structural changes described by k_f and k_u differ in the magnitude of atomic displacement. Hydrogen exchange in the folded proteins involves small atomic movements, probably around 1 Å, but sufficient to allow diffusion of OD^- and D_2O to the exchange site. In contrast, the unfolding of large segments of the backbone require displacing many atoms several Angstroms from their equilibrium positions in the native structure, and global unfolding requires gross movement of the entire backbone. Thus, exchange from the folded proteins (k_f) involves primarily low-amplitude motions (small displacement), while exchange from unfolded proteins (k_u) requires high-amplitude motions. Engen et. al. showed that ligand binding-induced changes in the exchange rates of rapidly exchanging NHs correlate with exchange directly from the folded protein, thereby signifying changes in low-amplitude motions.[17]

Two different H/D exchange techniques, continuous and pulsed labeling, have been developed to determine rates of folding and unfolding, as well as for identifying structures of folding and unfolding intermediates (**Figure 1.4**).[18] Continuous exchange involves exposing the protein to the deuterated medium during the incubation period. The labeled protein is thus a measure of all unfolding events that took place provided the exchange rate is much faster than the unfolding event. In pulse labeling, the deuterated protein is a snapshot

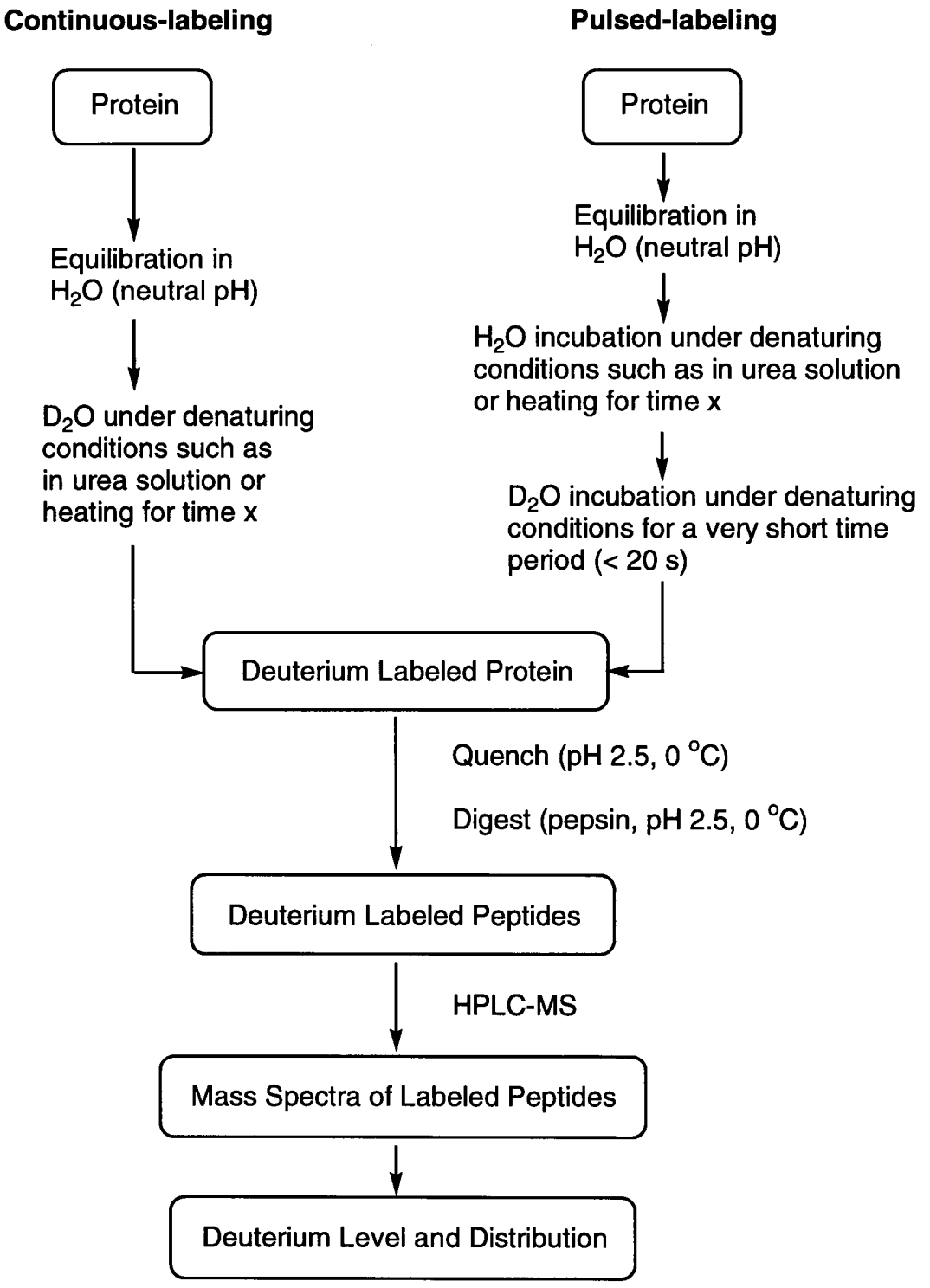

Figure 1.4. Experimental procedure for continuous and pulsed deuterium labeling

of the unfolded protein that existed during the pulse. Many unfolding and refolding events may have taken place during the incubation, but these are not recorded because there is no deuterium available for exchange between the pulses. Smith and co-workers have shown that continuous versus pulse labeling can help to show when both mechanisms (k_f and k_u in **Figure 1.3**) are operative in different regions of the protein if labeling under denaturing conditions occurs to give bimodal isotope distributions. Thus for rabbit muscle aldolase in 3M urea, when exchange in a given region of the folded state (k_f) is slow, a bimodal isotope distribution in the peptide used for study was observed in both experiments. When exchange was rapid, poorly resolved isotope distributions observed under continuous exchange conditions in peptides of certain regions of the protein, were nicely resolved into bimodal distributions in the pulsed labeling experiment.[18]

1.3 Thioredoxin

Thioredoxin (TRX) was chosen to study H/D exchange protocols in which HPLC-MS or -MS/MS techniques were used for the analysis. TRX is a small, (~12 kDa) multifunctional and ubiquitous protein characterized by having a redox-active disulfide/dithiol within the conserved active site sequence: -Cys-Gly-Pro-Cys-, the so-called "thioredoxin fold". TRX has been isolated and characterized from a wide variety of prokaryotic and eukaryotic species. Mammalian TRXs show about 25% sequence homology to the well-characterized *E. coli* protein with 108 residues. TRX has been found to have many activities *in vitro* in ribonucleotide reduction, photosynthesis, sulfite reduction, and DNA polymerase.

The disulfide linkage in the oxidized TRX is reduced by NADPH via the action of a flavoprotein enzyme, thioredoxin reductase (TR). The reduced TRX is a powerful protein disulfide reductase. Thus, TRX, TR, and NADPH, collectively called the thioredoxin system, operate as a powerful NADPH-dependent protein disulfide reductase system (**Figure 1.5**).[19] For this function, modifications of either active site cysteine (Cys-32 and Cys-35) through alkylation or site-directed mutagenesis, causes a loss of activity. TRX is also a required subunit in certain bacteriophage systems, including T7 DNA polymerase and filamentous phage assembly, where reduced thioredoxin is functional but oxidized thioredoxin is not.[20] The major determining factor in this difference does not appear to be the presence of free thiol groups, since mutants of TRX where one or both cysteines are replaced by Ala or Ser are also partly functional.[20] It suggests that the overall structure of the protein, and not the chemical properties of the cysteine residues are important to the regulation of this particular biological activity.

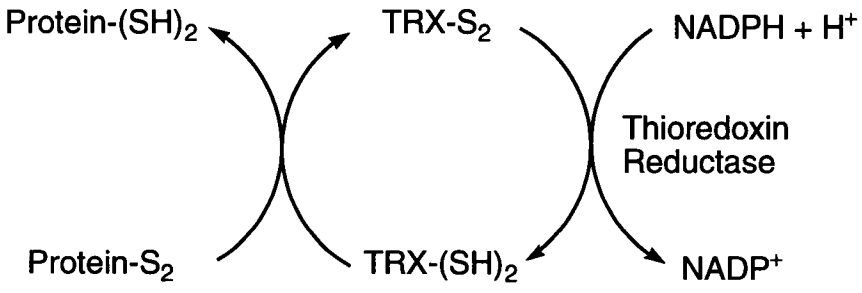

Figure 1.5. Electron transport sequences by thioredoxin system.

TRX has been well-characterized biochemically, and the high-resolution structures of oxidized and reduced forms of *E. coli* TRX have been determined by X-ray crystallography[21] and NMR spectroscopy[22] (**Figure 1.6**).

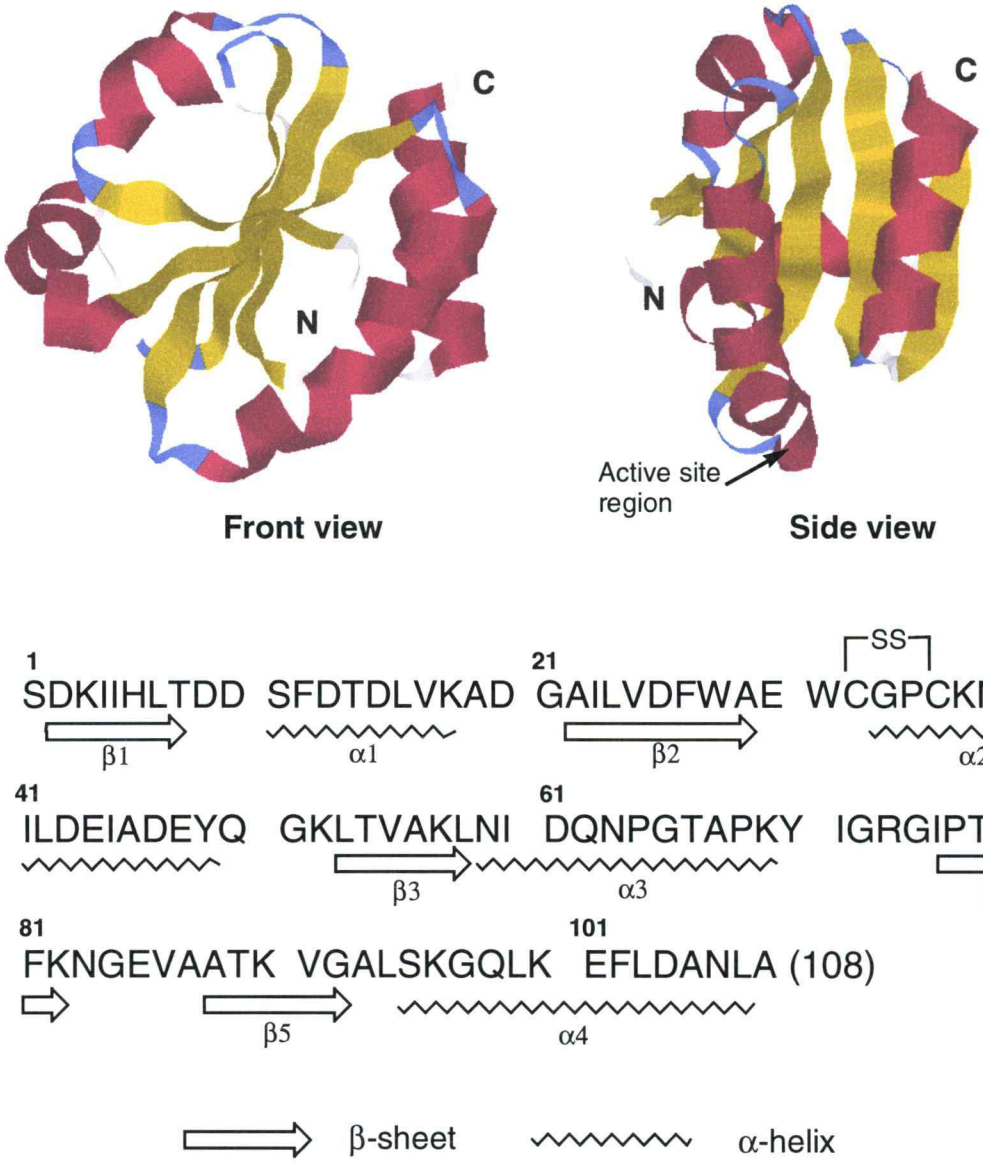

Molecular weight : 11673.86 (ESIMS)
11673.40 (calculated)

Total exchangeable hydrogens : 173
(backbone amide : 102, side chain : 68, terminal : 3)

Figure 1.6. NMR solution structure and sequence of oxidized *E. coli* thioredoxin.[12]

1.4 Electrospray ionization mass spectrometry (ESI-MS)

Electrospray ionization (ESI) is generally accomplished by forcing a solution of the analyte through a small biased capillary in the presence of a high electric field such that the fluid sprays into very fine droplets. This electric field is usually imposed between the tip of the spraying capillary and a counterelectrode (**Figure 1.7**). The initial fine droplets diminish in size due to simple evaporation of the solvent in a drying gas at atmospheric pressure or in a heated chamber at somewhat reduced pressure. As the droplets shrink, nonvolatile ions are retained. The resulting increase in the electrostatic repulsive forces between excess charges in the droplet eventually promotes electrohydrodynamic disintegration into many smaller droplets. Asymmetry in the distribution of charge at the droplet surface may stimulate "coulombic explosion" of the droplet before reaching the Rayleigh limit (the point at which repulsive forces between like charges in an electrolytic solution overcome the cohesive forces of the solvent) for stability of a spherical charged droplet. Finally, when the macroscopic solvent has evaporated, the analyte molecule finds itself with residual charges attached; for positive ESI, protons presumably attach at sites of high Lewis basicity.[6]

Because ESI can produce multiply charged ions, the mass-to-charge (*m/z*) value of ions of macromolecules (up to several million daltons) may fall within the mass range of most commonly used mass spectrometers. The high sensitivity and specificity of ESI-MS also make it a useful technique for the analysis of smaller compounds, such as those encountered in environmental and drug metabolite studies, which generally produce singly charged ions.

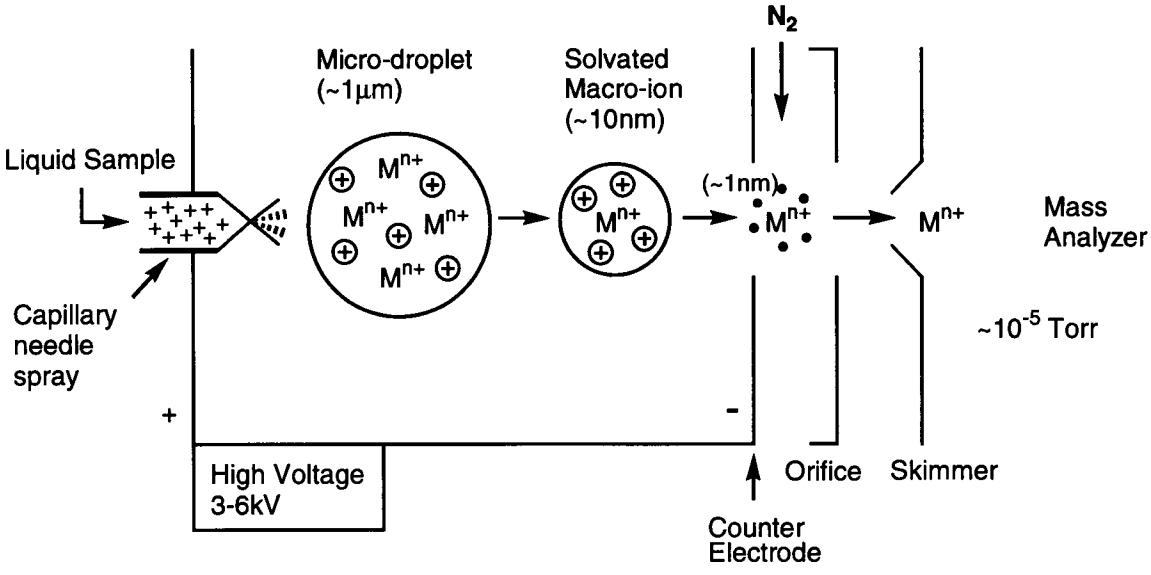

Figure 1.7. Electrospray Ionization Mechanism

The ESI technique has been a useful tool for the study of proteins and peptides, nucleic acids, carbohydrates and lipids, pharmacology and drug metabolism, and more recently organometallic and inorganic chemistry. Because ESI is a "soft" ionization technique, it permits investigations of noncovalent associations of large biomolecules such as proteins.

ESI-MS can be operated with continuous sample flow introduction, discrete sample injection as in flow-injection analysis (FIA), or on-line sample separation systems such as liquid chromatography (LC) and capillary electrophoresis (CE) (**Figure 1.7**). In particular, enzymes can be used to cleave a protein selectively, and the resulting peptide mixture is separated by either LC or CE, which is interfaced on-line to ESI-MS. ESI and assisted forms of ESI can produce sample ions from solution flow rates ranging from 25 nl/min to more than 1 ml/min.

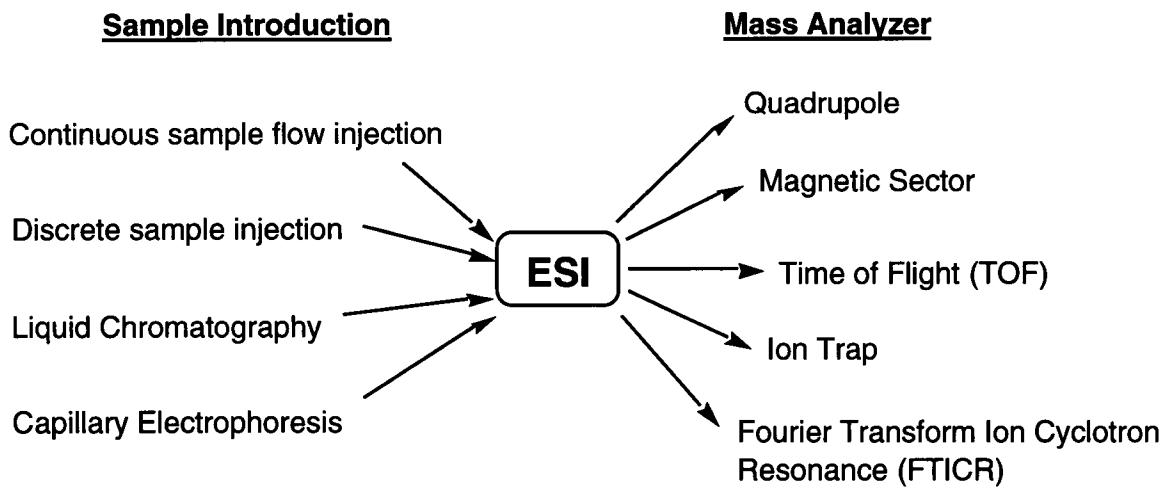

Figure 1.8. Sample introduction methods and mass analyzers for ESI.

The most common types of mass spectrometers for ESI are the quadrupole mass filter and ion trap. In the quadrupoles, mass separation is achieved by establishing an electric field in which ions of a certain *m/z* have stable trajectories through the field. The electric fields are created by placing a direct current (dc) voltage and an oscillating voltage (ac voltage at radio frequencies) on four metal rods, the quadrupoles. Adjacent rods have opposite polarity. Ions pass through the center of the rods inscribing circles as they pass the length of the rods. By increasing the magnitude of the dc and rf voltages while maintaining the appropriate dc-to-rf ratio, stable trajectories are created, allowing ions of greater *m/z* to pass through the quadrupoles and to reach the detector. The ion trap mass analyzer was developed at the same time as the quadrupole mass analyzer. The physics behind both of these analyzers is very similar. Ions inside an ion trap can be mass analyzed to produce a mass spectrum, or a particular ion can be trapped inside and made to undergo collisions to produce fragmentation information. The primary advantage of an

ion trap is that tandem mass spectrometry experiments can be performed without having multiple analyzers.

Charge state distributions generated by ESI depend on the conformation of the biomolecule in solution because different conformations in solution have different numbers of exposed basic sites. Factors such as temperature, solvent composition, and ionic strength can also influence biomolecular conformation in solution. When the fraction of organic solvents such as methanol, acetonitrile, and acetone is increased, a shift to higher charge states is observed in the ESI-MS spectra.[23] The influence of solution temperature upon charge state distributions shows that at low temperatures, low charge states are favored; at high temperatures where thermal denaturation can occur, high charge states are observed.[24]

There is some evidence suggesting that gas-phase protein ions retain the distribution of conformations that are present in solution. The evidence indicates that ion structures in the final stages of ESI are influenced by both the properties of the solution and the nature of the gas-phase ions that are formed.[25] Most H/D exchange studies to probe protein conformations have been conducted in solution. Recently gas-phase H/D exchange has been used to probe gas-phase ion conformations. Comparison of H/D exchange data between these two phases should also provide information on the role of water in protein structures particularly where conformational changes take place as in folding pathways. McLafferty and co-workers used fourier-transform ion-cyclotron-resonance (FTICR) MS to investigate the conformations of cytochrome c; trapped ions were exposed to dilute concentrations of D_2O vapor (ca. 10^{-7} torr), and exchange levels were monitored for extended time periods.[26b] Under these conditions, cytochrome c was found to exist as multiple conformational states that were stable for hours, while in solution, H/D

exchange involves nearly all of the exchangeable hydrogens indicating rapid equilibration among conformers.

ESI is relatively gentle and does not produce a significant abundance of fragment ions, in contrast to electron ionization which produces many peaks in the spectrum. Therefore, it has been necessary to develop techniques such as tandem mass spectrometry (MS/MS) to induce fragmentation. Tandem mass spectrometry (abbreviated MS^n - where n refers to the number of MS experiments, i.e. MS^3 means MS/MS/MS) allows one to induce fragmentation and mass analyze the fragment ions. This is accomplished by collisionally induced dissociation (CID) of a particular ion and then mass analyzing the fragment ions (**Figure 1.9**). A precursor ion is selected using MS-1, collisionally activating it in a region of relatively high pressure between MS-1 and MS-2, and then observing the product (fragment) ions by scanning the second mass filter, MS-2.

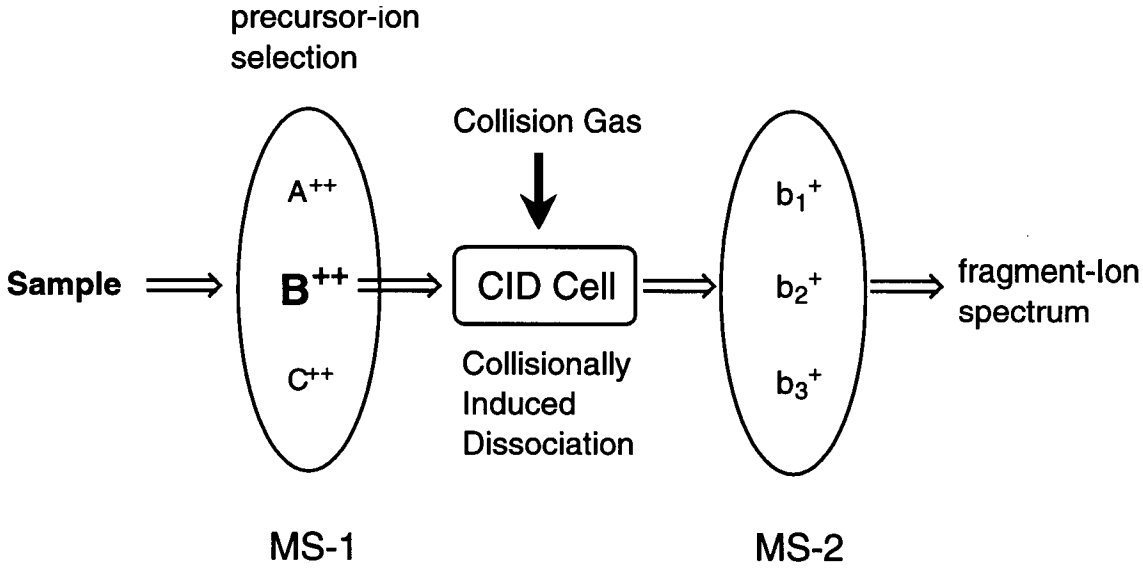

Figure 1.9. Schematic diagram of tandem mass spectrometry.

For peptides and proteins, the polypeptide backbone is fragmented in the CID cell in a predictable way giving rise to an ion series from which most of the sequence can be deduced (**Figure 1.10**).[27] The fragment ions produced in this process can be separated into two classes. One class retains the charge on the N-terminus while cleavage is observed from the C-terminus. This fragmentation can occur at three different positions, each of which is a sequence of ions designated as types a_n, b_n, and c_n. The second class of fragment ions generated from the N-terminal end retains the charge on the C-terminal end, while cleavage is observed from the N-terminus. Like the first class, this fragmentation can occur at three different positions, types x_n, y_n, and z_n.

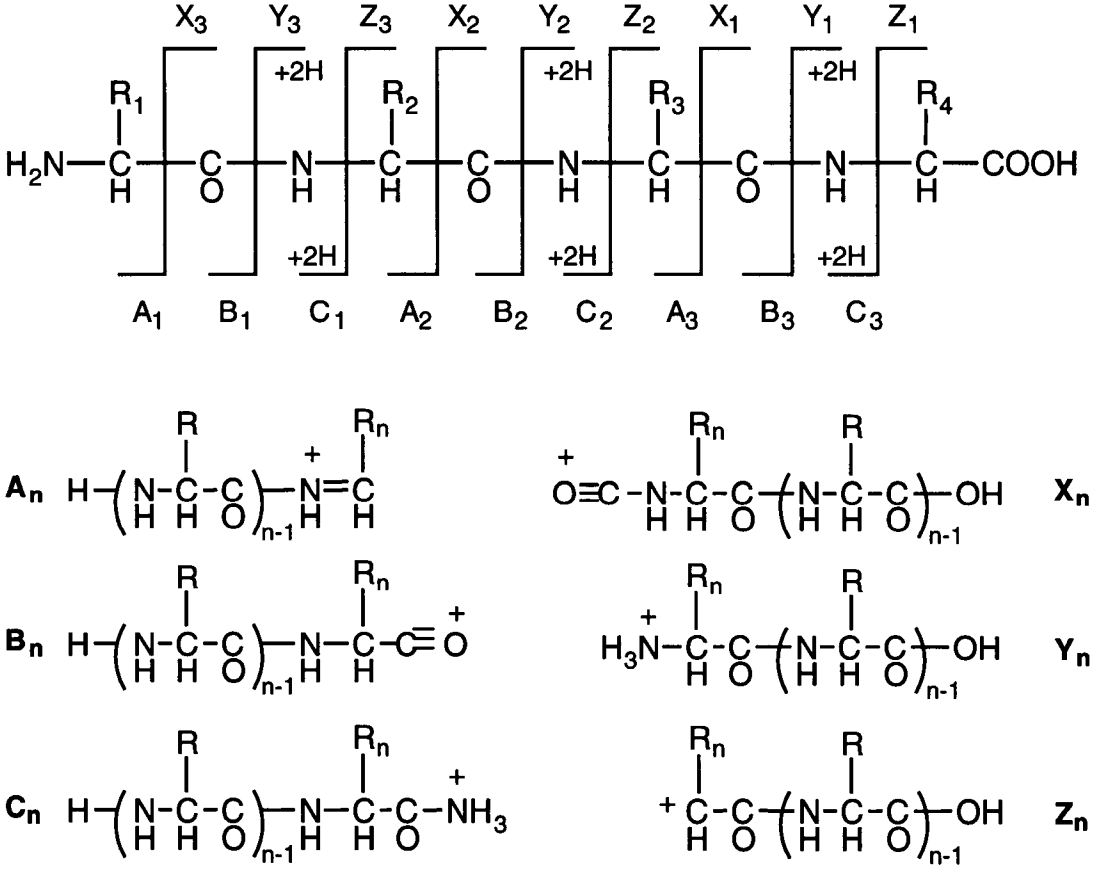

Figure 1.10. Fragment Ions Obtained from Cleavage of a Peptide Backbone.[27]

Sequence information can be obtained for peptides with molecular weights up to 2500 Da. Larger peptides reveal at least partial sequence information that often suffices to solve a particular problem. MS/MS data on proteolytic peptides can be used to obtain the sequence and solve other structural problems even for relatively large proteins. Partial sequence information by itself can be very informative. In many cases, the sequence of the peptide is already known, and any sequence information from MS/MS experiments can potentially point to where modification sites are located.

NMR spectroscopy has been used as a practical method for determining the rates of deuterium incorporation at individual amide sites by measuring the disappearance of the relevant proton resonance signals. Amide hydrogen/deuterium content can also be measured by tandem mass spectrometry at individual amino acid residues, however the results must be interpreted with caution because of the potential for randomization during the collision process. Deuterium present on amide nitrogens will be evident in a shift to higher masses of the of the isotopic clusters of sequence ions as for example in the b_n and y_n ions when compared to the non-deuterated peptides. From these data the H/D ratios at individual amide nitrogens can be determined.

For these determinations to succeed, a sequential set of ions must be observed. Although earlier studies made use of several different ion series, such as the b_n, y_n, and z_n, more recent studies rely mostly on the b_n ions.[28] A potential problem in using y_n ions is that they are believed to be formed by the transfer of a hydrogen from the N-terminal side of the cleavage site (**Figure 1.11**).[29] This transfer of hydrogen or deuterium during analysis obviously would lead to errors if not accounted for. In this case analysis of the b_n ions is preferable since no transfer of hydrogens in forming the acylium ions occurs

during fragmentation. However, high energy collisions required for fragmentations in CID MS/MS experiments can cause intramolecular scrambling of the amide hydrogens. Randomization occurs by the 'mobile proton', i.e. by the added proton that forms the MH+. All exchangeable hydrogens are subject to interchange[26a] and extensive H/D scrambling was also observed in SORI-CID dissociation of cytochrome c[26b] analyzed by ESI-FTMS though α-helical regions were found to remain intact by salt bridge stabilization. There is some evidence that electron capture dissociation of cytochrome c causes much less H/D scrambling.[30]

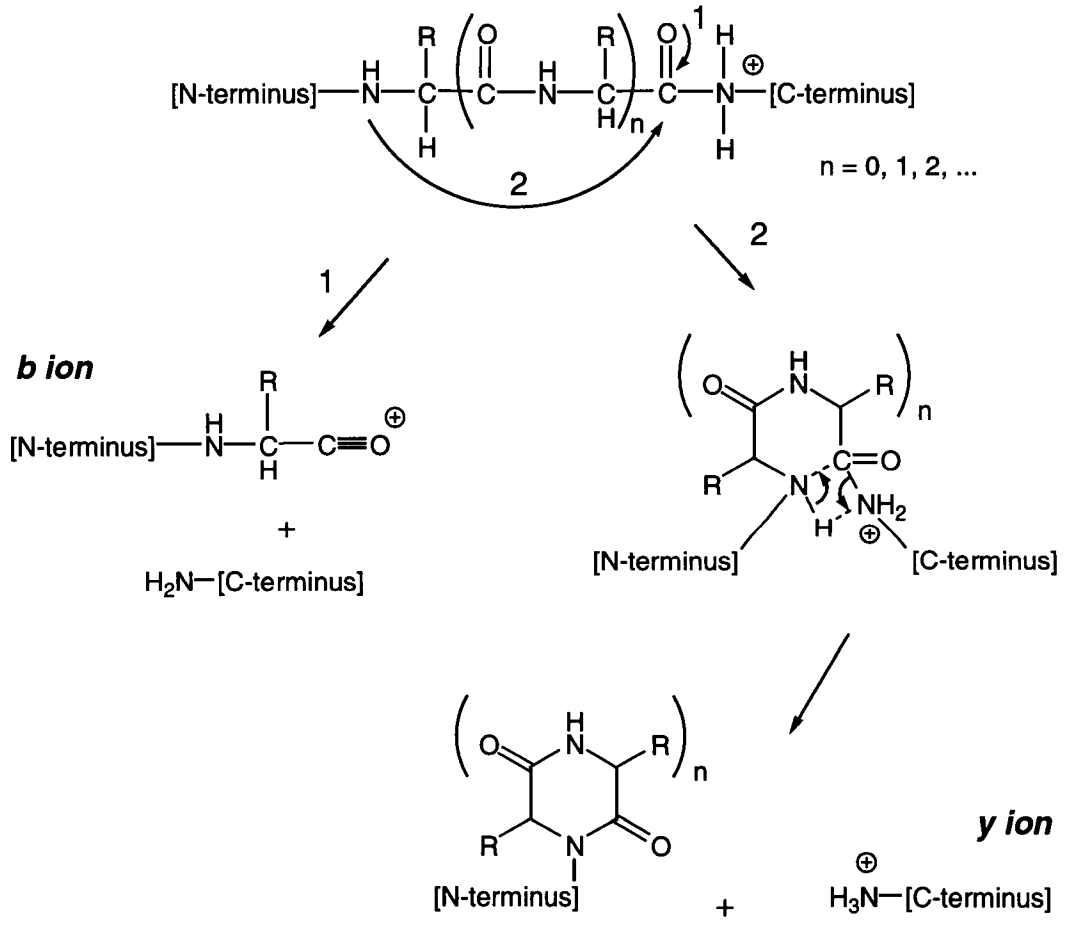

Figure 1.11. Mechanisms for the formation of *b* and *y* ions

Deng et al. showed the feasibility of detecting H/D exchange at peptide amide linkages by mass spectrometry.[31] Cytochome c was selectively labeled at specific linkages and analyzed by CID MS/MS. They found a high level of correlation between the predictions based on NMR and the CID *b*-fragments. Similar analysis of the *y* ions showed several discrepancies, but, for the most part the *y* ion series in their studies correlated very well with the NMR H/D exchange rate constants. Thus, their results implied that CID MS/MS can be confidently used to estimate deuterium levels at individual peptide amide linkages.

In the following sections, H/D exchange experiments were carried out on *E. coli* TRX and its alkylated adducts using thermally induced denaturation and analysis by LC-ESIMS and LC-ESIMS/MS. In these schemes, the main effort as focused on investigating the conformational change induced from the reduction of TRX and noncovalent interactions between the alkylated portions and the rest of the protein structure.

CHAPTER 2

RESULTS AND DISCUSSION

2.1 Alkylation of *E. coli* thioredoxin and identification of the adducts

The tripeptide, glutathione, is abundant in most cells.[32] Glutathione reductase acts unidirectionally, so that the ratio of reduced glutathione to oxidized glutathione in most cells is about 500 to 1. Because of its free thiol group, it represents a major protective mechanism against oxidative stress caused by a variety of chemical species such as hydrogen peroxide and organic peroxides.

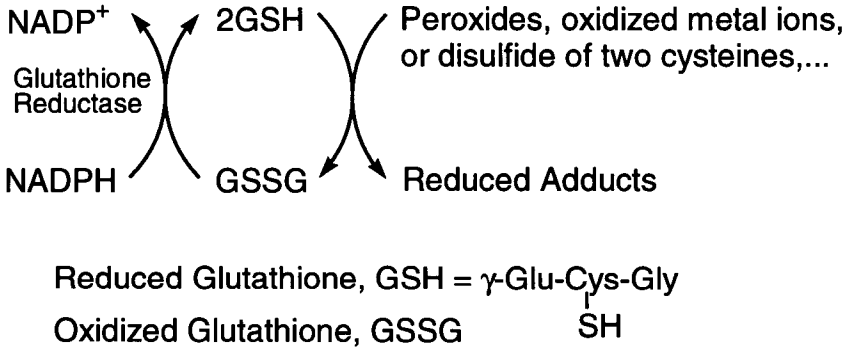

Figure 2.1. Electron transport sequences by glutathione system

The mutagenicity of 1,2-dihaloethanes is highly dependent upon its conjugation to glutathione by the enzyme glutathione *S*-transferase.[33] The conjugates thus formed can react with a variety of biomolecules such as nucleic acids and proteins.[34] Glutathione conjugation can induce cytotoxicity by forming

S-(2-chloroethyl)glutathione (CEG), as a consequence of 1,2-dichloroethane exposure. It can be hypothesized that the active site of proteins containing "thioredoxin fold" such as thioredoxin, thioredoxin reductase, and protein disulfide isomerase are *in vivo* targets for alkylation by glutathione conjugates. Reduced *E. coli* thioredoxin was alkylated by the episulfonium ion derived from CEG or *S*-(2-chloroethyl)cysteine (CEC).[34c, 35] Tandem mass spectrometry was used to confirm the position of alkylation on the protein.

2.1-1 Synthesis of alkylating agents.

S-(2-Chloroethyl)-glutathione (CEG) was synthesized *in vitro* from the reduced glutathione (GSH) and 1-bromo-2-chloroethane according to the method of Guengerich (**Figure 2.2A**).[34a] The CEG was obtained by precipitation and used for alkylation of the protein without further purification. The molecular weight of CEG was confirmed by mass spectrometry [369.83 (calculated), 369.8 (observed)] and the purity of CEG was found to be 60-70 % measured by HPLC. *S*-(2-chloroethyl)-cysteine (CEC) was synthesized from cysteine and 1-bromo-2-chloroethane by the same method. It was known that CEG reacts with DNA through an episulfonium ion intermediate.[35b]

2.1-2 Reduction and alkylation of *E. coli* thioredoxin by CEG and CEC.

The disulfide linkage between Cys 32 and 35 of *E. coli* TRX was reduced by the phosphine derivative, tris(2-carboxyethyl)phosphine (TCEP). Disulfides are reduced by TCEP via a mechanism similar to that of the trialkylphosphines, which have been used to quantitatively reduce organic disulfides.[36] The advantages of TCEP include its high solubility in water, activity below neutral pH,

resistance to air oxidation, and selectivity towards disulfide bonds. Only a small molar excess of TCEP is needed to quantitatively reduce disulfides.

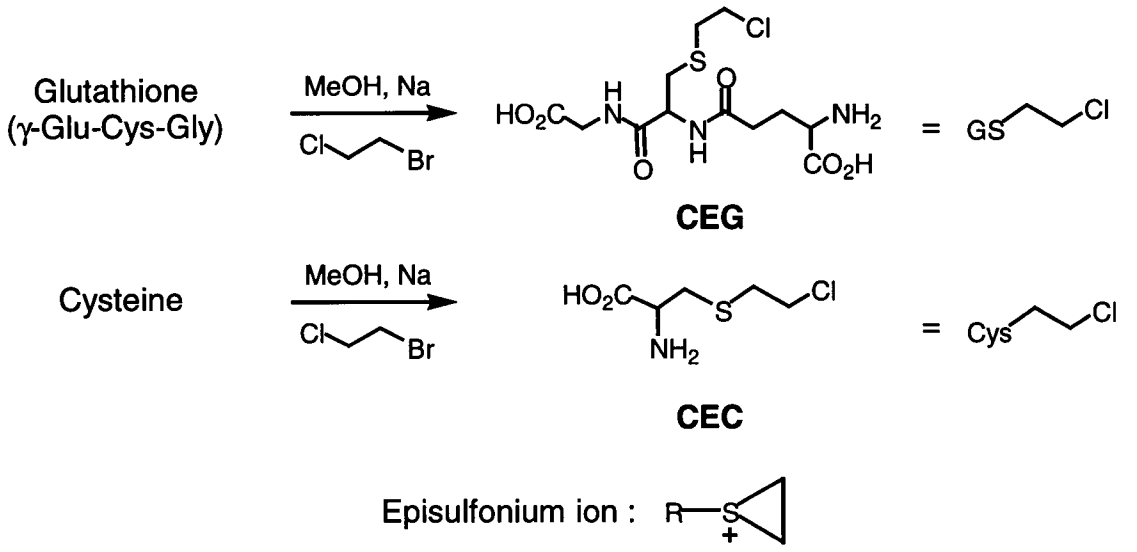

Figure 2.2(A). Syntheses of alkylating agents

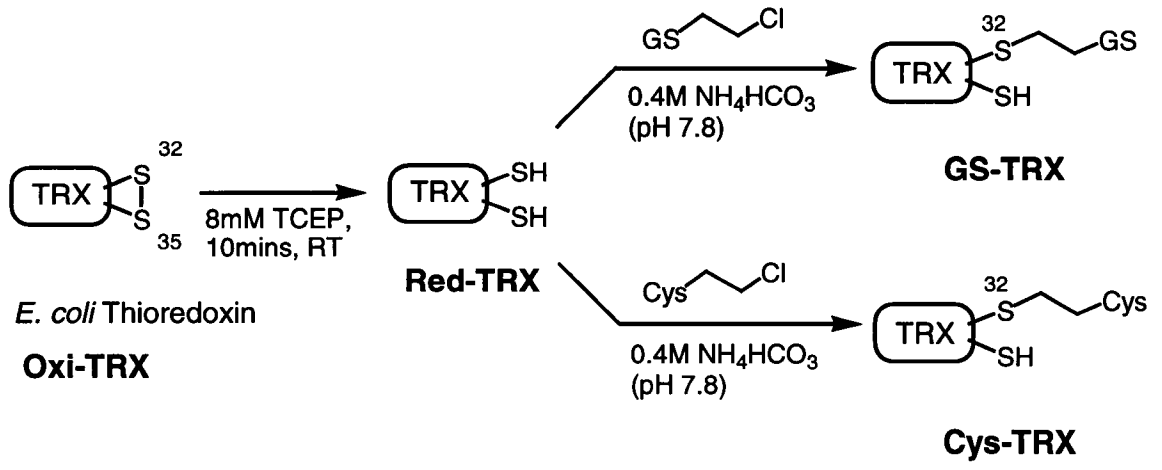

Figure 2.2(B). Alkylation of *E. coli* thioredoxin by CEG and CEC. The alkylation positions were determined by tandem mass spectrometry.

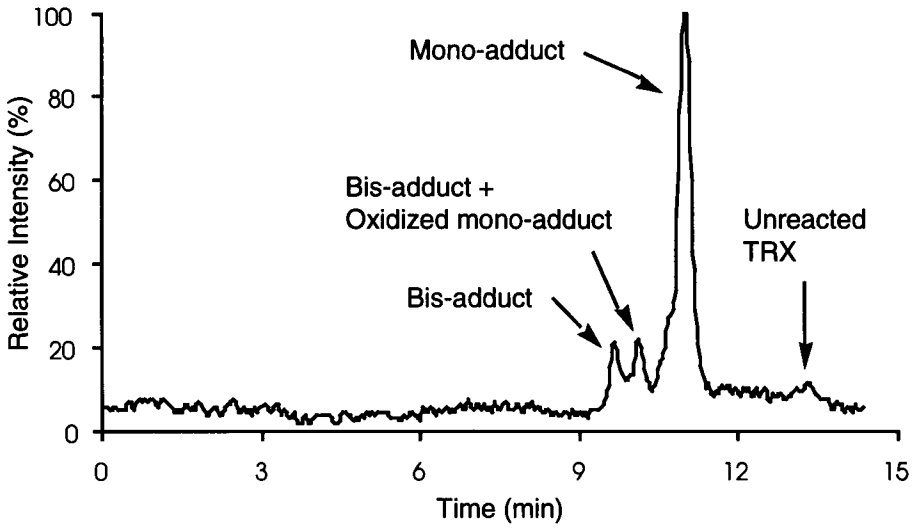

	Observed MW	Calculated MW
Oxi-TRX (unreacted)	11673.78	11673.45
Mono-adduct	12007.10	12008.83
Oxidized mono-adduct*	12023.48	12024.83
Bis-adduct	12342.22	12342.20

Figure 2.3. Total ion chromatogram of the reaction mixture of GS-TRX and the observed and calculated molecular weights of TRX adducts.
* Possible oxidation products of Met residues.

The reaction pathway was monitored by HPLC. The reduction of *E. coli* TRX by TCEP was completed within 10 min. Then, CEG or CEC in buffer solution was added in 50-fold excess to the solution of Red-TRX because CEG or CEC can also react with water in aqueous buffer solution. The alkylation reaction proceeds for about 1 hour at room temperature. For the completion of the reaction, i.e. complete consumption of reduced TRX as monitored by HPLC, more CEG or CEC was added (2 x 25-fold). The reaction mixture was then purified by preparative reverse phase HPLC. Mono-alkylated TRX adduct was collected and freeze-dried under high vacuum. The molecular weights of TRX

adducts were measured by mass spectrometry. Minor side products included bis- and oxidized mono-adduct (**Figure 2.3**).

2.1-3 Identification of modified sites in the alkylated TRXs by ESI-MS/MS

The modified site on GS-TRX was identified by enzymatic digestion and tandem mass spectrometry. It is already known that cysteine 32 is a major alkylation site,[34c] and MS/MS experiments were carried out to confirm that alkylation did, in fact, occur at this site. In the case of the mono-adduct, it was, indeed, found that one of two cysteines is alkylated and the other is free. The free thiol group in the mono-adduct was alkylated by iodoacetamide (IAA) to produce the carboxamidomethylated derivative. Alkylation of the cysteine prevented dimerization that otherwise occurs through intermolecular disulfide bond formation. Urea (10 M) was added to denature the protein. Trypsin was added to the protein solution. After 5 hours of incubation at 37 °C, the digestion mixture was separated and mass-analyzed through reverse-phase HPLC-ESI-MS. A very small peak in the total ion chromatogram was identified as the T3 fragment derived from CEG and IAA. Ions for the peptide, T3 (average MW 2371.7), showed the peaks at *m/z* 791.6 (+3) and 1186.8 (+2) (**Figure 2.4**). MS/MS experiments were carried out on these two ions to identify the exact alkylation site. CID experiments were carried out on both ions over the range of collision voltages, 15V to 25V. However, the expected daughter ion peaks, y_5 or b_{14}, that would identify the CEG-modified sites were not detected. Only weak b_2, b_3, b_4, b_5, b_6, b_7, and y_4 ions were detected. This result was thought to be due to the low intensity of parent ions (*m/z* 791.6 and 1186.8). To obtain higher intensities for these ions, several digestion and separation conditions were tested, however, those conditions were not effective, either.

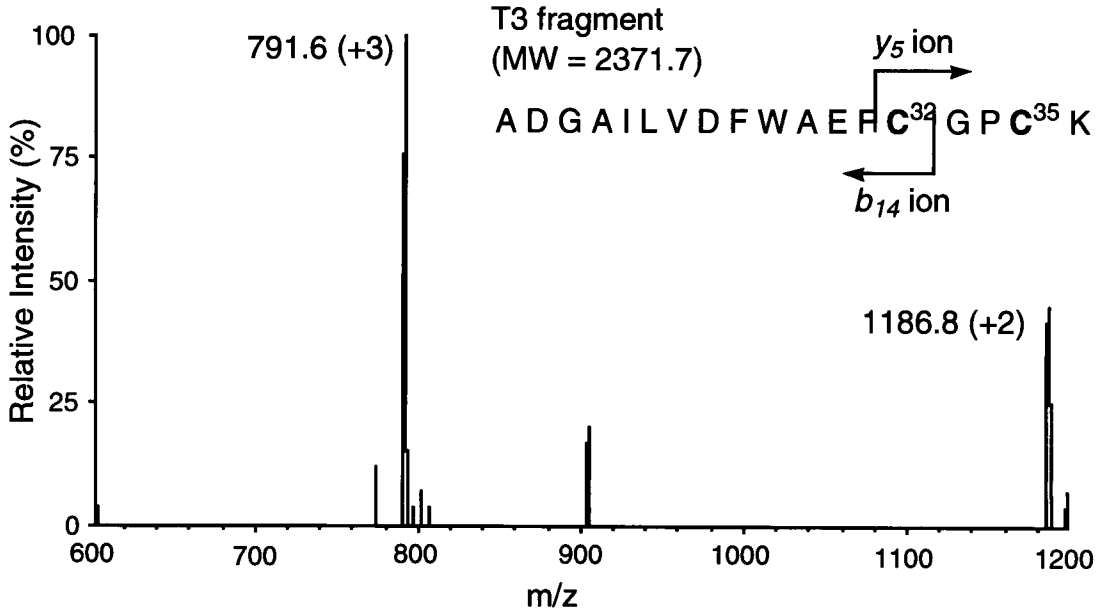

Figure 2.4. ESI mass spectrum of alkylated T3 fragment of GS-TRX.

Since the trypsin digest did not yield the expected data to support alkylation at Cys-32, it was decided to use another enzyme. Pepsin was selected as an alternative proteolytic enzyme to digest TRX under acidic conditions which involved 0.1M citrate buffer (pH 3.0). Initially digestions were carried out with the free thiol group of GS-TRX not alkylated by IAA. HPLC-purified mono-adduct was digested by pepsin in 4 M urea/0.1 M citrate solution. Through LC-MS, a fragment including the modified site was found. The measured mass value of this fragment (1543.3) corresponded to the mass of the residue consisting of amino acid 28-37 (Trp-Ala-Glu-Trp-Cys*-Gly-Pro-Cys*-Lys-Met, average MW 1543.8) with one of two cysteines* alkylated. The doubly charged ion peak (*m/z* 772.4) was subjected to CID to produce a series of *b* and *y* fragment ions. At 25 V collision energy, the selected fragment which included the alkylated site was

unambiguously characterized (**Figure 2.5** and **Table 3.1**). The daughter ion spectrum indicates that the site of alkylation was Cys-32 exclusively as there was no alkylation at Cys35. The ion denoted by y_6 (*m/z* 971.2) corresponds to Cys32*-Gly-Pro-Cys35-Lys-Met (an asterisk indicates alkylated Cysteine). The y_5 ion (*m/z* 535.2) corresponds to Gly-Pro-Cys35-Lys-Met. The mass difference between y_6 and y_5 ions (436.0) exactly matches the molecular weight (436.5) of 2-(*S*-glutathionyl) ethylcysteine at position 32. The y_6 ion loses a glutamic acid residue (E) from the ethylglutathionylated adduct to produce the signal at *m/z* 842. All fragment ions that included covalently attached glutathionyl group, y_7, y_8, and y_9, showed similar patterns with the glutamic acid residue missing (curved arrows).

A minor bis-adduct was isolated from the alkylation product mixture, which when digested with pepsin, produced two CEG-modified peptides. One is the peptide that contains Cys-32, and the other contains Tyr-49. It was assumed, therefore, that the second alkylation site is Tyr-49, since previous studies had shown that the OH of this amino acid can be alkylated.[34c] However, because of the low intensity of parent ions, it was not possible to confirm by MS/MS experiments that Tyr-49 was, in fact, alkylated.

Sequencing of Cys-TRX was accomplished in the same manner. The cysteinylethyl group also was attached at the Cys 32 position (**Figure 2.6** and **Table 3.2**). The reason for the exclusive alkylation at Cys-32 is most likely due to the fact that the pKa of the Cys-32 thiol group is lower by several pH units than is normally observed for cysteine residues. This is supported by possible favorable interactions between this thiolate anion and the effective positive charge at the N-terminal of the α-helix.[37] In addition, further stabilization of the thiolate anion can also arise from interactions with positively charged groups such as the basic residues, Arg and Lys.[38]

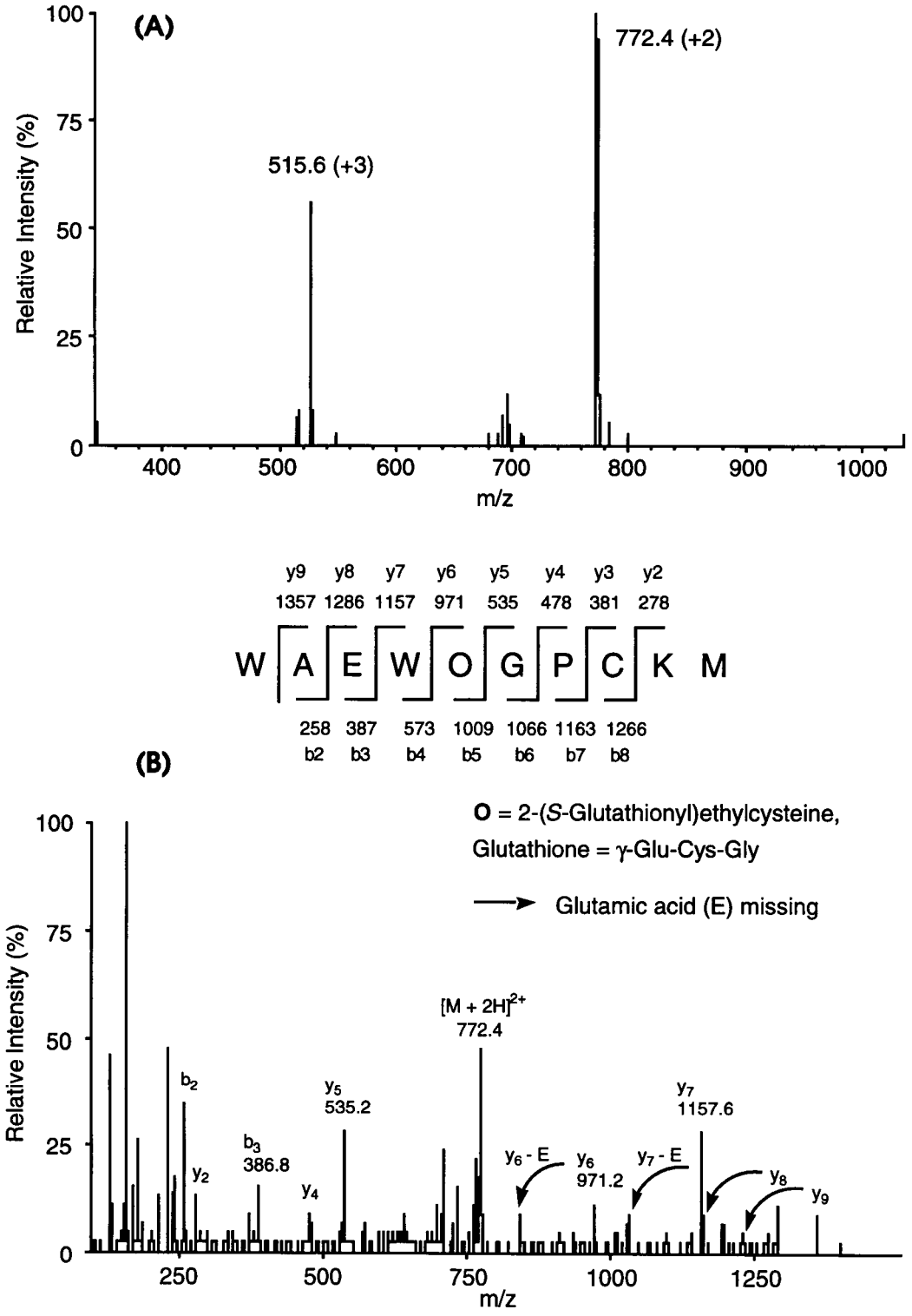

Figure 2.5. (A) The ESI spectrum of a peptic fragment 28-37 of GS-TRX. **(B)** The CID spectrum of 2+ charged ion (*m/z* 772.4) of fragment 28-37.

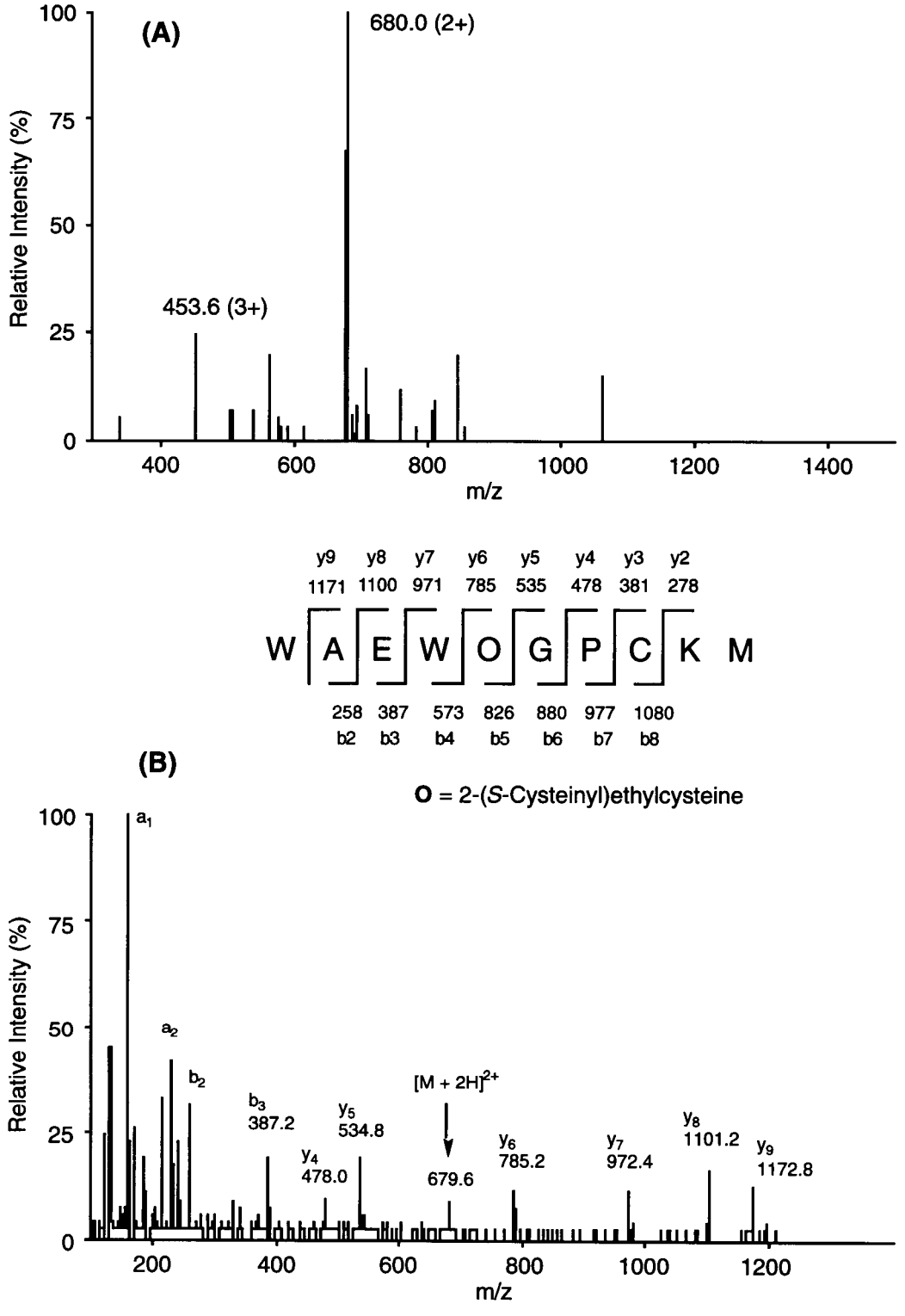

Figure 2.6. (A) The ESI spectrum of a peptic fragment 28-37 of Cys-TRX. **(B)** The CID spectrum of 2+ charged ion (*m/z* 680.0) of fragment 28-37.

2.1-4 Sample pretreatment of purified modified TRXs

The charge state distribution spectrum of HPLC-purified GS-TRX at 25 °C (**Figure 2.7 (C)**), unexpectedly shows that the majority of GS-TRX molecules are populated as unfolded or open conformers. Charge states from 10+ to 16+ represent the unfolded or open conformers; charge states from 7+ to 9+ represent the compact or folded conformers. This unexpectedly high proportion of unfolded GS-TRX is believed to be due to the use of C18 reverse-phase HPLC for separation. A number of cases of protein structure disruption have been reported when using LC for separation.[39]

Temperature-dependent alteration of ESI mass spectra of purified GS-TRX was monitored by heating the protein stock solution to 85 °C. ESI mass spectra at 45 °C (**Figure 2.7 (B)**) indicated very low intensities of ions in the charge state envelopes for the unfolded form, i.e. these spectra showed stable, compact conformers. Above 45 °C, the intensities of charge states representing unfolded conformers (10+ to 16+) appeared, i.e. protein molecules start to melt. Ion peaks representing charge states +7, +8, and +9 were attributed to the folded form F. Ion peaks representing charge states +10 to +15 were ascribed to the unfolded form U (see experimental details in **section 2.2-3**). The effect of temperature was determined on the function of folded conformers in the mixture by measuring F/(F+U) (**Figure 2.8** and **Table 3.3**). At around 45 °C, the F/(F+U) ratio was found to be a maximum. After initial equilibration at 45 °C for 15 min, the charge state distribution of GS-TRX indicated that there was a constant F/(F+U) from 20 to 45 °C and a melting point at ~55 °C. This result suggests that the charge state distribution in a protein ESI spectrum reflects the heterogeneity of conformational states in protein folding.[40] After reverse-phase HPLC separation, the structure of protein may be disrupted in a high-energy unfolded

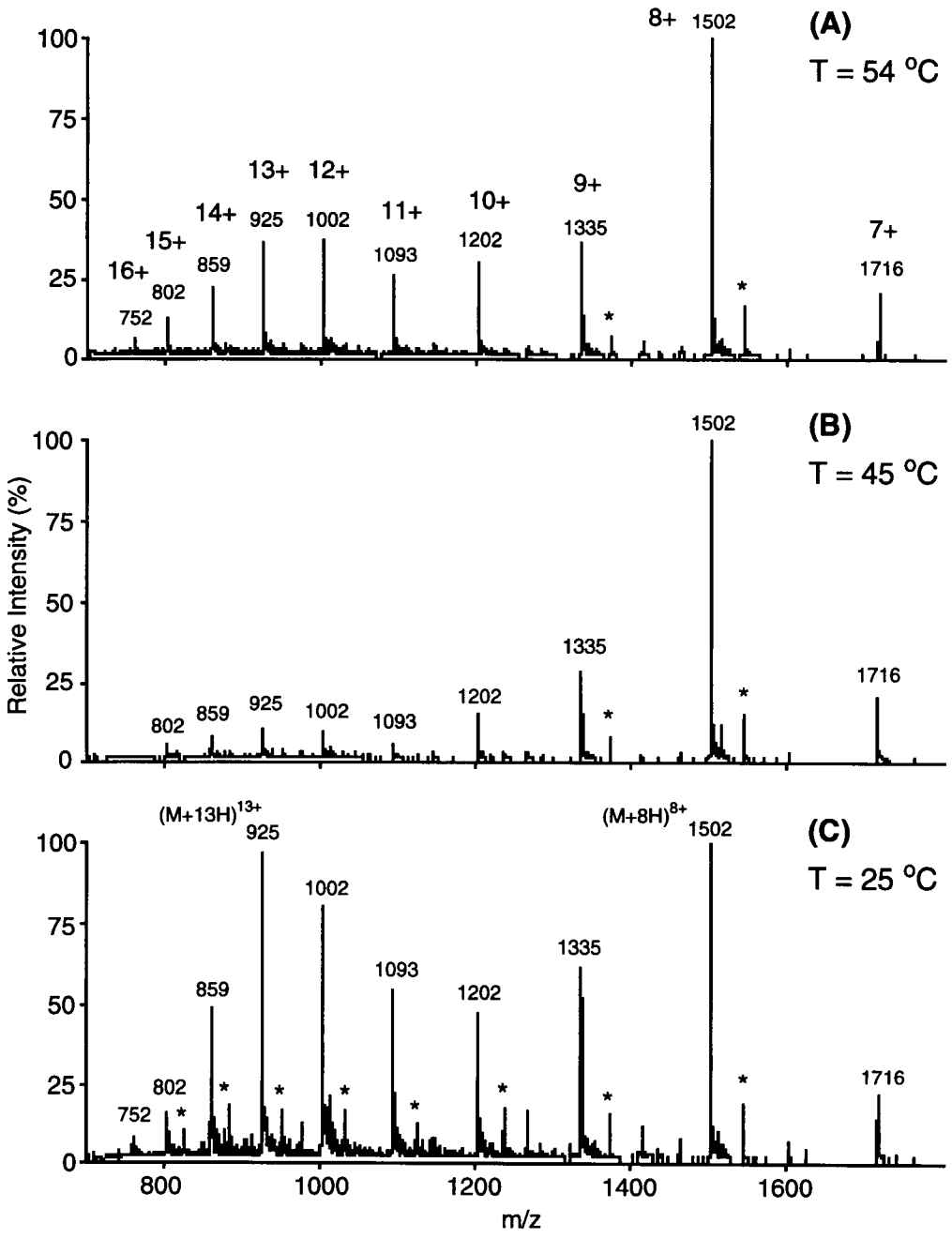

Figure 2.7. The ESI mass spectra of HPLC-purified GS-TRX in 1% acetic acid at different temperatures: (A) 54 °C, (B) 45 °C, and (C) 25 °C. Bis-alkylated adducts are marked with an asterisk.

state. With sufficient energy to overcome this kinetic trap, the conformation of the protein became stabilized in a compact, native-like conformation. A decrease of both the actual charge and the width of distinct charge state distributions at 45 °C can be interpreted in terms of the funnel-like nature of an energy landscape which directs the ensemble of protein molecules toward more compact structures, and ultimately to the native structure.[41] Hence, alkylated TRXs, GS- and Cys-TRX, had to be pretreated by incubation in 1 % acetic acid at 45 °C for 15 min and cooled down to room temperature before being used in the experiments.

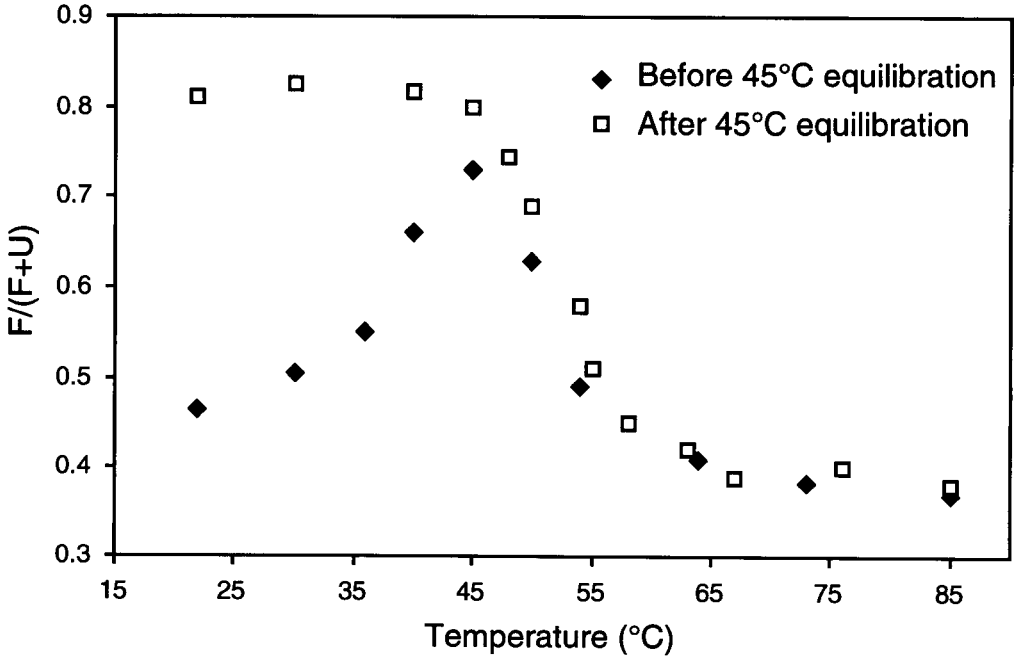

Figure 2.8. Temperature dependent variation of F/(F+U) for GS-TRX before and after 45 °C equilibration.

2.2 Thermal denaturation of *E. coli* thioredoxin and its derivatives (TRXs)

Thermally-induced unfolding of proteins has been studied extensively to improve our understanding of the fundamental tenets of protein stability and folding. Calorimetry is making enormous contributions to this area because it provides a means of directly measuring enthalpy and entropy changes due to unfolding.[42] The variation of amide hydrogen exchange rates with temperature, which may be a useful method for the thermal unfolding studies of proteins, has received some attentions. Structural and dynamic changes induced by temperature have been studied by amide hydrogen exchange.[43]

ESI mass spectra exhibit charge state distributions characteristic of the conformational states in solution which enable one to differentiate between folded, more compact and unfolded, less compact states. Some experimental evidence is available showing the relationship between observed charge state distributions in ESI mass spectra and the solution structures.[44] There is a general agreement that higher charge states correspond to unfolded, less compact conformations and vice versa.

2.2-1 Online H/D exchange and ESI-MS experiments

This study was an attempt to learn more about the temperature-induced denaturation of TRXs and the conformational dynamics during thermal denaturation. ESI mass spectrometric approaches, of necessity, make use of volatile buffer solutions. Hiraoki et al. noted that the stability of TRX was unchanged at pH 2.5 and 25 °C, and no signs of denaturation were detected by proton NMR spectroscopy.[45] Consequently, aqueous acetic acid was chosen as the solvent system and the concentration was optimized to 1 % because it

showed a uniform charge distribution pattern for the unmodifed as well as the modified TRXs. Low pH and high temperatures show a synergistic denaturing effect that decreases the melting temperature, T_m, thereby allowing direct monitoring of the thermal unfolding transition of TRX by mass spectrometric methods.

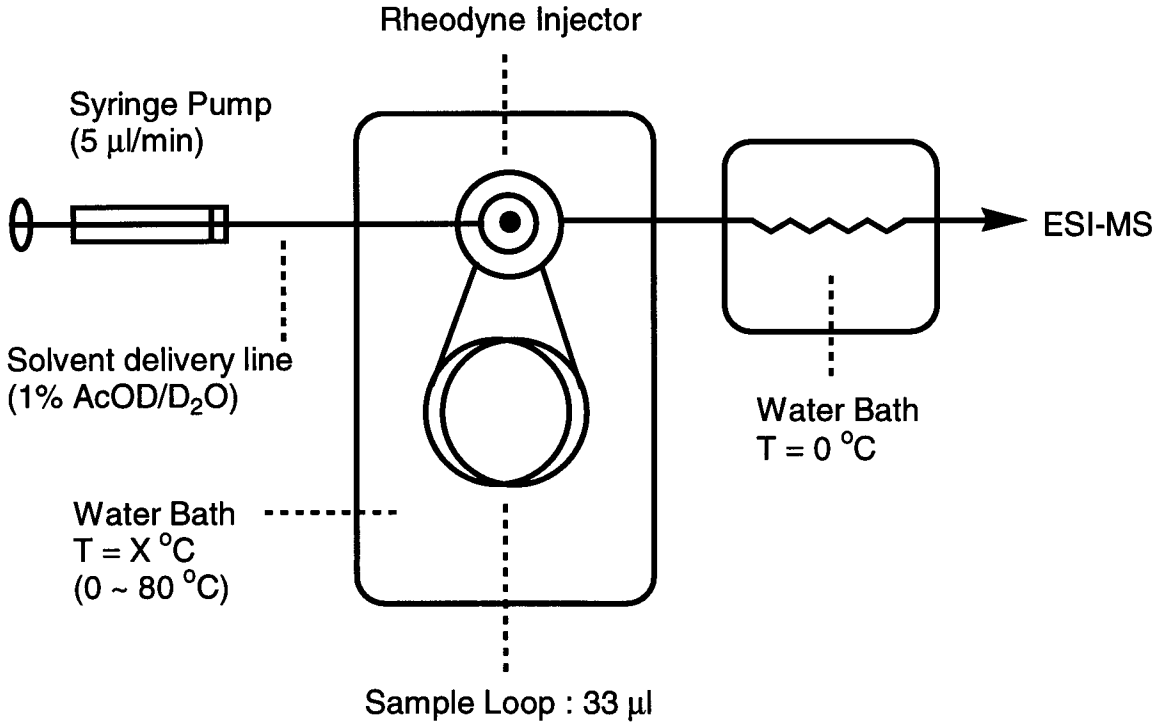

Figure 2.9. Instrumentation for on-line H/D exchange-in experiments

The conformational dynamics of TRX during thermal denaturation were investigated by performing online H/D exchange-in experiments as a function of temperature and time. The method is based on a continuous flow setup (**Figure 2.9**). The solvent delivery line, the sample loop, and the injection valve were

immersed in a water bath and equilibrated at the desired temperature (X °C). The sample loop was used as exchange reaction capillary.

H/D exchange was initiated by a 50-fold dilution of a 0.85 μM protein stock solution in 1% acetic acid into ice-cold 1% AcOD/D_2O which resulted in a final protein concentration of 0.018 μM. The protein solution was injected as quickly as possible into the sample loop in the desired temperature. The injection took approximately 15-20s. To minimize exchange during this period, the glass body of the syringe was precooled prior to injection. After the deuterium exchange reaction in the sample loop, the protein solution was transferred from the sample loop into the ESI source via a fused silica capillary which was immersed in an ice bath to quench exchange-in and to facilitate refolding to thermally unfolded TRX. The reported incubation periods represent the time that the protein spent in the sample loop exposed to the H/D exchange conditions. The maximum H/D exchange reaction time, i.e. incubation time, depends on the volume of the sample loop and the flow rate. The estimated exchange reaction time for this setup (**Figure 2.9**) was 5 min for a flow rate of 6 μl/min or 10 min for 3 μl/min. To obtain a strong ion signal, the flow rate had to be maintained over 5 μl/min. The total ion chromatogram indicated a strong and constant ion intensity for about 5 min (**Figure 2.10**).

The mass spectrum of Oxi-TRX in 1 % AcOH/H_2O exhibits a broad distribution of charge states ranging from 7+ to 14+ (**Figure 2.11**). The mass derived from deconvolution of the multiply-charged ions is 11,673.78 Da, a figure which is consistent with the predicted mass, 11,673.45 Da. The conformational dynamics from thermal unfolding of TRX and its alkylated adducts was monitored by online H/D exchange-in experiments as a function of time and temperature.

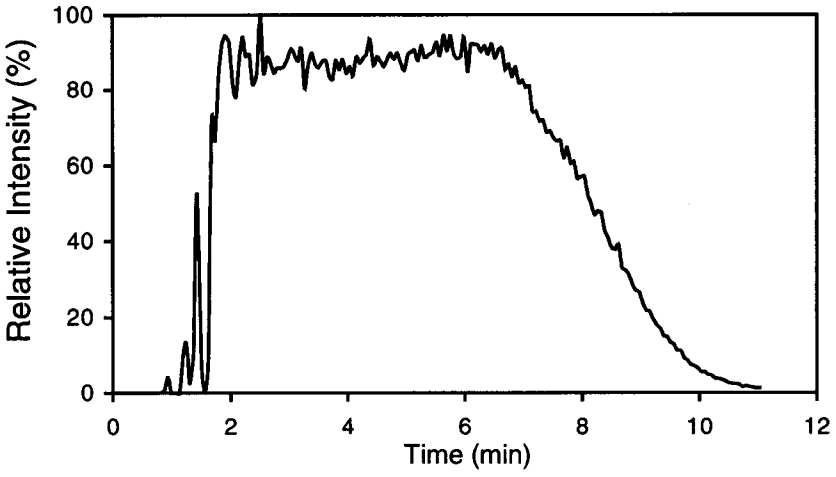

Figure 2.10. Total ion chromatogram of H/D exchanged Oxi-TRX. The volume of the reaction mixture (size of sample loop) was 33 µl. The flow rate was 6µl/min.

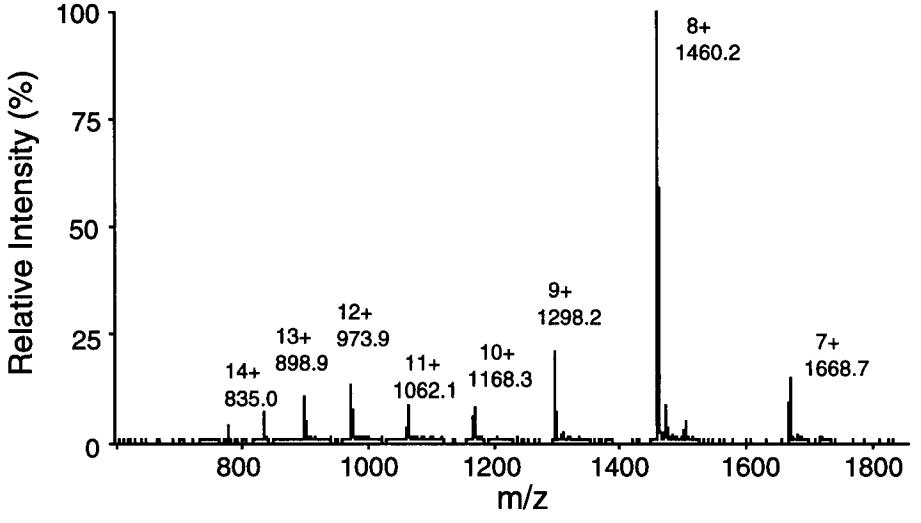

Actual peak	Intensity	Charge	Compound mass
835.00	50,000	14	11,675.89
898.90	88,333	13	11,672.60
973.90	116,667	12	11,674.71
1062.10	72,500	11	11,672.01
1168.30	70,000	10	11,672.92
1298.20	190,833	9	11,674.73
1460.20	858,333	8	11,673.54
1668.70	150,000	7	11,673.84

Avg. compound mass **11,673.78**, Std. Deviation: 1.28

Figure 2.11. Charge state distribution of Oxi-TRX in 1 % acetic acid. Molecular weights were calculated by deconvolution of the multiply-charged ions.

This continuous flow design allowed direct monitoring of protein unfolding by ESI-MS. In these experiments, charge staes +7, +8, and +9 were ascribed to the compact conformational state of TRX. Because of its high intensity, the 8-fold charged ion peak was used to make quantitative comparisons of the ion peaks after an exchange-in period of 105±10s (**Figure 2.12**). During the online exchange-in experiment at 40 °C, the *m/z* value of the 8-fold charged ion peak of Oxi-TRX increased to *m/z* 1468.1 after 105 sec which indicated an incorporation of roughly 65 deuteriums (37% of exchangeable hydrogens). As the exchange-in was monitored at 60 °C, the ion peak became broader and showed slight peak splitting. At around 70 °C the spectrum showed two distinct peaks, *m/z* 1472.0 and 1476.8. The ion peak at lower mass value corresponds closely to the ion peak which was observed during the hydrogen exchange experiment under nondenaturing conditions (40 °C), and the peak at the higher mass value was very close to the mass value that was observed for the ion of fully deuterated TRX. Fully deuterated protein ions are shown as dotted peaks (**Figure 2.13**). These were obtained from the fully denatured proteins that were incubated in 1% AcOD/D_2O at 80 °C for 1 hour. Reduced and alkylated adducts (GS- and Cys-TRX) already showed two distinct peaks at approximately 50 °C and only one peak at around 70 °C whose *m/z* value is very close to the ion peak of the fully deuterated protein. This result suggests that Red-TRX and its alkylated adducts have more unstable structures than Oxi-TRX because they showed the conversion from EX2 to EX1 mechanism at lowered temperature.

As the exchange-in time increased, the ion peak at the higher *m/z*-value increased in intensity, and the ion peak at the lower *m/z*-value diminished (**Figure 2.13**). Peak evolution patterns at 50 °C were significantly different between the Oxi-TRX and modified TRXs. Oxi-TRX showed it to be stable in the EX2 kinetics, in which the mass spectrum shows a peak that gradually shifts with

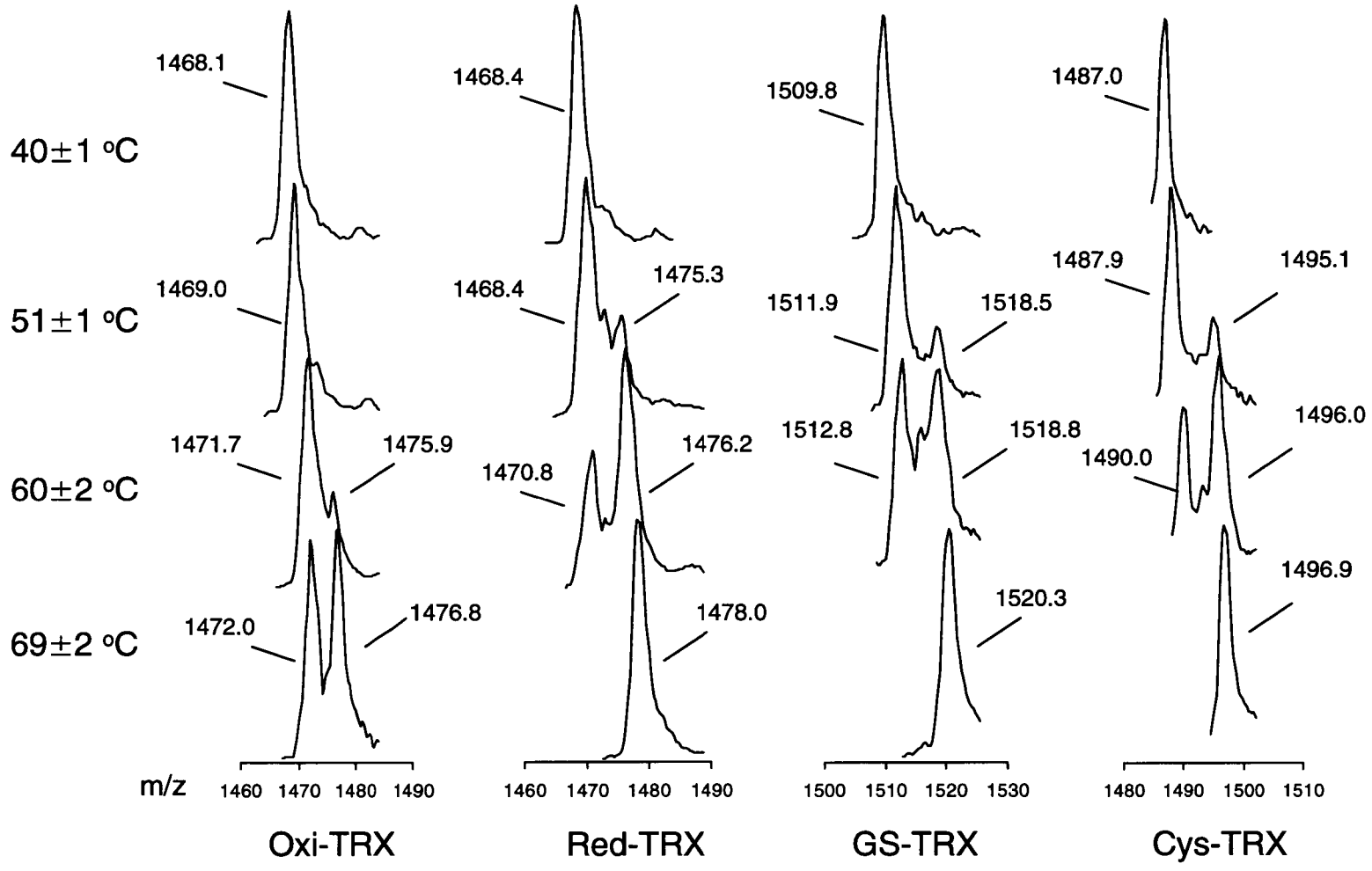

Figure 2.12. Temperature-dependent alteration of the exchange mechanism (Comparison of the 8-fold charged ion peak of TRXs at different temperatures after an exchange-in period of 105±10 s in 1% AcOD/D_2O)

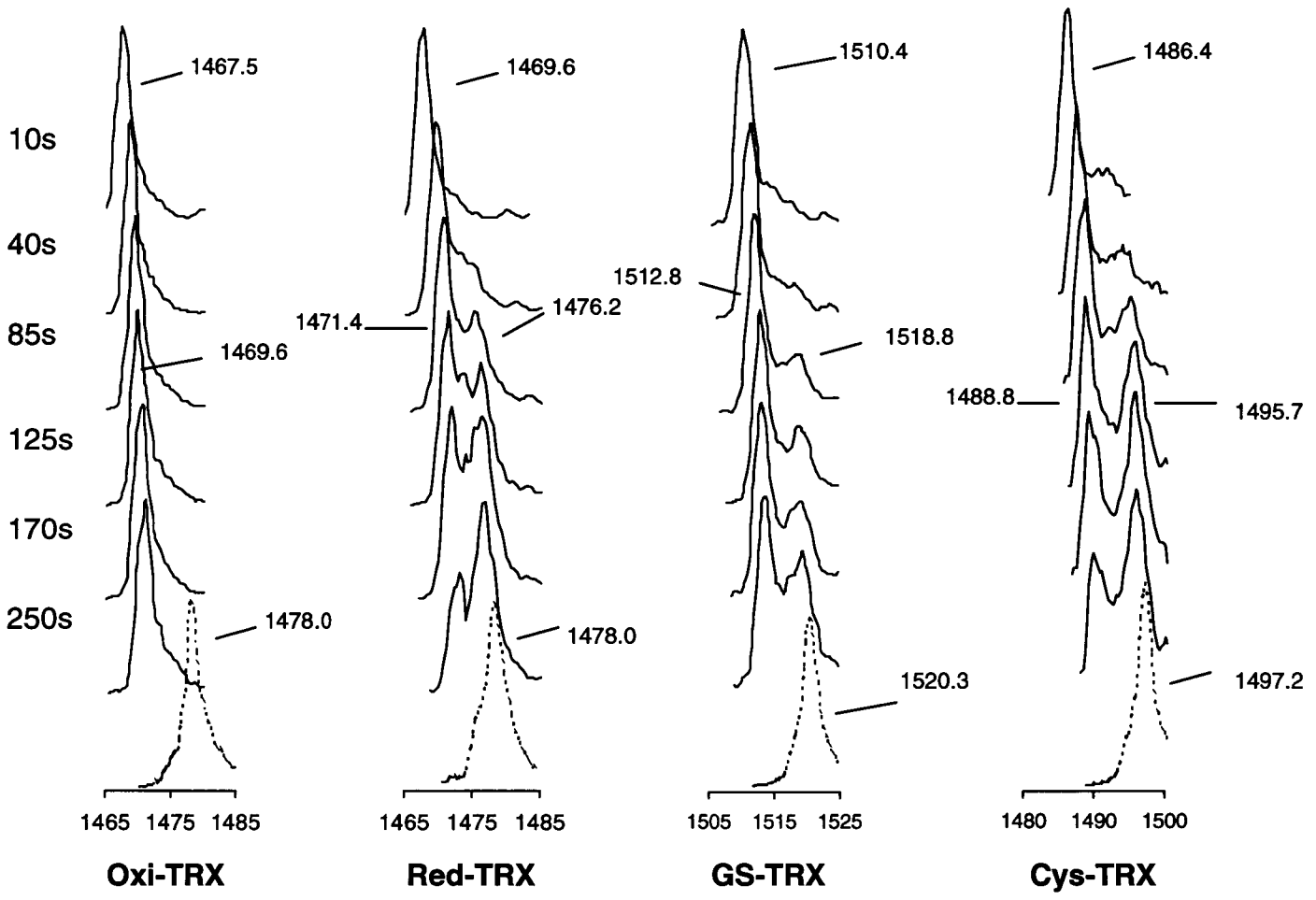

Figure 2.13. Evolution of the 8-fold charged ion peaks of TRXs during on-line H/D exchange-in experiments in 1% AcOD/D_2O at 50 °C. Time points refer to H/D exchange periods. Dashed peaks were obtained by mass spectral measurements of the fully deuterated proteins.

increasing exchange-in time to higher masses. In contrast, Red-TRX and its alkylated adducts showed that two distinct mass peaks developed after a short exchange-in time indicating that the exchange took place by the EX1 mechanism. Deconvolution of the profiles by a non-linear algorithm (PeakFit v.4, AISN software) shows several peaks between the lower and higher mass peaks in the 8-fold charged ion peak of Red-TRX after an incubation in 1% AcOD/D_2O for 170 sec (**Figure 2.14**). Presumably, these peaks are produced from partially unfolded intermediates or molten globule states that consist of core hydrophobic β-sheets that resist unfolding. These unfolding intermediates can be rationalized on the basis of "regional melting" of the Oxi-TRX,[45] in which some amino acid residues consisting of core β-sheets show very slow isotopic exchange rates. Miranker et al. reported a similar pattern of transient protein folding intermediate in the refolding study of hen lysozyme. The transient protein folding intermediates were thought to be a result of cooperative folding of protein domains.[10c]

The evolution of the 8-fold charged ion peaks showed different rates of conversion from lower mass (*m/z*) peaks to higher mass (*m/z*) peaks. The conversion rate constants for TRXs were estimated from the varying intensities of two separated 8-fold charged ion peaks at different temperatures. To simplify the calculation, the mass peaks from partially unfolded intermediates were excluded, and only the two extreme peaks (peaks A and D in **Figure 2.14(A)**) from undenatured (folded) protein and fully denatured (unfolded) protein were chosen. The conversion rate constants (k_{obs}) were calculated by fitting the experimental results, $f/(f+u)$, to an equation $f/(f+u) = A\exp(-k_{obs}t)$ where f and u are the intensities of peaks A and D, respectively.[46] The conversion rate constants of TRXs at 50, 55, and 60 °C were obtained from the curves based on $f/(f+u)$ and time (**Figure 2.15 A-C** and **Table 3.4 ~ 3.6**).

Time dependent analysis for the deconvolution of 8-fold charged ion peaks were performed for Red-, GS-, and Cys-TRX (**Figure 2.14(B)**). The deconvoluted peaks indicated three or four envelopes of isotope peaks corresponding to three or four different structures. It is hard to say that whether there are one or two intermediates between folded and unfolded forms (peaks A and D in **Figure 2.14(A)**) because the resolution of the mass peak was not good enough to determine the exact number of intermediates. For example, the first two small peak tops (peaks A and B in **Figure 2.14(A)**) separated by about 2 Da amounts to a resolution of ~800. To be able to determine the minimum number of real peaks hidden within these profiles, a resolving power of at least an order of magnitude greater would be required.

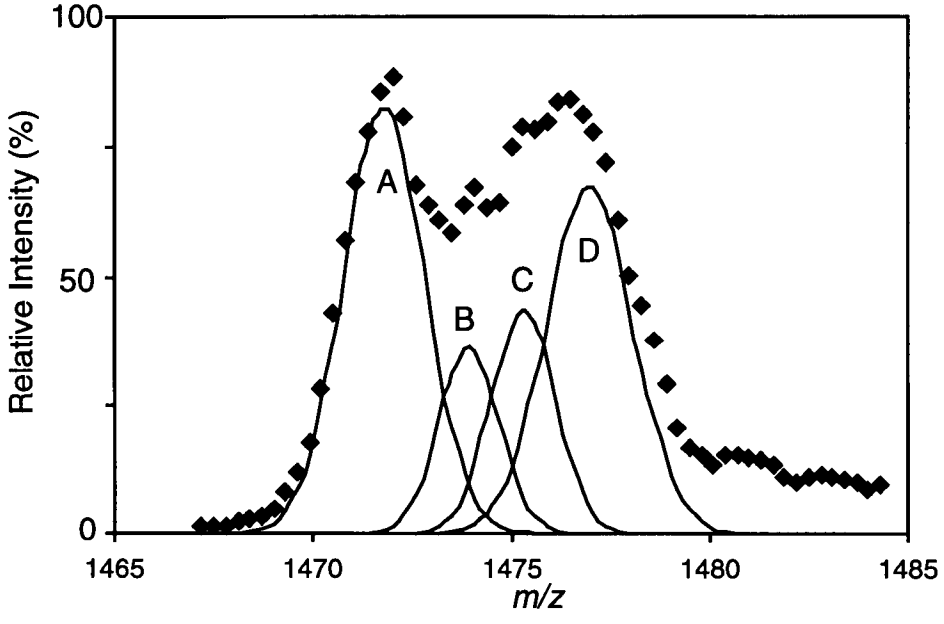

Figure 2.14(A). 8-Fold charged ion peak (◆) of Red-TRX after incubation in 1% AcOD/D_2O for 170 sec at 50 °C. Deconvolution of raw data was obtained using a non-linear deconvolution algorithm (PeakFit).

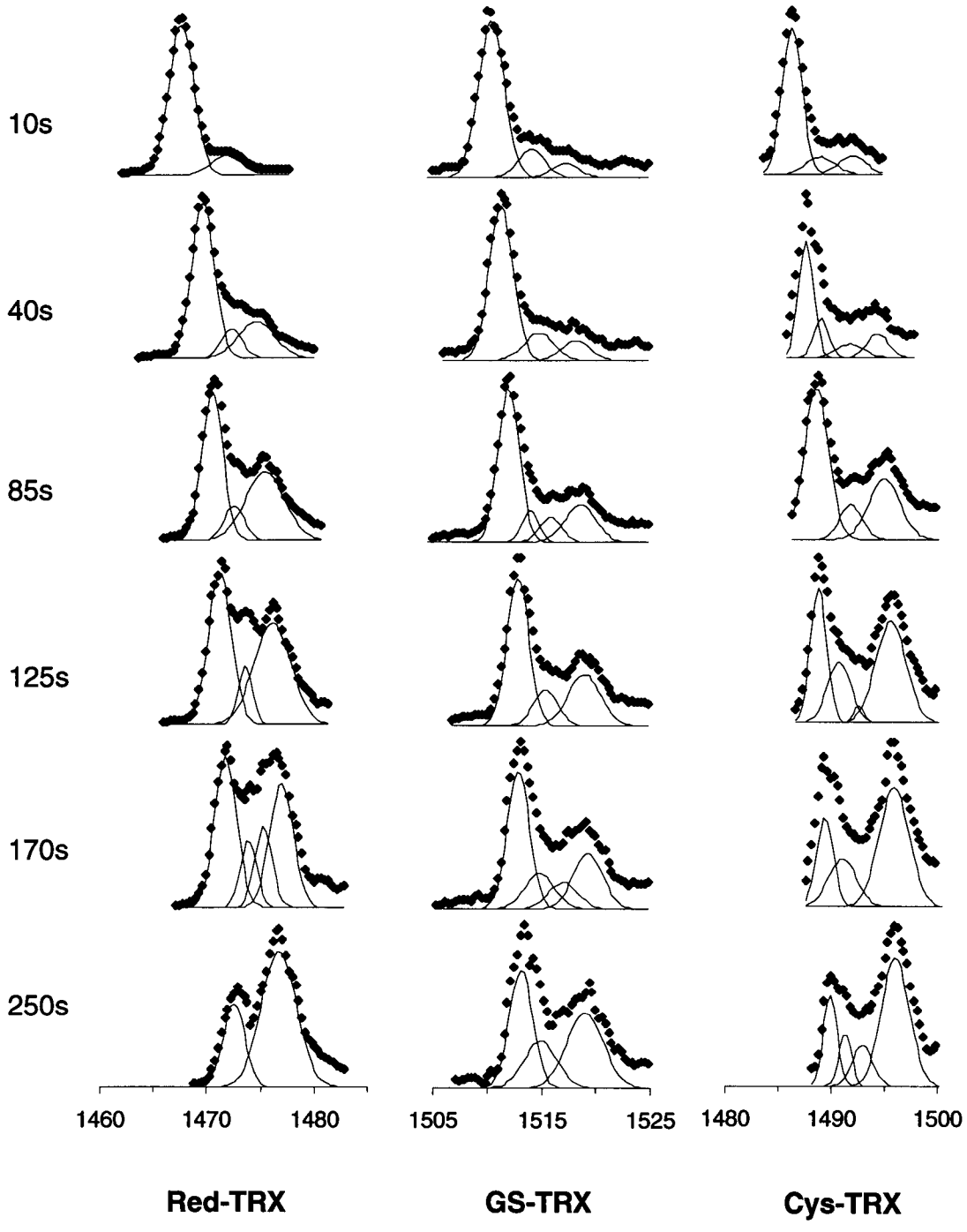

Figure 2.14(B) 8-fold charge ion peaks (◆) of Red-, GS-, and Cys-TRX and their fitting with Gaussian functions during the on-line H/D exchange-in experiments in 1% AcOD/D_2O. Time points refer to H/D exchange periods.

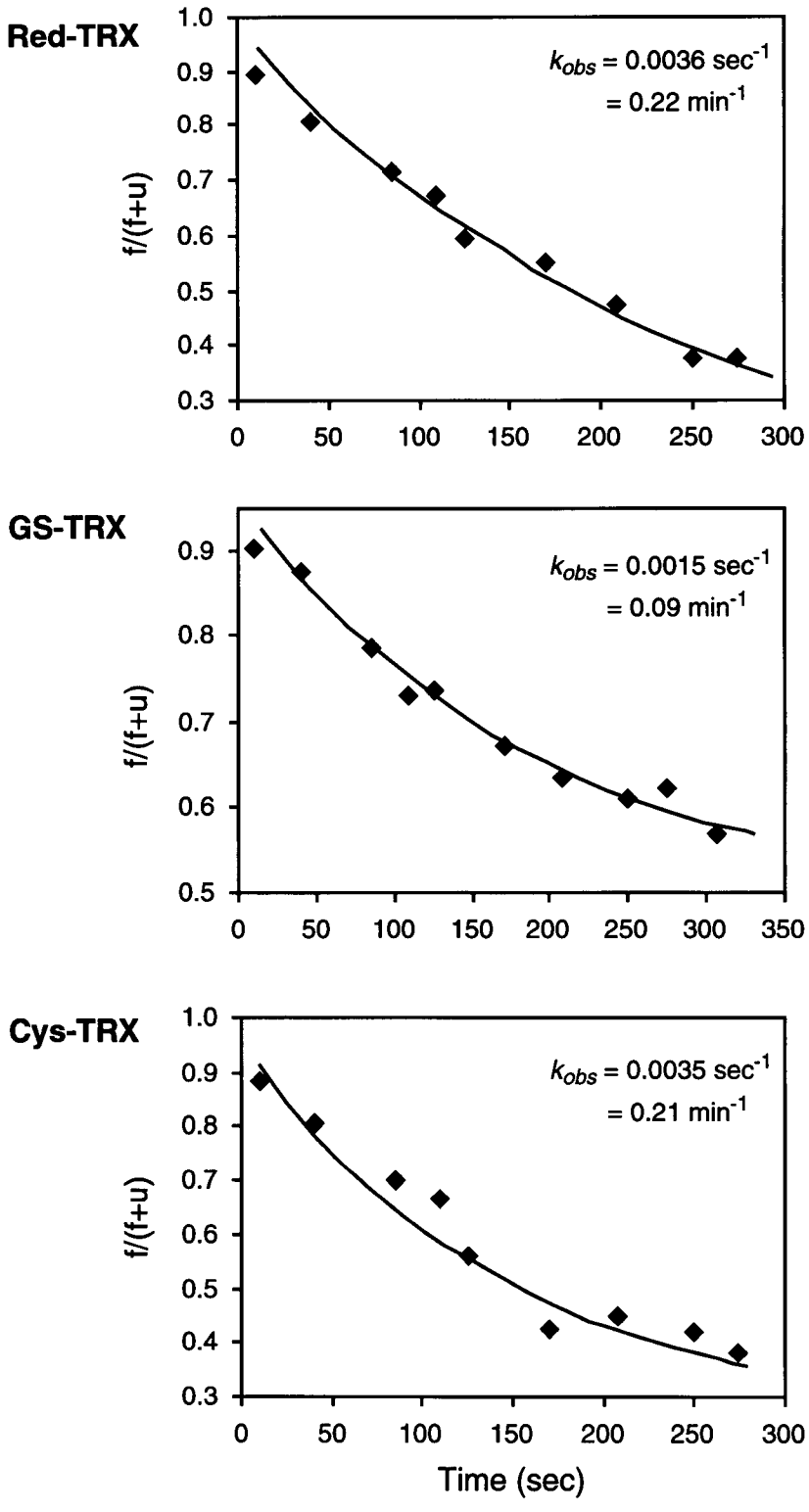

Figure 2.15 (A). Change in the fraction of folded conformers at 50 °C with time. The rate constant k_{obs} was obtained using equation f/(f+u) = Aexp(-k_{obs}t).

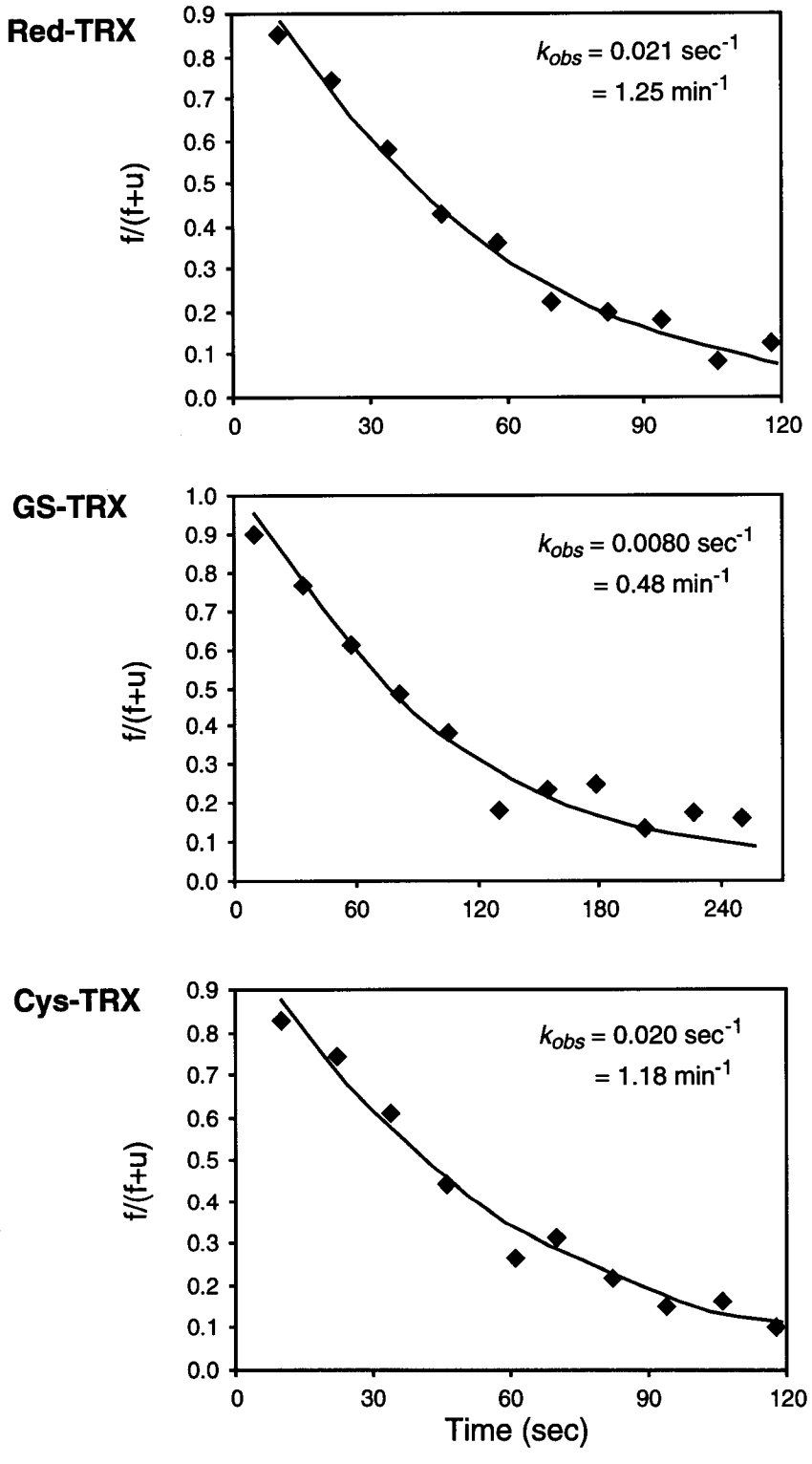

Figure 2.15 (B). Change in the fraction of folded conformers at 55 °C with time. The rate constant k_{obs} was obtained using equation f/(f+u) = Aexp(-k_{obs}t).

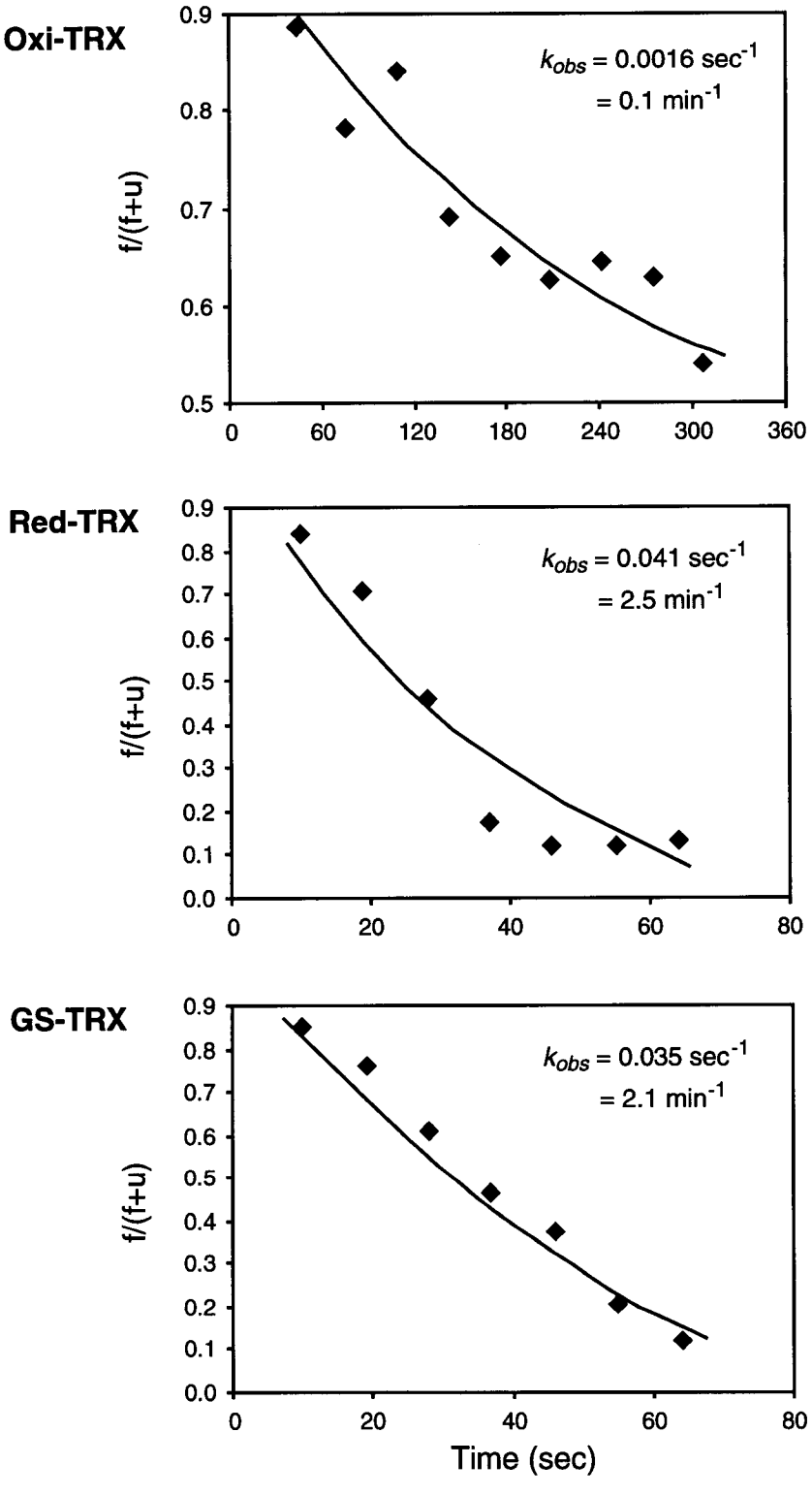

Figure 2.15 (C). Change in the fraction of folded conformers at 60 °C with time. The rate constant k_{obs} was obtained using equation f/(f+u) = Aexp(-k_{obs}t).

The conversion rate constants of TRXs are summarized (**Table 2.1**). Cys-TRX and Red-TRX indicated similar rate constants of conversion at 50 °C, whereas GS-TRX had a much smaller rate constant. As the temperature approached 60 °C, this difference in rate constants became smaller. At higher temperatures, Red-TRX and alkylated adducts showed similar rate constants for unfolding. However, at 50 °C, GS-TRX indicated a more compact structure relative to Red- and Cys-TRX. This result suggests that the attached glutathionyl group in GS-TRX has some interactions with TRX protein body which stabilizes the adducted protein conformation.

Although the conversion rate constant, k_{obs}, has almost the same meaning as the unfolding rate constant, k_1, in eq (5), they are not equivalent because k_{obs} was calculated with only mass peaks A and D (**Figure 2.14**) and the unfolding intermediates were not taken into account. It is assumed that the actual unfolding processes are much more complicated than the two-process H/D exchange model (**Figure 1.3**).

Table 2.1. Conversion rate constants k_{obs} (min^{-1}) of TRXs in 1% acetic acid solution.

T (°C)	Oxi-TRX	Red-TRX	GS-TRX	Cys-TRX
50	- [a]	0.22	0.09	0.21
55	- [a]	1.3	0.48	1.2
60	0.1	2.5	2.1	- [b]
80	2.1 [c]	-	-	-

[a] Separated peaks not detected. [b] Only the higher mass peak from fully unfolded protein was observed. [c] Measured in 2 % acetic acid-d solution.[29]

2.2-2 Offline H/D exchange and ESI-MS experiments

The H/D exchange behavior of TRXs at room temperature was monitored by offline H/D exchange (**Figure 2.16**). In this method, the protein stock solutions were equilibrated in 1 % acetic acid solution (pH 2.6, 25 °C) and diluted 50-fold with 1 % acetic acid-d/D_2O (25 °C). At the moment of dilution, the timer was started to measure the length of time for H/D exchange. At appropriate time intervals, small aliquots of solution were taken from the diluted solution and injected into the sample loop for mass measurement. A time-dependent mass profile was obtained by plotting the percentage of deuterium incorporation versus H/D exchange time (**Figure 2.17 and Table 3.7 ~ 3.10**). The side chain deuteriums were not back exchanged because D_2O based delivery solvents were used. The percentage of deuterium incorporation was calculated using eq (7). Molecular weights of deuterated proteins were calculated by deconvolution with multiply-charged ions from 7+ to 9+ because they showed strong peak intensities.

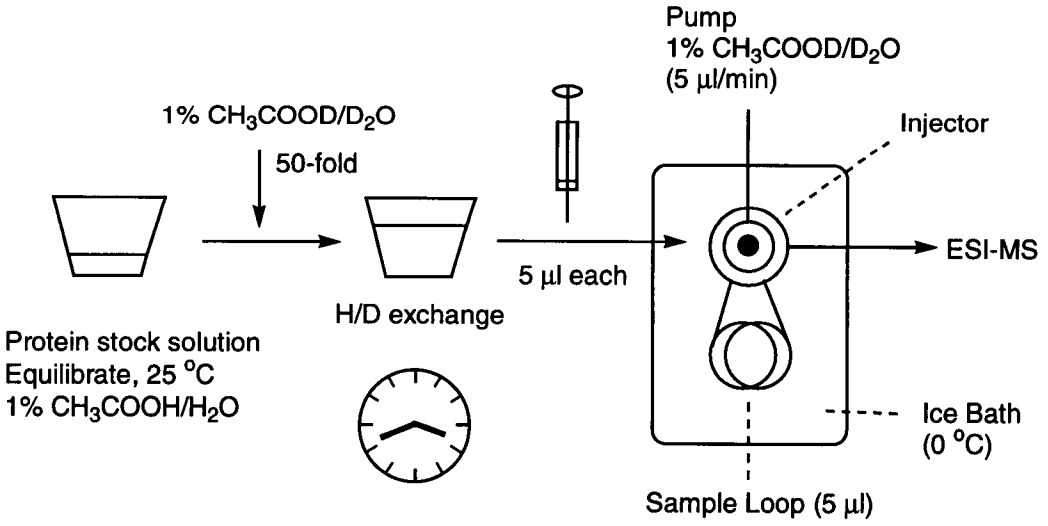

Figure 2.16. Experimental setup for offline H/D exchange-in.

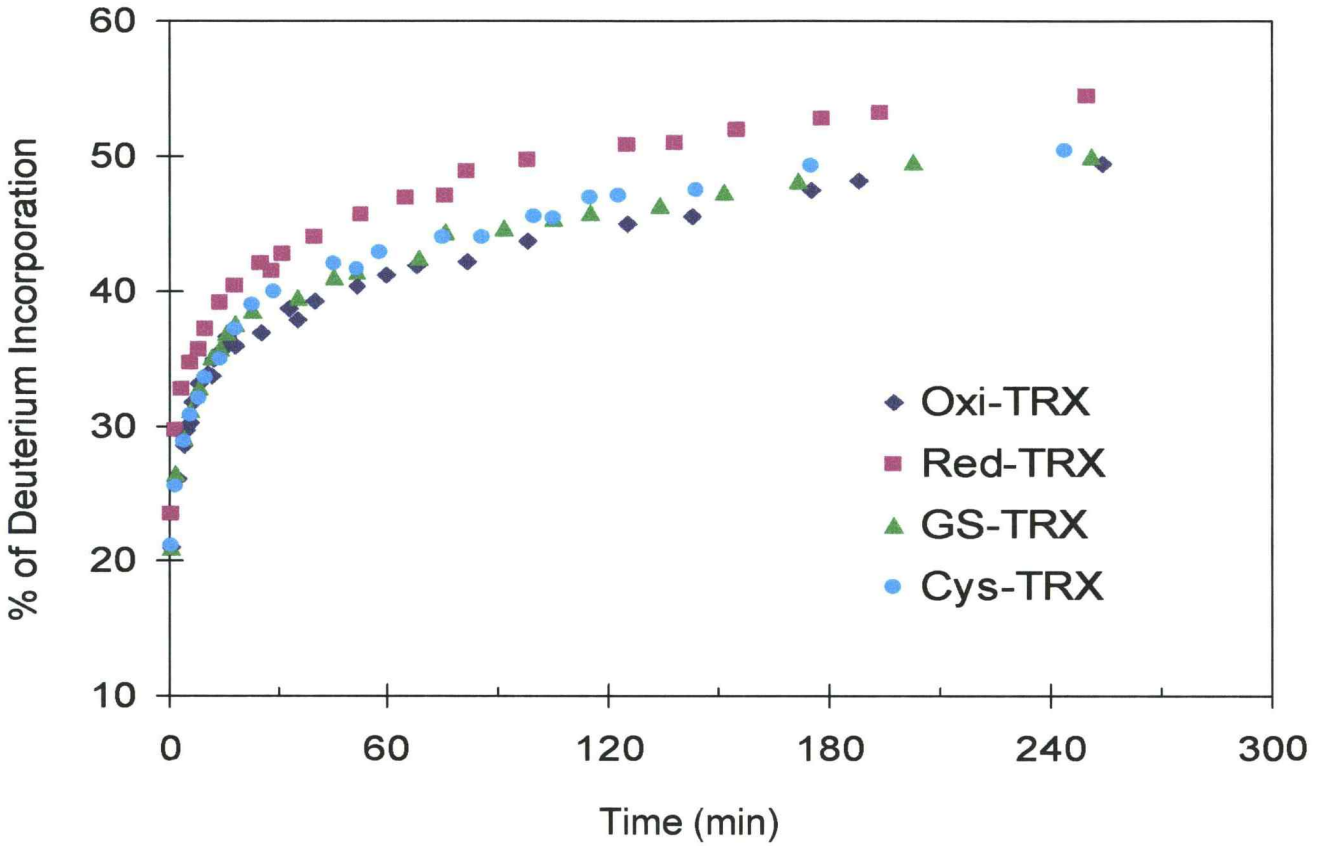

Figure 2.17. H/D exchange time courses for TRXs in 1% AcOD/D_2O at 22 °C

$$\frac{\text{Deuterated M.W. (exp.) - Undeuterated M.W. (cal.)}}{\text{The number of exchangeable hydrogens}} \times 100 = \% \text{ of D incorporation} \quad (7)$$

The extent of H/D exchange of Red-TRX compared to Oxi-TRX indicated approximately 7% increase in deuterium (D) incorporation. GS- and Cys-TRX showed almost the same exchange profile with Oxi-TRX. The alkylated TRXs showed a slight increase in protection against H/D exchange in comparison with Red-TRX. There was no clear difference in D incorporation between GS- and Cys-TRX. These results suggest that the reduction of a disulfide linkage exposes some protected amide hydrogens to the solvent. It is expected that conformational changes take place, and that in addition the alkylated portions in GS- and Cys-TRX prevent H/D exchange of some unprotected hydrogens in Red-TRX. These might be protected through noncovalent interactions such as H-bonding and shielding. In order to localize the regions of TRX where exchange was prevented by alkylation, the peptic digests were analyzed by LC-ESI-MS and LC-ESI-MS/MS (chapter **2.3-2 and 2.3-3**).

2.2-3 Analyses of bimodal charge state distributions

The charge state distributions of TRXs were monitored as a function of temperature. The distribution of the charge states significantly changed as the solution temperature was increased to 50 °C or above (**Figure 2.18**). The experimental setup was the same as that used for online H/D exchange (**Figure 2.9**). The only difference was that all solvents for delivery and protein dilution were normal H_2O based solvents. Mass analyses of the injected protein samples in the sample loop were preceded by at least 2 minutes incubation periods to

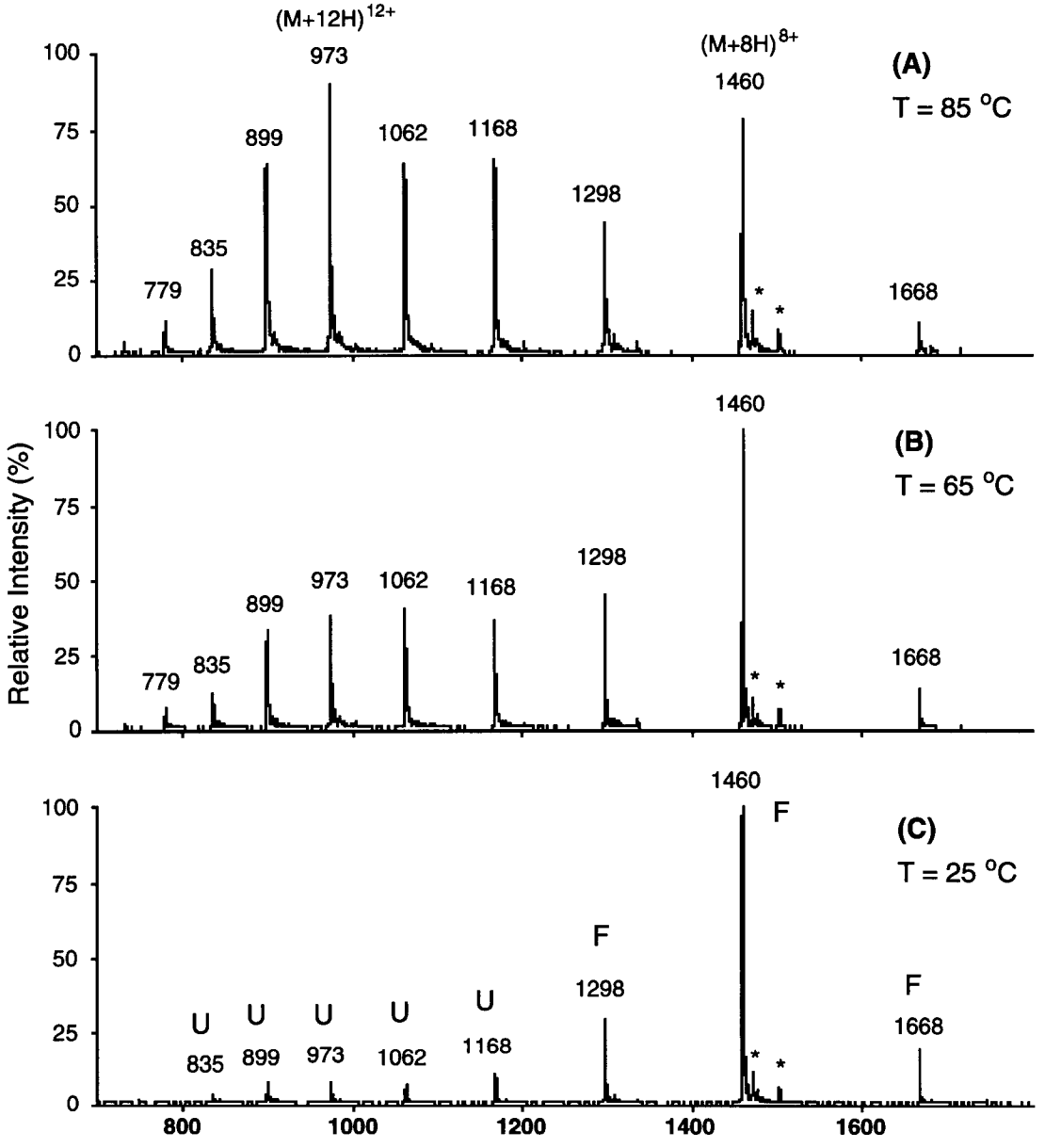

Figure 2.18. ESI mass spectra of Oxi-TRX in 1% acetic acid at different temperatures: (A) 85 °C, (B) 65 °C, and (C) 25 °C. Ion peaks at *m/z* 1668, 1460, and 1298 representing charge states 7+, 8+, and 9+, respectively, were attributed to the folded form, F. Ion peaks at *m/z* 1168, 1062, 973, 899, 835, and 779 representing charge states 10+ to 15+ were attributed to the unfolded form, U. A minor unidentified impurity is marked with an asterisk.

establish equilibrium. The changes in charge state distributions are evident in the denaturation transition curves plotted as a function of temperature and F/(F+U) (**Figure 2.19** and **Table 3.11**). The intensity of the folded conformer is designated F, which is the summation of the peak intensities from 7+ to 9+ charge states. The unfolded conformer, U, is represented by the summation of 10+ to 16+ charge state peak intensities.

As the temperature is gradually increased toward conditions that favor unfolding, the folded conformation initially changes very little, if at all. There may be increases in flexibility and localized conformational alterations, but the average structure is unchanged. This stable phase was observed as gradually decreasing absorption intensities by near UV-CD experiments (**Figure 2.22** and **2.23**). The protein then unfolds completely within a narrow range of temperature, of about 10 °C. The abruptness of the unfolding transition is indicative of a very cooperative transition for thermal unfolding.

At room temperature, Oxi-TRX is the most compact conformer, and Red-TRX has the least compact structure. The difference in F/(F+U) between Red- and Oxi-TRX is more than 0.2. This result is comparable to those from an NMR study, in which Red- and Oxi-TRX were found to have very similar rates of H/D exchange, and thus were assumed to have similar structural or backbone dynamics.[47] Significant differences were observed only in the active site sequence and regions close to the active site. GS-TRX has an intermediate fluffiness, while Cys-TRX and Red-TRX showed almost the same F/(F+U). The difference in melting temperature (T_m) between Oxi- and Red-TRX is about 15 °C, which is in close agreement with previously reported data from NMR and CD studies.[45] Cys-TRX showed almost the same T_m as that of Red-TRX, while GS-TRX showed a little higher T_m value relative to Cys-TRX. These results also

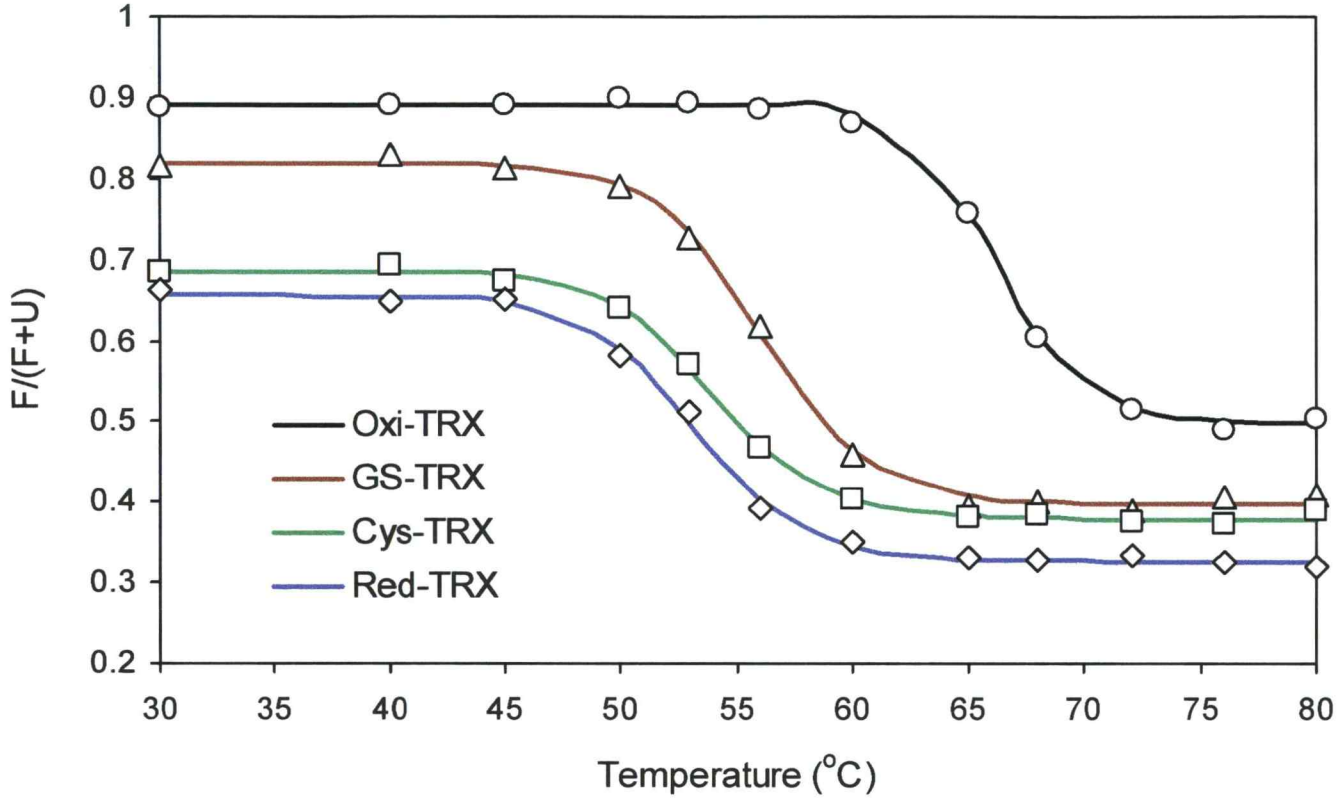

Figure 2.19. Denaturation curves of TRXs in 1% acetic acid.

reflect that the glutathionyl group on GS-TRX has some stabilizing effects on the conformation of the protein whereas the cysteinyl group does not.

2.2-4 Spectroscopic experiments : UV absorption and circular dichroism

The ultraviolet (UV) absorption spectra of TRXs in 1% acetic acid solution were obtained (**Figure 2.20**). The reduction of the disulfide bond in the protein causes small but significant changes in the absorption spectrum. In the range between 230 nm and 300 nm, the effects of aromatic amino acids - Phe, Tyr, and Trp - contribute to the absorbance. The most intense band is due to tryptophan (W) at around 280 nm. The small changes in absorbance means that there is a change in the chemical environments of the two tryptophans - W28 and W31- near the active site. The conformational changes due to reduction and alkylation may cause the alteration of environments of two tryptophans because they are very close to the active site.

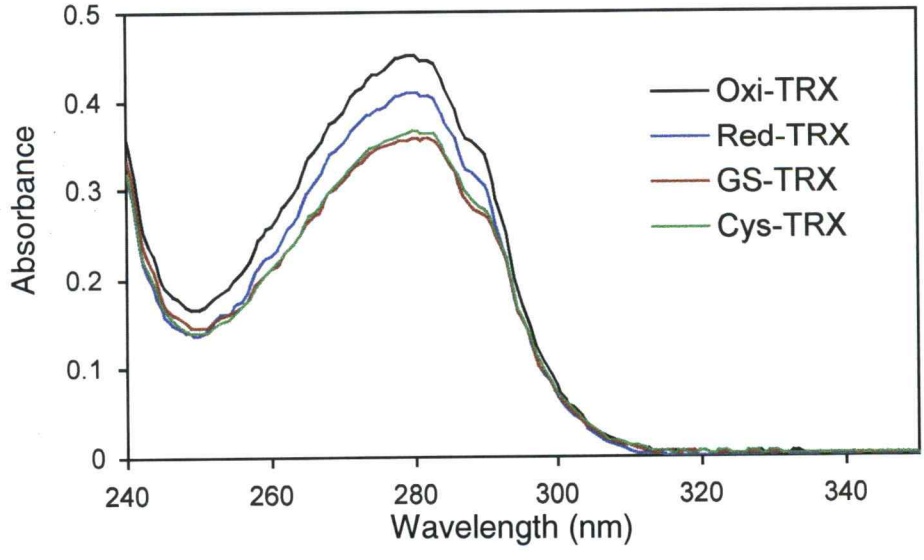

Figure 2.20. UV spectra of TRXs (34 μM in 1% AcOH).

The aromatic region of the CD spectra of TRXs were measured in the near-UV range (250-360 nm) (**Figure 2.21**). The reduction of the disulfide bond and alkylations bring about significant changes in the near UV-CD spectrum, which suggests at least some of the aromatic residues acquire a different environment and/or conformation. These changes seem to take place without the involvement of the backbone. There are significant differences between Red-TRX and modified TRXs, while no difference seems to exist between GS- and Cys-TRX, which is similar to the pattern observed in the UV spectra.

CD spectra are widely used for detecting and measuring the various conformational components of proteins in solution.[48] The temperature-dependent unfolding transition determined by analysis of the charge state distributions in the ESI mass spectra coincided with the unfolding transition observed in the near-UV CD that reflected the collapse of the tertiary structure (**Figure 2.22**). The change of intensities at 280 nm are shown (**Figure 2.23** and **Table 3.12**). The unfolding transitions, i.e. the melting temperatures (T_m), indicate similar results in comparison with the graph (**Figure 2.19**) from the analyses of the charge state distribution in the mass spectra.

Far UV-CD spectra of TRXs at 25 °C and pH 2.5 were measured (**Figure 2.24**). All proteins show the broad minimum at around 220 nm, the cross-over points between 205 and 207 nm, and the positive maxima around 197 nm. The secondary structural elements were calculated from these spectra and a basis set of 20 proteins by singular value decomposition.[48] The calculated secondary structural elements of TRXs (**Table 2.2**) shows significant changes in α-helix and β-sheet by the reduction of the disulfide bond in Oxi-TRX, which suggests that the reduction changed the position of the backbone, which is not in agreement with results from NMR experiments.

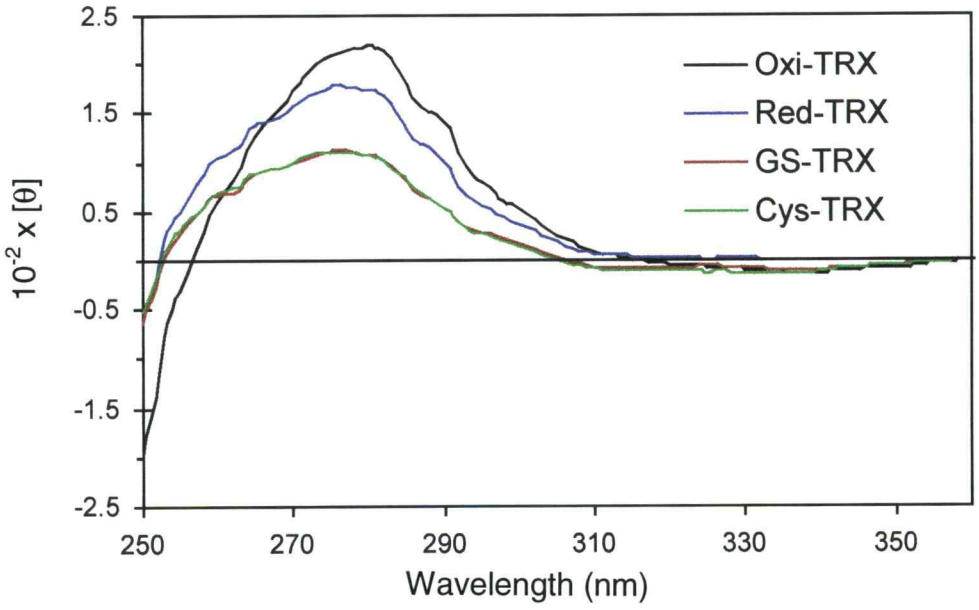

Figure 2.21. Near UV CD spectra of TRXs (34 μM in 1% AcOH, pathlength 1 cm)

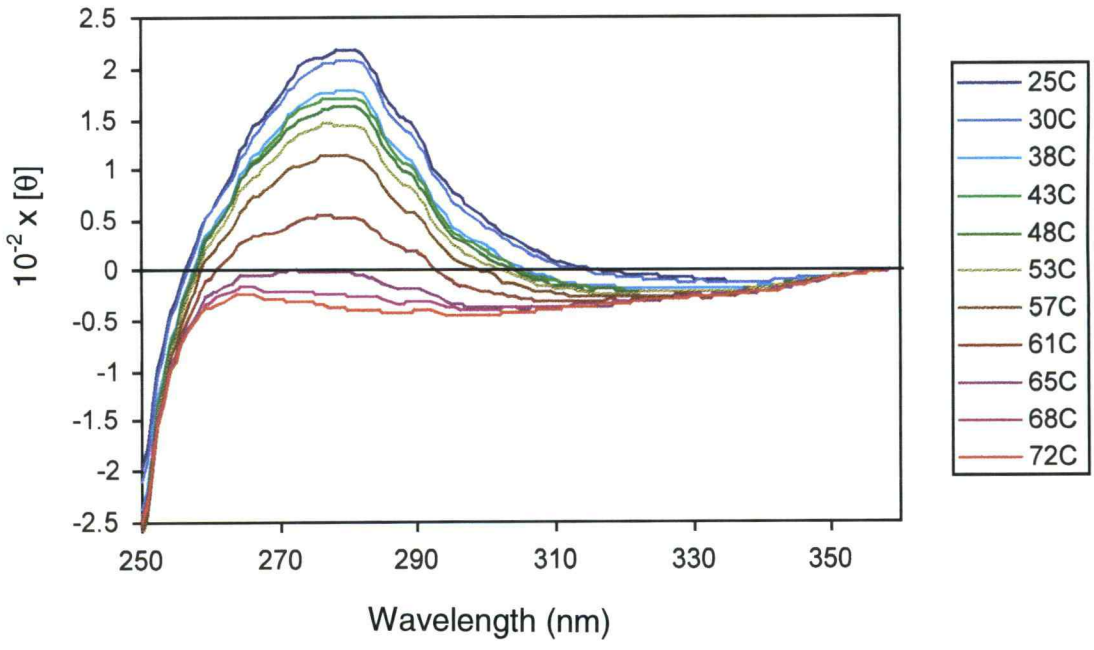

Figure 2.22. Near UV CD spectra of thermal denaturation of Oxi-TRX (34 μM in 1% AcOH, pathlength 1 cm)

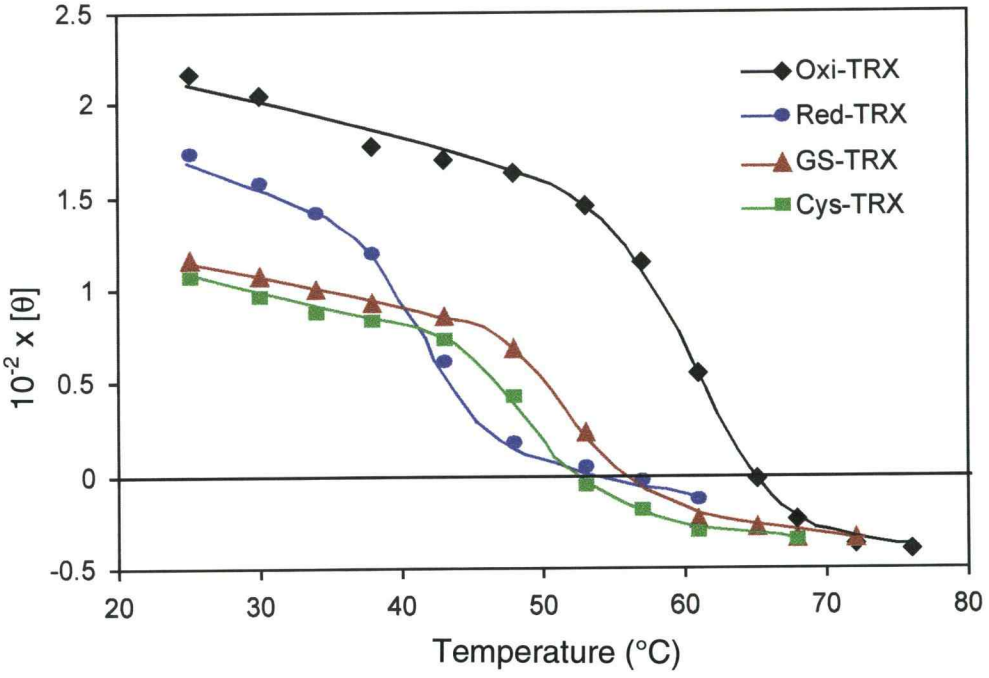

Figure 2.23. Denaturation curves from the analyses of near UV CD spectra. Each data point is from the intensity measured at 280 nm

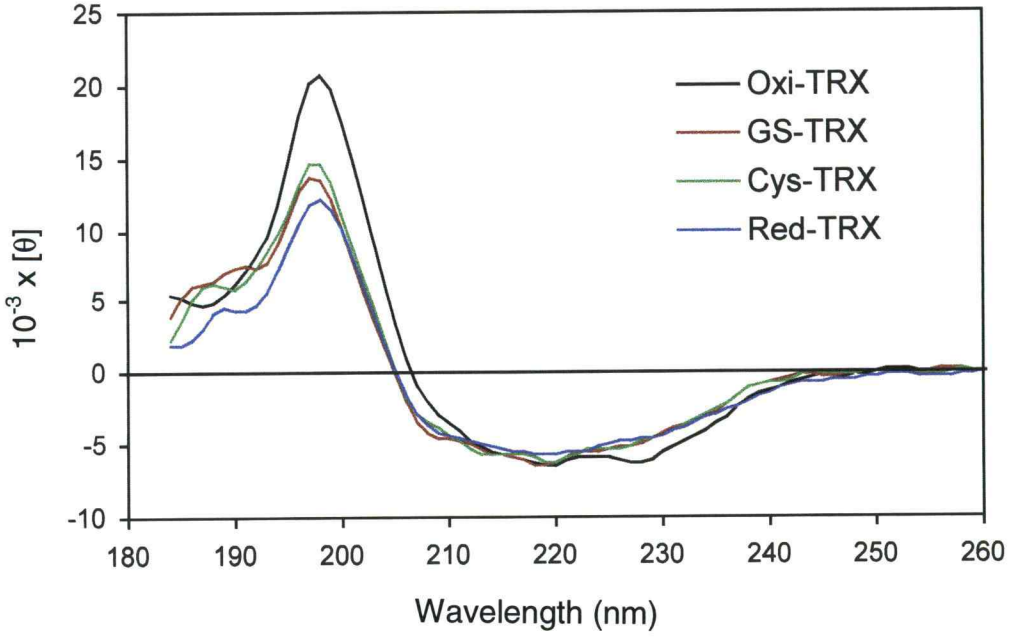

Figure 2.24. Far UV CD spectra of TRXs (10 mM TRIS.HCl, pH 2.5, path length 0.01 cm)

Table 2.2. Estimation of secondary structural elements of TRXs based on far UV CD spectra and singular value decomposition.[48]

	α-Helix	3_{10}Helix	β-sheet	β-Turn	PolyPro	Others
Oxi-TRX	.34	.07	.13	.10	.13	.23
Red-TRX	.17	.04	.28	.10	.08	.35
GS-TRX	.19	.03	.25	.10	.10	.33
Cys-TRX	.19	.02	.26	.09	.09	.35

The CD spectra for many proteins can be predicted successfully using this calculation. However, some protein CD spectra are not analyzed successfully due to insufficient basis sets or equations to solve for all of the unknowns that contribute to the CD. At least, this calculation showed the changing in CD spectra with the reduction of the disulfide linkage and alkylation.

2.3 Structural features of TRXs analyzed by H/D exchange

The protein fragmentation/MS method was used to locate sites of amide hydrogen exchange on *E. coli* TRX and its alkylated adducts. H/D exchange experiments were preceded by the identification of peptic peptides because pepsin cleaves proteins unpredictably. For fragment-specific H/D exchange information, TRXs were equilibrated in 1% acetic acid (pH 2.6) because the results are then comparable with global H/D exchange obtained under the same conditions (**section 2.2**). For site-specific H/D exchange experiments, TRXs were equilibrated in 10 mM phosphate buffer (pH 5.7) when the results were to be compared with NMR rate constant data. Previous spectroscopic data showed that the influence of pH on the near-UV CD spectrum of Oxi-TRX between pH 3.0 and 6.5 was small.[49] It suggested that local conformational changes, observed through the aromatic side chains, take place without affecting the backbone structure. NMR data also indicated that the influence of pH was negligible in both Oxi- and Red-TRX in the pH range from 2.5 to 12.[45] It is assumed that the conformational differences of TRXs at two different pHs, 2.6 and 5.7, are negligible.

2.3-1 Peptide mapping and sequencing of thioredoxins (TRXs)

Proteolytic digestion of TRXs with pepsin at a weight ratio of enzyme to substrate E/S = 1/2 under slow H/D exchange conditions (1% acetic acid, pH 2.6, 0 °C, 5 min) were successful except in the case of Oxi-TRX. This protein form was poorly digested (**Figure 2.25**), which supports the notion that it has the most compact 3-D structure. However, with just a small amount of proteolytic fragmentation, peptide mapping of Oxi-TRX digest was possible. The peptic

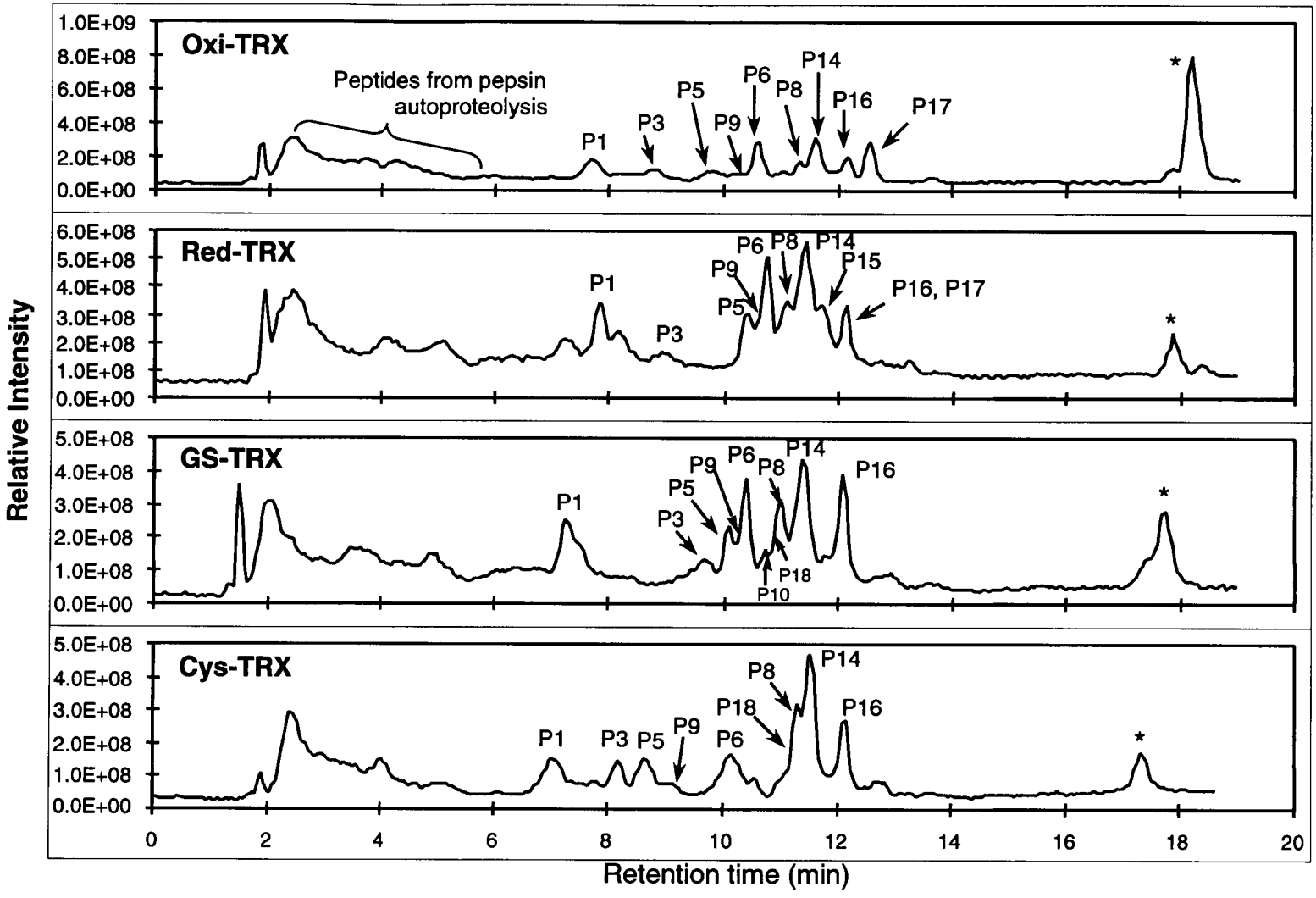

Figure 2.25. Total ion chromatograms of peptides produced from peptic digestion of TRXs. Asterisks represent undigested proteins. Peaks from 2 min to 5 min retention time resulted from autoproteolysis of pepsin. Peptide numbers are assigned according to **Figure 2.28**.

peptides of TRXs were observed between 7 and 13 min retention time. The fragments from pepsin autoproteolysis were easily recognized through the blank test. The retention time of these fragments was 2-5 min.

Digestion was quenched simply by injecting the peptic digest onto an LC column. Peptic peptides were separated and identified by on-line HPLC-MS (**Figure 2.26**). Because peptide mapping and sequencing are necessary and preliminary experiments for H/D exchange, digestion and separation were adjusted for slow H/D exchange conditions. The entire system from the injection valve to the column outlet just before the mass spectrometer were immersed in an ice-bath.

Since pepsin cleaves proteins rather unpredictably, peptide masses alone are insufficient for the unambiguous determination of their identification. Therefore, all peptides were identified with a combination of molecular weight information and MS/MS data. An example of this ambiguity, and its resolution, is demonstrated for mass peak, *m/z* 1145.1, from the digest of Oxi-TRX (**Figure 2.27**). Seven possible peptides from the sequence of Oxi-TRX could correspond to the mass *m/z* 1145.1 ± 1 with charges of 1+ or 2+ (**Figure 2.27 (A)**). The MS/MS spectrum of the mass peak, *m/z* 1145.1, was identified as corresponding to fragment 80-101 (**Figure 2.27(B)**). Seventeen peptides identified through this procedure for each TRX (**Figure 2.28**) represented about 94% of the total protein sequence. All these fragments were confirmed by tandem mass spectrometry (**Table 3.13**). In the active site region, pepsin showed different patterns of digestion for the alkylated TRXs. In the native TRXs, Oxi- and Red-TRX, segments 28-39 were obtained, whereas only segments 28-37 were found for the alkylated TRXs. It was assumed that the peptic cleavage site was changed by alkylation of the protein.

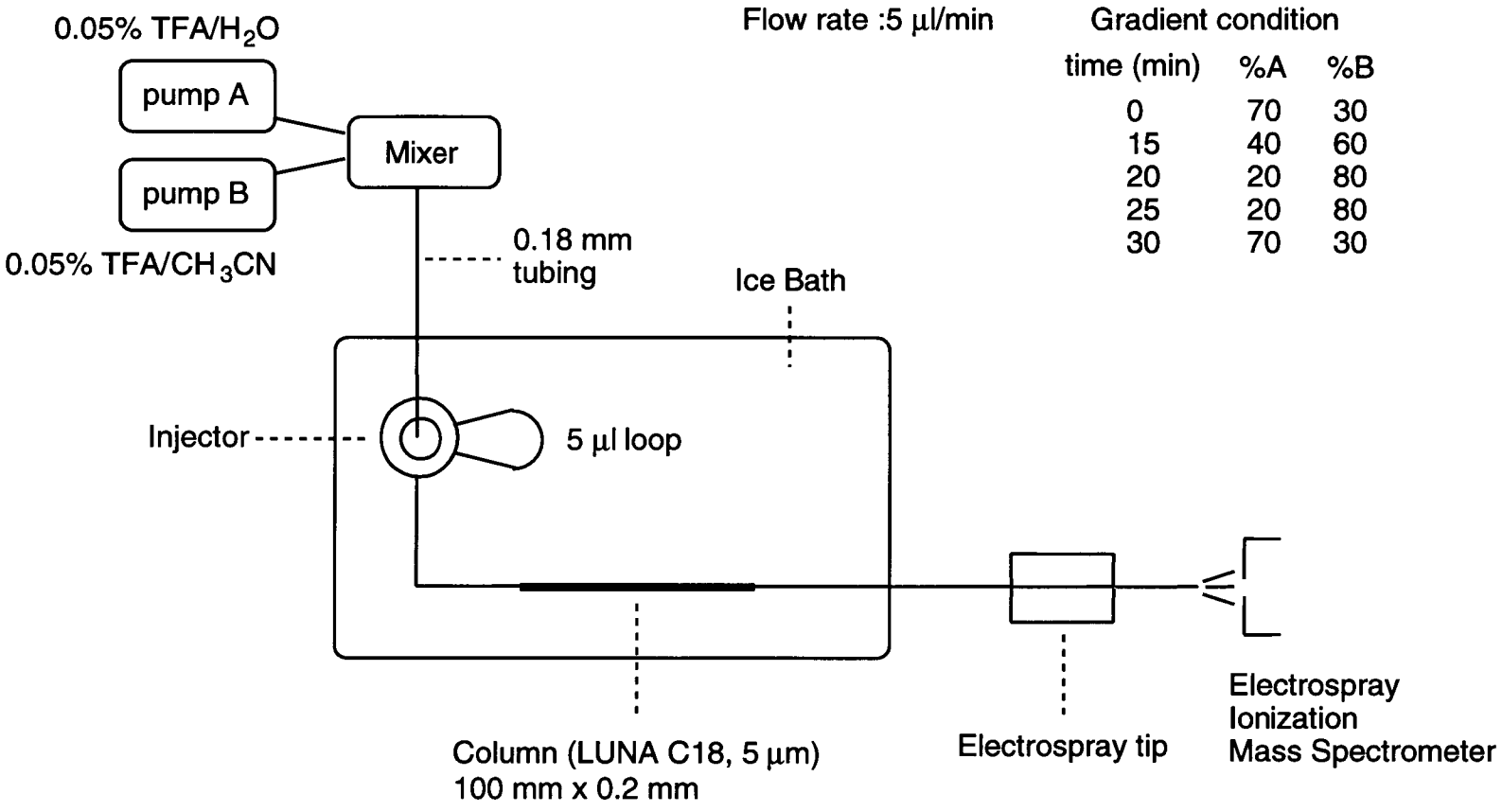

Figure 2.26. Instrumentation (HPLC-MS) for peptide mapping and sequencing of pepsin digest of TRXs.

A

M. W.	Residues	Charge	Sequence
2287.73	66 - 86	2	G <TAPKYIGRGIPTLLLFKNGEV> A
1143.62	82 - 93	1	F <KNGEVAATKVGA> L
2288.68	82 - 103	2	F <KNGEVAATKVGALSKGQLKEFL> D
2288.68	**80 - 101**	2	L <**LFKNGEVAATKVGALSKGQLKE**> F
1144.59	62 - 72	1	D <QNPGTAPKYIG> R
2287.56	3 - 23	2	D <KIIHLTDDSFDTDLVKADGAI> L
2287.55	45 - 65	2	E <IADEYQGKLTVAKLNIDQNPG> T

B

Residues 80-101
L-F-K-N-G-E-V-A-A-T-K-V-G-A-L-S-K-G-Q-L-K-E

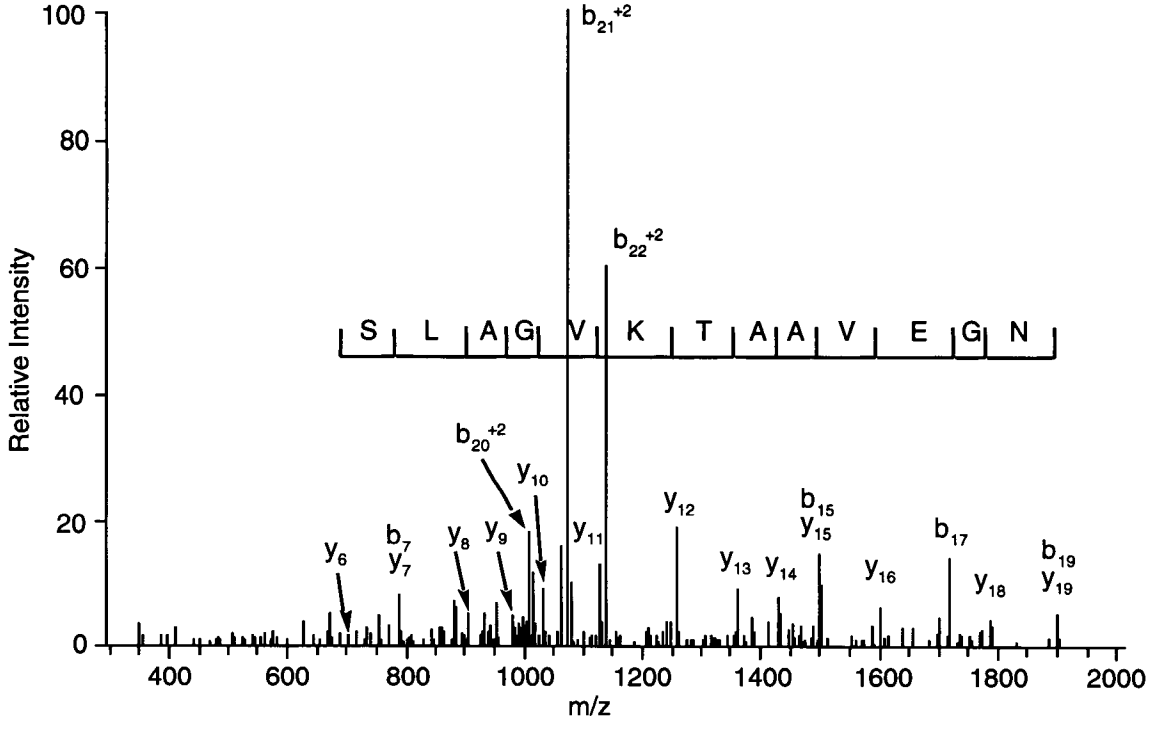

Figure 2.27. Peptic peptide identification. A: A list of possible peptides with *m/z* 1145.1 and charges of 1+ to 2+. B: MS/MS spectrum of *m/z* 1145.1 peak representing residues 80-101 of TRX.

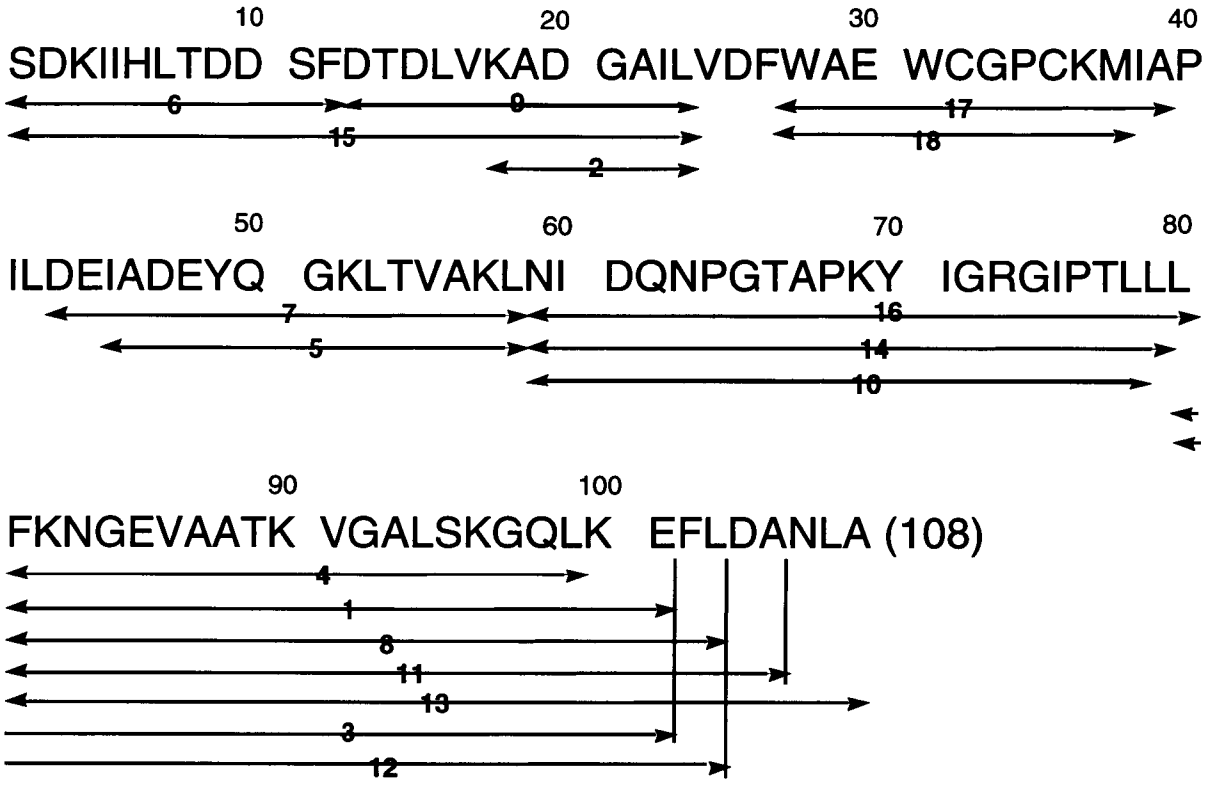

Residues : *m/z* (charge state)

P1: 81-101 : 1088.6 (+2)
P2: 18-24 : 687.6 (+1)
P3: 80-101 : 1145.0 (+2)
P4: 81-99 : 959.9 (+2)
P5: 45-58 : 1548.8 (+1)
P6: 1-12 : 1390.8 (+1)
P7: 43-58 : 897.3 (+2)
P8: 81-103 : 1218.7 (+2)
P9: 13-24 : 1230.6 (+1)
P10: 59-78 : 1063.4 (+2)
P11: 81-105 : 1311.6 (+2)
P12: 80-103 : 1275.1 (+2)
P13: 81-108 : 1460.7 (+2)
P14: 59-79 : 1120.0 (+2)
P15: 1-24 : 1302.1 (+2)
P16: 59-80 : 1176.6 (+2)
P17: 28-39 : 1392.7 (+1) Oxi-TRX
1394.7 (+1) Red-TRX
P18: 28-37: 772.4(+2) GS-TRX
679.4(+2) Cys-TRX

Figure2.28. Peptides identified in the pepic digests of TRXs by tandem mass spectrometry

2.3-2 H/D exchange of TRXs, proteolysis, and the determination of deuterium content in peptide segments

The general procedure used in the protein fragmentation/MS approach for determining amide hydrogen exchange content in intact proteins is based on a protein fragmentation method described previously (**Figure 2.29**).[12] Following the deuterium exchange-in step, isotopic exchange at peptide amide linkages is usually quenched by reducing the pH and temperature. The extent of back-exchange was minimized by performing the digestion and HPLC separation at 0 °C and pH 2-3.[50] In this experiment, simply decreasing temperature to 0°C was sufficient because the pH was already at 2.6. Isotopic exchange in unfolded polypeptides is slowest at pH 2-3 (**Figure 1.1**). For this quench condition, the half-life for isotopic exchange of peptide amide linkages is 30-120 min.[13b, 12b]

The same microbore HPLC-MS system that was used for peptide mapping was used for separation and mass analysis of the H/D-exchanged TRX samples (**Figure 2.26**) although the gradient conditions for the HPLC were slightly changed. All peptic peptides were eluted from the LC column within 10 min retention times in order to minimize deuterium loss. Because the amide deuterium level was determined directly from the molecular weights of the peptides, it was not necessary to isolate the peptides prior to analysis. By optimizing the chromatography for speed rather than resolution, the extent of back-exchange that occurred during analysis was kept low. Results were obtained by incubating proteins in 1% AcOD/D_2O (pD 2.6) at room temperature for different incubation periods. Five-microliter (0.4 nanomole) aliquots of the incubation mixture were removed, adjusted to 0°C to quench hydrogen exchange, and digested with pepsin for 5 min. The proteolytic digests were analyzed by HPLC-ESIMS to determine the deuterium content of the peptides.

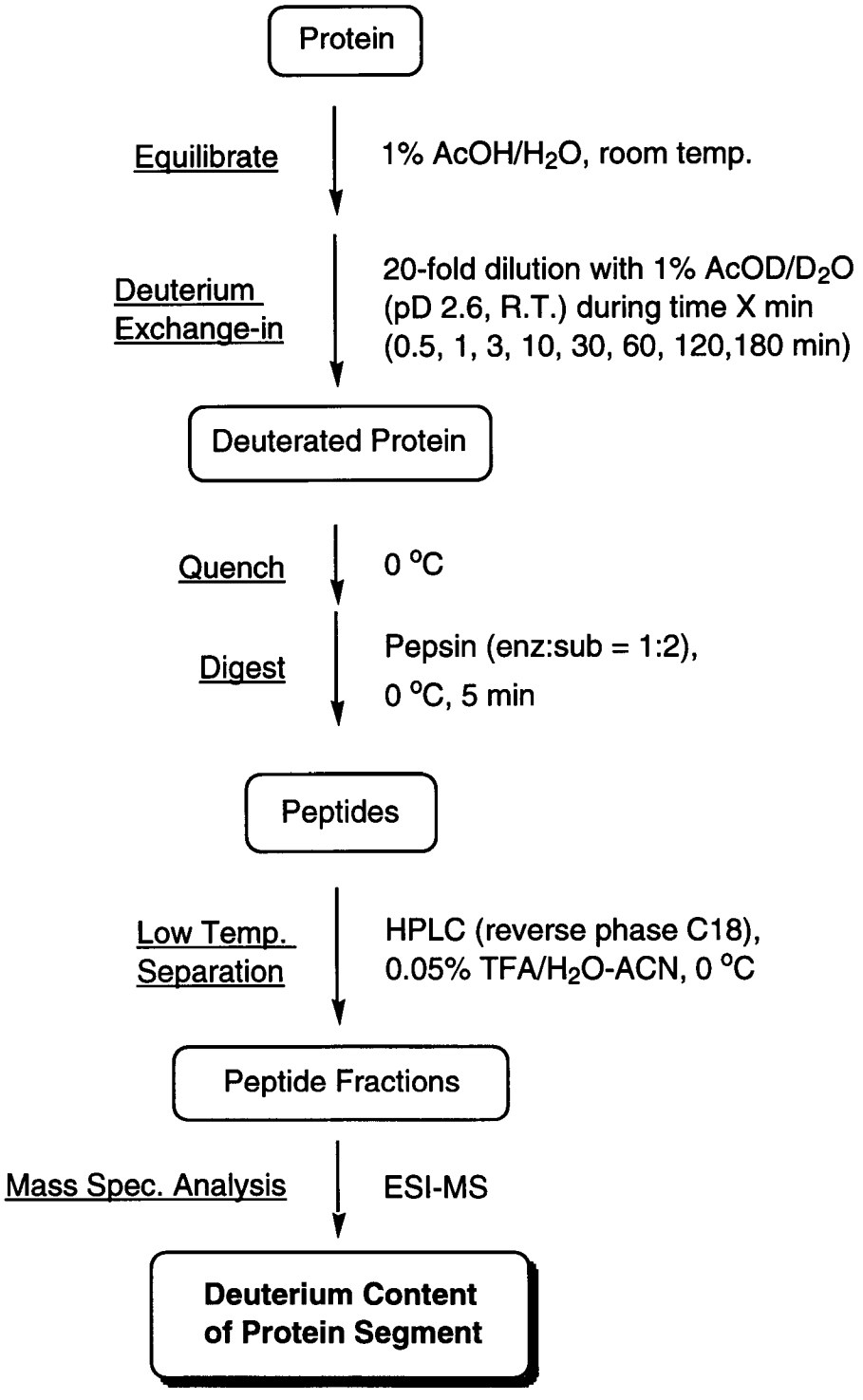

Figure 2.29. Diagram of the general procedure used to determine the deuterium content of the peptic peptides in H/D exchanged TRXs.

Amide and side chain hydrogens in peptides underwent isotopic exchange with the solvent during digestion and fractionation by HPLC. Even under slow H/D exchange conditions (0°C and pH 2-3), deuteriums located on side chains and on the N- and C-termini of the peptides are completely back-exchanged to protons during HPLC separation because the exchange rates of these hydrogens are several orders of magnitude faster than the exchange rates of peptide amide hydrogens. As a result, the increase in the molecular weights of peptides analyzed by this procedure is a direct measure of the number of peptide amide deuteriums present in the peptide.

ESI mass spectra of two peptic fragments, which include residues 28-39 and 59-80, will be used to illustrate two very different types of hydrogen exchange behavior found when Oxi-TRX was labeled continously for 0.5, 10, and 30 min (**Figure 2.30**). Reference spectra of the same peptides taken from Oxi-TRX that contained no deuterium (0% ref) and Oxi-TRX that was completely exchanged in D_2O (100% ref) are presented in the top and bottom panels. These reference spectra were used to determine the extent of deuterium loss during digestion and HPLC separation. In addition, the 0% ref and 100% ref spectra served as references for totally folded and unfolded states of proteins.

Doubly charged ion peaks of fragment 28-39 showed gradually increasing one envelope mass peaks (**Figure 2.30 (A)**). Each of the molecular ion patterns have contributions from the natural abundance of isotopes (^{13}C, ^{15}N, ^{18}O, etc.) and/or an excess of deuterium. This fragment is structurally homogeneous in all Oxi-TRX molecules during the entire time of incubation. For the region including the fragment 28-39, opening and refolding occurs many times before exchange takes place, i.e. this fragment follows EX2 mechanism ($k_2 << k_{-1}$).

In contrast, triply charged ion peaks of fragment 59-80 displayed a bimodal isotope pattern after a short incubation period in D_2O (**Figure 2.30 (B)**),

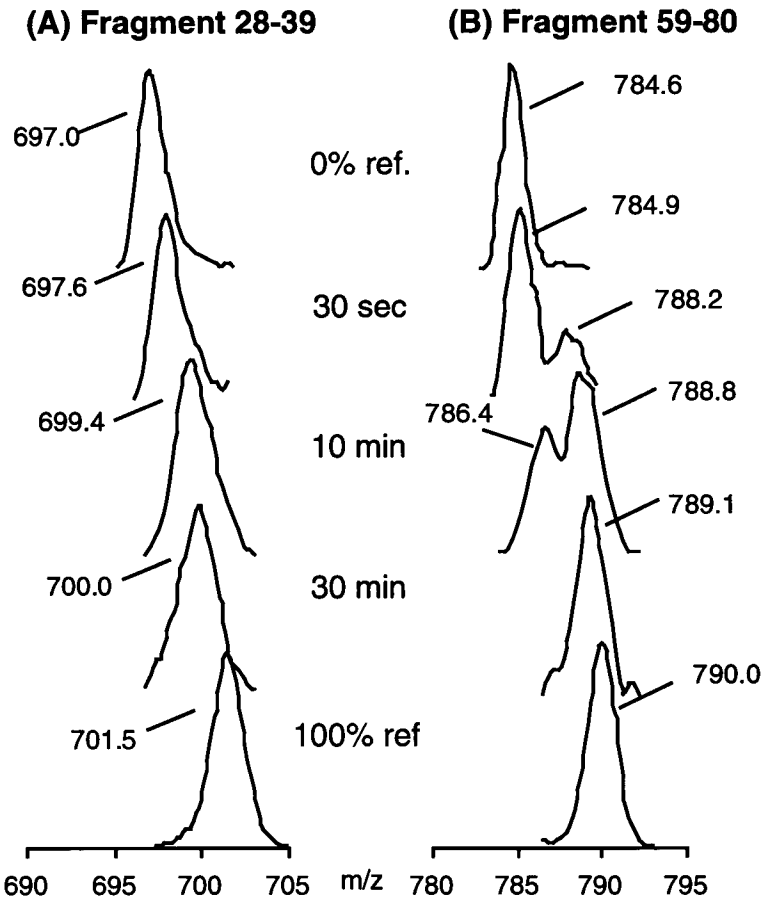

Figure 2.30. ESI mass spectra of the doubly charged molecular ions of fragment 28-39 and the triply charged molecular ions of fragment 59-80 derived from non-deuterated (0% ref), partially deuterated and completely deuterated (100% ref) Oxi-TRX.

suggesting that hydrogen exchange is very slow in this segment of some Oxi-TRX molecules and very fast in other molecules. The increasing higher mass peaks suggest that this segment had spent enough time in the unfolded state before refolding to allow its amide protons to completely exchange with deuteriums, i.e. this fragment follows the EX1 mechanism ($k_2 >> k_{-1}$). The intensity of the low-mass envelope of isotope peaks indicates that the fraction of Oxi-TRX that was folded during the period of incubation, while the intensity of the

high-mass envelope of isotope peaks indicates the fraction of molecules that was unfolded during the incubation period. The observed mass difference between high- and low-mass envelopes, 2.8 ± 0.5 (*m/z*), corresponded to 8.4 ± 1.5 deuteriums. Only fragments 59-80 and 81-101 of Oxi- and Red-TRX showed bimodal isotope peak patterns, i.e. the EX1 mechanism (**Table 2.3**). This result suggests that the region including amino acid residues 59-108 of Oxi- and Red-TRX is more flexible than that same region in alkylated TRXs.

Table 2.3. Summary of EX1(●) and EX2 (O) kinetics of peptic peptides obtained from H/D exchange-in experiments of TRXs in 1% AcOD/D_2O

Fragments	Oxi-TRX	Red-TRX	GS-TRX	Cys-TRX
1-12	O	O	O	O
13-24	O	O	O	O
28-39 or 37	O	O	O	O
45-58	O	O	O	O
59-80	●	●	O	O
81-101	●	●	O	O

The first step for estimating the EX2 mechanism is an accurate determination of the deuterium level for each mass peak under different D_2O incubation times. As mentioned above, some isotopic exchange occurs during both digestion and HPLC analysis. The deuterium content of the peptides may increase or decrease during digestion, depending on the D_2O level in the digest. Since the HPLC mobile phase contains no D_2O, the peptides can only lose

deuterium during HPLC analysis. Measured deuterium levels can be adjusted for artifactual isotopic exchange that occurs during digestion and HPLC fractionation (eq (8)).

$$D = \frac{m - m_{0\%}}{m_{100\%} - m_{0\%}} \times N \qquad (8)$$

In the expression (eq (8)), D is the number of deuteriums present in a particular segment of the protein after incubation in D_2O for time t, and $m_{0\%}$, m, and $m_{100\%}$ are the average molecular masses of a peptide obtained by analysis of nondeuterated, partially deuterated and fully deuterated samples, respectively. N is the total number of peptide amide hydrogens in the peptide.

The deuterium content in the peptide fragment 28-39 of Oxi-TRX was determined from the centroid of a Gaussian-shaped peak that resulted from the isotopic composition of the ion (**Figure 2.30**). The deuterium content of the 28-39 segment in the protein was deduced from the deuterium content of this peptide, after adjusting for deuterium gain/loss during digestion and HPLC separation. To make this adjustment, nondeuterated as well as fully deuterated Oxi-TRX was analyzed by the same procedure. Completely deuterated proteins were obtained by incubating TRXs in 1% AcOD/D_2O at 80 °C for 1h. Having chosen experimental parameters to minimize isotopic exchange at peptide amide linkages during analysis, the peptic peptides of TRXs showed that recoveries of deuterium at peptide amide linkages were in the range 80 - 90%.

Data were processed by centroiding an isotopic distribution corresponding to the +1, +2, or +3 charge state of each peptide. Deuterium levels were plotted versus the exchange-in time and fitted with a series of first-order rate terms according to eq (9) where D is the number of deuterium present, N is the number

of peptide amide linkages in a segment, and the k_i are hydrogen-deuterium exchange rate constants for each peptide linkage. The exchange rate constants, k_i, were varied to obtain the best fit between the experimental data and eq (9).[17]

$$D = N - \sum_{i=1}^{N} \exp^{-k_i t} \tag{9}$$

Deuterium levels for peptic fragments of all TRXs were plotted versus D_2O incubation time (**Figure 2.31~34** and **Table 3.14 ~ 3.17**). Although specific exchange rate constants have not been determined for each amide hydrogen, the range and distribution of rate constants can be estimated by fitting parameters into the first-order rate expression, eq (9), with the experimental results. A quantitative assessment of hydrogen exchange rates was made by fitting data to the following expression, which represents a four-component model, eq (10), modified from eq (9).[12b]

$$y = N - (P_1 \exp^{-P_2 x} + P_3 \exp^{-P_4 x} + P_5 \exp^{-P_6 x} + (N - P_1 - P_3 - P_5)\exp^{-P_7 x}) \tag{10}$$

According to this model, the total number of amide hydrogens, N, is divided into four groups, P_1, P_3, P_5, and (N-P_1-P_3-P_5), with exchange rate constants P_2, P_4, P_6, and P_7, respectively. Values for $P_{1\text{-}7}$ for each peptide of the TRXs are given by fitting deuterium levels to eq (10) (**Table 2.4**). Four different exchange rate constants, P_2, P_4, P_6, and P_7, represent four categories of rate constants, very fast, fast, slow, and very slow, grouped according to their exchange rates. For the exchange times used in this study, 30 s to 3 h, only those rate constants in the range 0.003 – 3 min^{-1} could be determined.

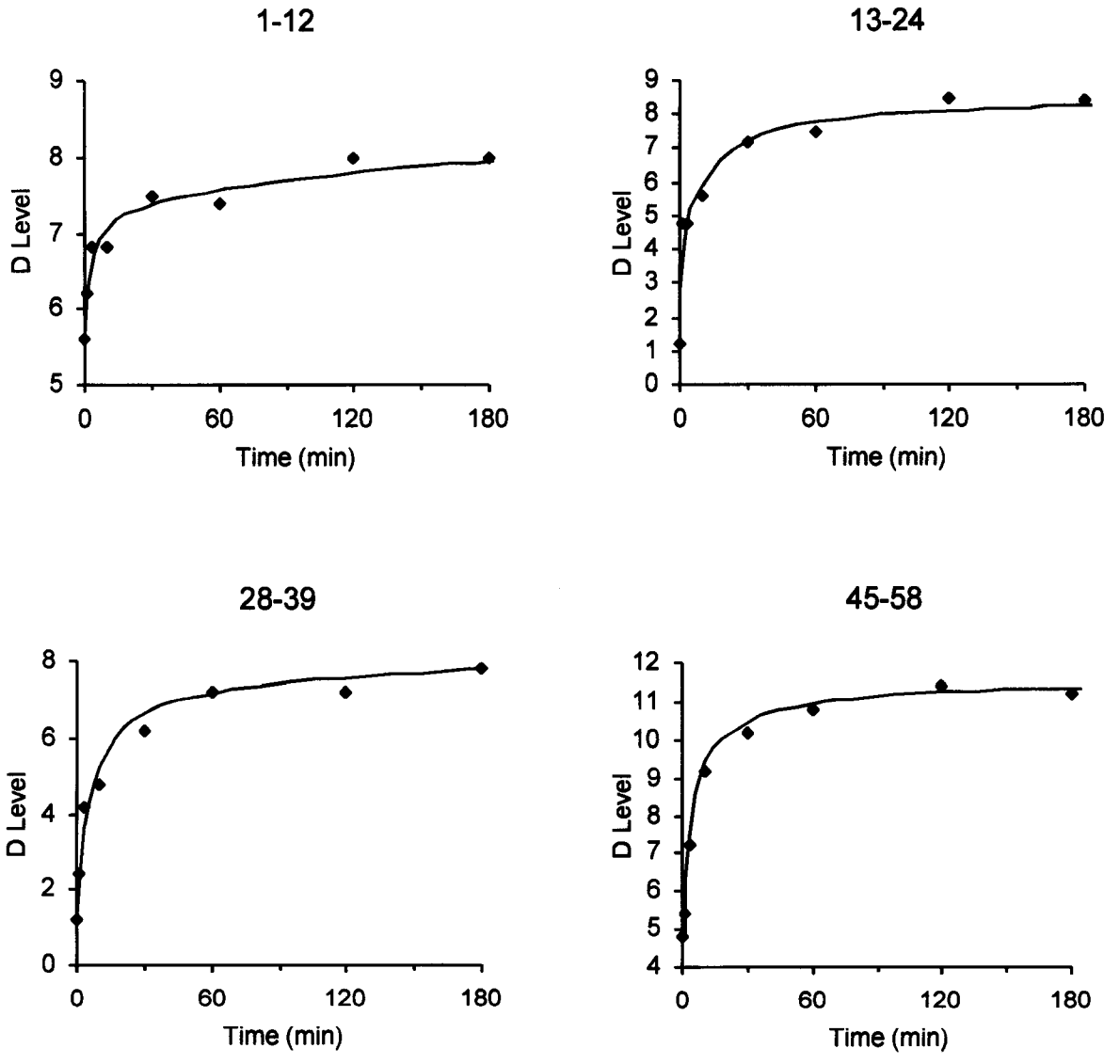

Figure 2.31. Deuterium levels found in segments 1-12, 13-24, 28-39, and 45-58 of Oxi-TRX with different incubation times in 1% AcOD/D_2O. The solid lines were drawn by fitting the experimental data to parameters in eq (10).

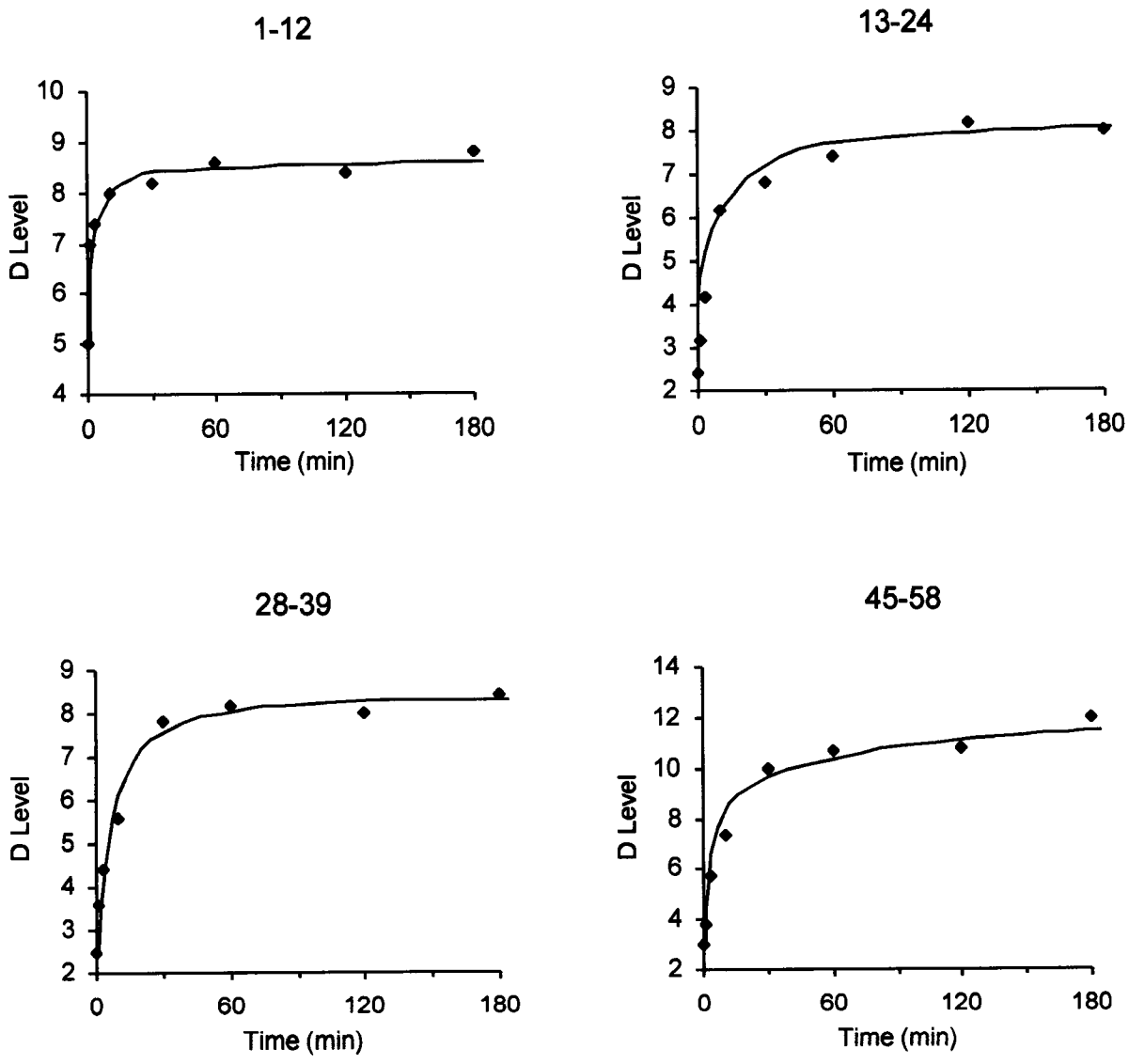

Figure 2.32. Deuterium levels found in segments 1-12, 13-24, 28-39, and 45-58 of Red-TRX with different incubation times in 1% AcOD/D_2O. The solid lines were drawn by fitting the experimental data to parameters in eq (10).

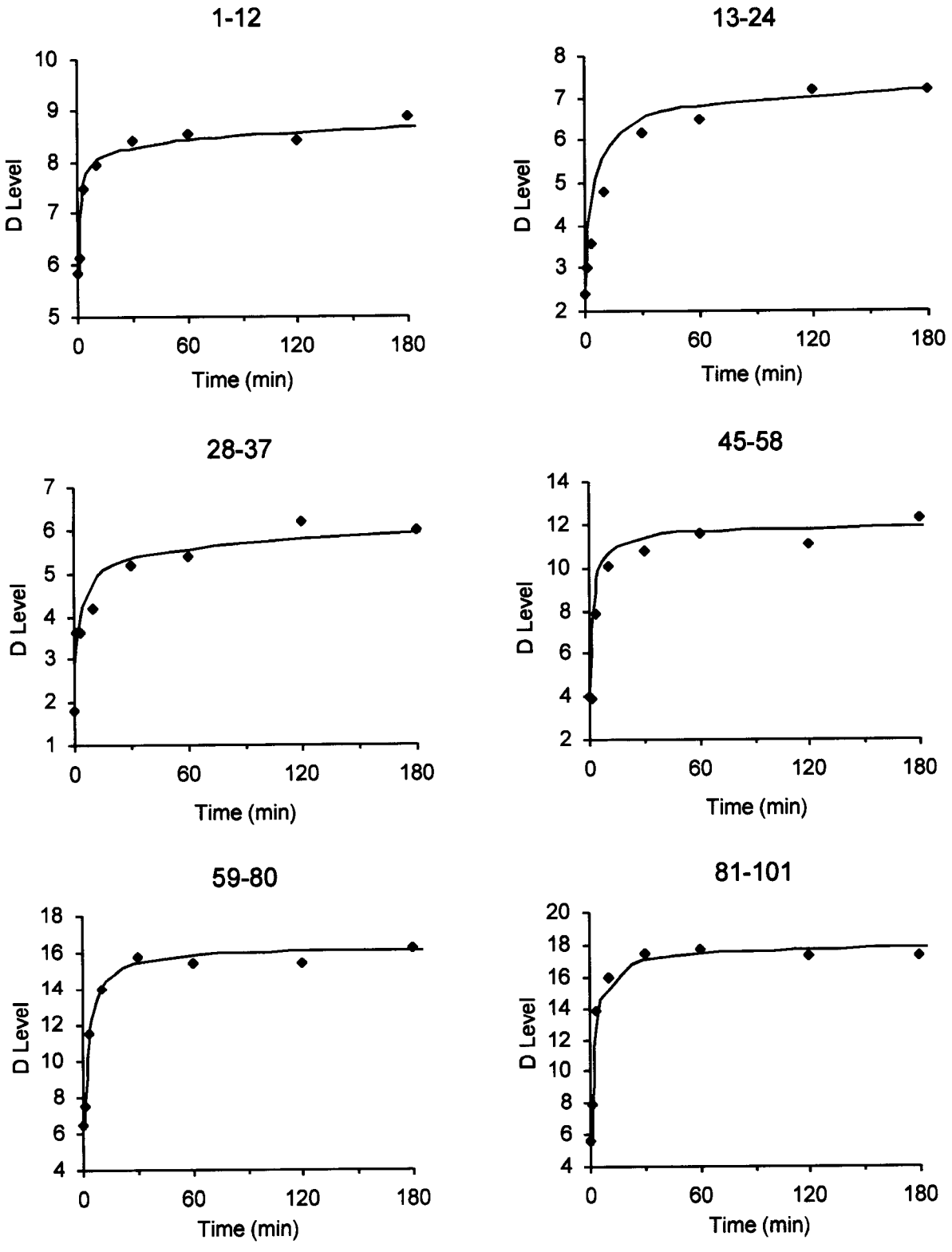

Figure 2.33. Deuterium levels found in segments 1-12, 13-24, 28-37, 45-58, 59-80, and 81-101 of GS-TRX with different incubation times in 1% AcOD/D_2O. The solid lines were drawn by fitting the experimental data to parameters in eq (10).

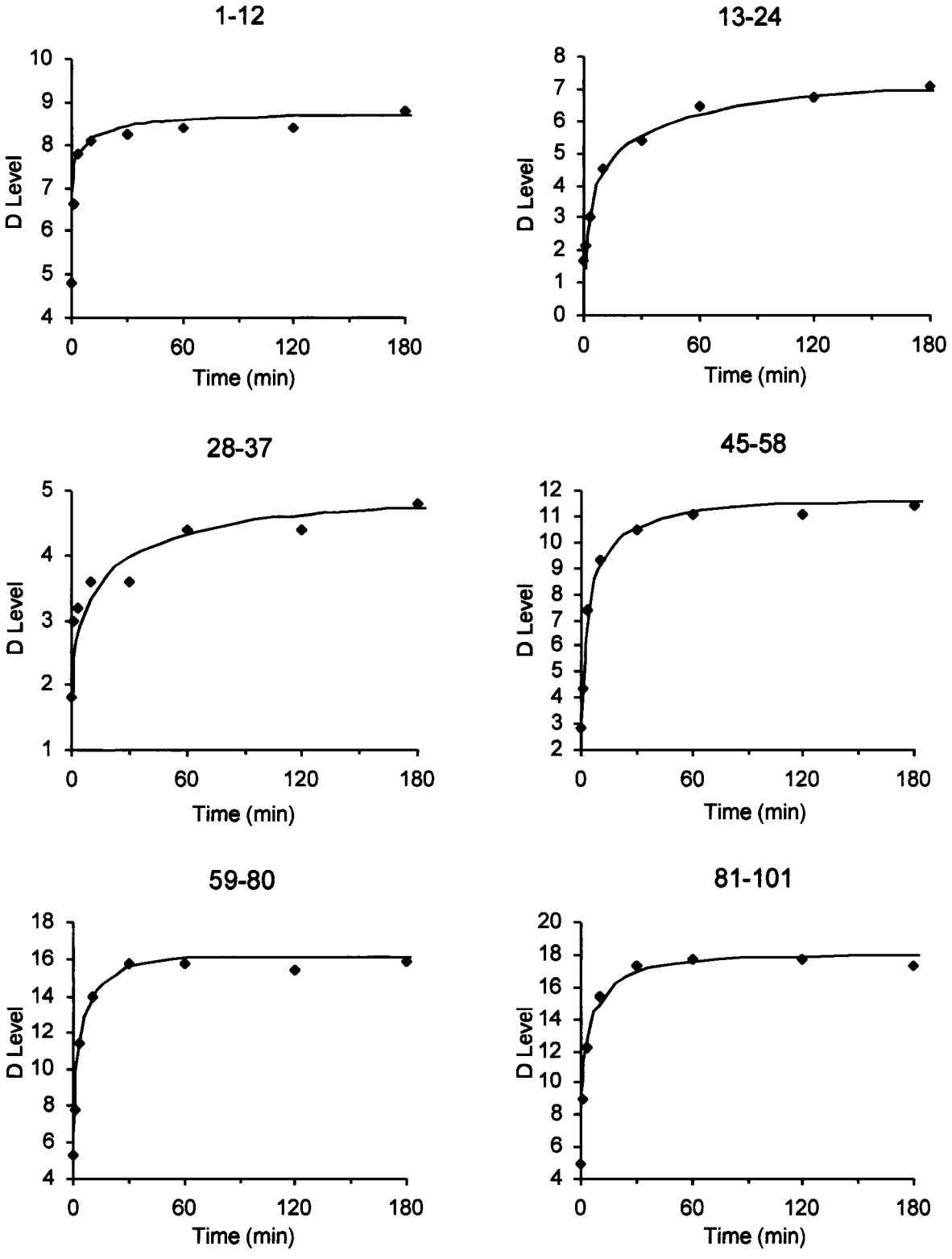

Figure 2.34. Deuterium levels found in segments 1-12, 13-24, 28-37, 45-58, 59-80, and 81-101 of Cys-TRX with different incubation times in 1% AcOD/D_2O. The solid lines were drawn by fitting the experimental data parameters in eq (10).

Table 2.4. Numbers of amide hydrogens that have exchanged with H/D exchange rate constants (rate groups) for common peptides from TRXs.[a]

Peptides	TRXs	# of NH	Rate groups[b]			
			very fast	fast	slow	very slow[c]
1-12	Oxi-TRX	11	4.0 (>3.0)	2.5 (1.3)	1.0 (0.04)	3.5 (<0.003)
	Red-TRX	11	4.0 (>3.0)	2.5 (1.14)	1.9 (0.1)	2.6 (<0.003)
	GS-TRX	11	5.0 (>3.0)	2.6 (0.6)	0.7 (0.1)	2.7 (<0.003)
	Cys-TRX	11	4.2 (>3.0)	3.0 (1.0)	1.1 (0.1)	2.7 (<0.003)
13-24	Oxi-TRX	11	1.0 (>3.0)	4.0 (0.2)	2.5 (0.05)	3.5 (<0.003)
	Red-TRX	11	2.0 (>3.0)	3.0 (0.3)	2.6 (0.04)	3.4 (<0.003)
	GS-TRX	11	2.8 (>3.0)	2.8 (0.1)	1.6 (0.01)	3.8 (<0.003)
	Cys-TRX	11	1.6 (>3.0)	3.1 (0.2)	1.3 (0.02)	5.0 (<0.003)
28-39	Oxi-TRX	10	0.5 (>3.0)	4.0 (0.4)	2.7 (0.04)	2.8 (<0.003)
	Red-TRX	10	2.0 (>3.0)	3.0 (0.5)	3.0 (0.05)	2.0 (<0.003)
28-37	GS-TRX	9	1.5 (>3.0)	2.5 (0.3)	1.0 (0.1)	4.0 (<0.003)
	Cys-TRX	7	1.0 (>3.0)	2.0 (0.9)	1.0 (0.03)	3.0 (<0.003)
45-58	Oxi-TRX	13	4.0 (>3.0)	4.0 (0.3)	3.3 (0.03)	1.7 (<0.003)
	Red-TRX	13	2.1 (>3.0)	3.3 (0.4)	4.9 (0.06)	2.7 (<0.003)
	GS-TRX	13	2.0 (>3.0)	7.1 (0.4)	2.1 (0.05)	1.8 (<0.003)
	Cys-TRX	13	1.0 (>3.0)	6.9 (0.6)	3.0 (0.06)	2.1 (<0.003)
59-80	GS-TRX	18	5.3 (>3.0)	8.3 (0.2)	1.7 (0.14)	2.7 (<0.003)
	Cys-TRX	18	4.2 (>3.0)	8.5 (0.2)	3.0 (0.17)	2.3 (<0.003)
81-101	GS-TRX	20	1.0 (>3.0)	14.0 (0.7)	3.5 (0.06)	1.5 (<0.003)
	Cys-TRX	20	4.0 (>3.0)	10.0 (0.3)	3.7 (0.06)	2.3 (<0.003)

[a] Distribution of rate constants for H/D exchange of peptide amide hydrogens estimated by fitting deuterium exchange results shown in Figures 2.31~34 to eq (10). [b] The number of amide hydrogens that exchange with the rate constant (min^{-1}) indicated in parentheses. [c] The number of very slowly exchanging amide hydrogens was determined by subtracting the number of amide hydrogens exchanged in 3h from the total number of amide hydrogens in each segment, i.e. (N-P_1-P_3-P_5) (eq (10)).

For the N-terminal peptide of Oxi-TRX consisting of residues 1-12, there is a total of 11 amide hydrogens in the backbone; 4.0 exchange with rate constants greater than 3 min^{-1}, 2.5 exchange with rate constants equal to 1.3 min^{-1}, 1.0 exchanges with a rate constant equal to 0.04 min^{-1}, and 3.5 exchange very slowly with rate constants less than 0.003 min^{-1}. The categories of very fast and very slow include amide hydrogens that exchange either too fast ($k_{ex} > 3$ min^{-1}) or too slow ($k_{ex} < 0.003$ min^{-1}). The fast and slow exchange categories were assigned on a relative basis in each peptic segment. For example in GS-TRX, the rate constant 0.1 min^{-1} for peptide 13-24 is in the fast category, whereas for peptide 1-12 it is in the slow category.

The results in **Table 2.4** were plotted to more easily show the number of amide hydrogens that exhibit similar exchange rates for common peptic peptides from TRXs (**Figure 2.35**). The number of amide hydrogens that exchange in the very fast category, i.e. $k_{ex} > 3$ min^{-1}, is indicated on the right of each panel, while the number of amide hydrogens with very slow exchange rates is indicated on the left of each panel. In the data analysis, only very fast and very slowly exchanging amide hydrogens have been focused because they are directly connected to the protein's conformational changes such as ligand binding or partial unfolding.[41]

Small changes observed in the four rate groups for peptide 1-12 suggest that either the reduction of the disulfide linkage between Cys-32 and Cys-35 or alkylation of the Red-TRX causes slight changes in the conformation and stability of this segment. In peptide 13-24, the reduction and alkylation increases the number of very fast exchanging amide hydrogens by 0.6~1.8. For slowly exchanging amide hydrogens, only Cys-TRX showed an increase, that was about one. This result suggests that the conformational changes resulting from

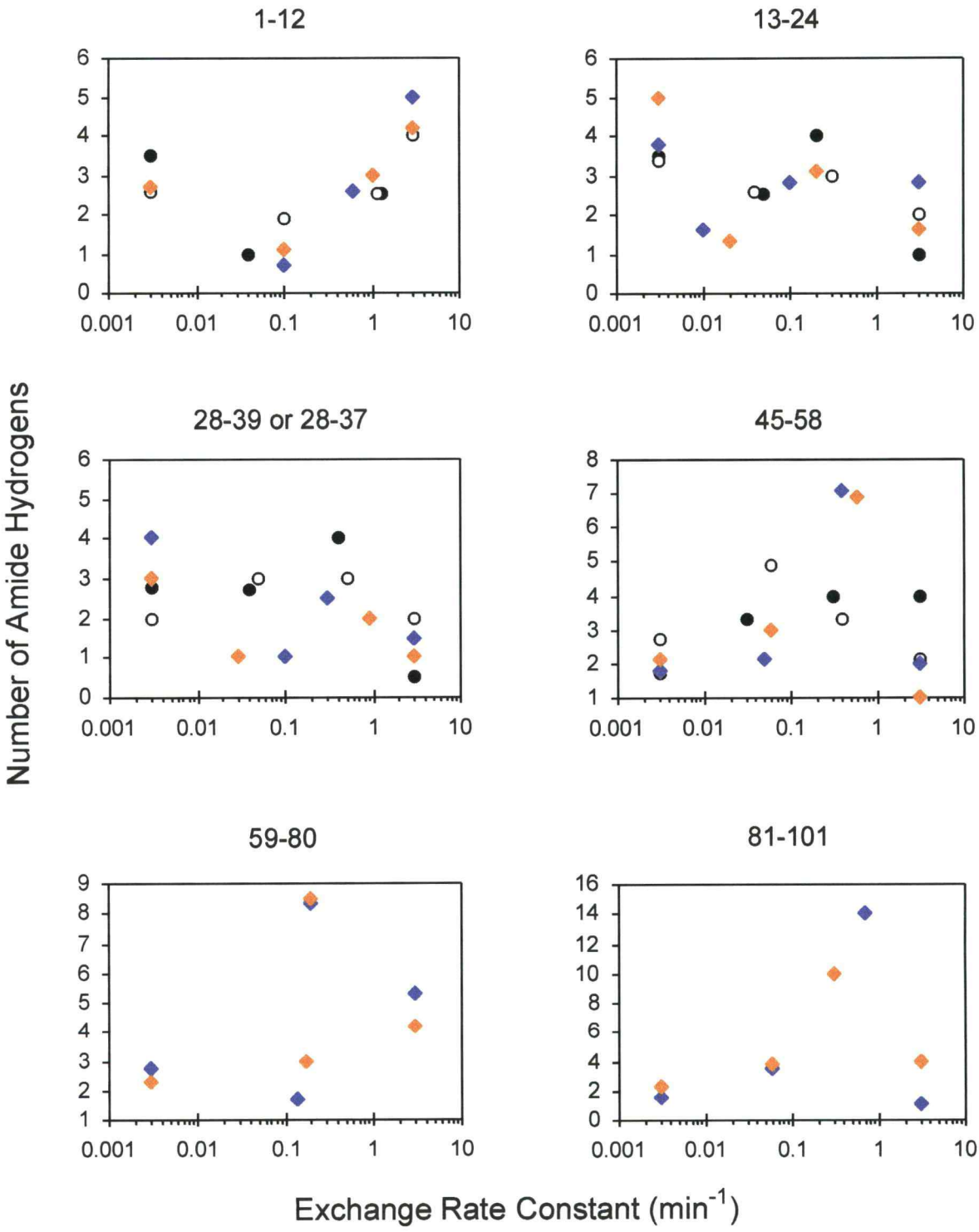

Figure 2.35. Distribution of amide hydrogen exchange rates in peptic fragments of Oxi-TRX (●), Red-TRX (○), GS-TRX (◆), and Cys-TRX (◆). The number of amide hydrogens that have exchanged versus their mean exchange rates is displayed. Results were obtained by fitting parameters in eq (10) to deuterium exchange results. The fragments 28-39 were taken from Oxi- and Red-TRX, and fragments 28-37 were taken from GS- and Cys-TRX.

the reduction and alkylation in the active site which contains Cys-32 and 35 residues influence the adjacent segment 13-24, however, slightly.

Four component model analysis clearly differentiates the conformational changes in the active site segments 28-39 or 28-37. Even though it is not appropriate for these segments to be compared because they have different numbers of peptide amide hydrogens, the results show they are significantly different. The very fast and very slow rate groups showed dramatic changes which were caused by reduction of the disulfide linkage and by the alkylation at Cys-32. The reduction increased the number of very fast exchanging amide hydrogens by 1.5. The alkylation decreased the hydrogen number in the very fast rate group of Red-TRX by 0.5 and 1 for GS-TRX and Cys-TRX, respectively. The very slow rate group showed that 2, 2.8, 3, and 4 of very slowly exchanging hydrogens were found in Red-, Oxi-, Cys-, and GS-TRX, respectively. These results suggest that the reduction and alkylation changed the conformation in the active site. That is, the increase of very fast amide hydrogens by reduction implies there is enhanced flexibility in the vicinity of the active site. The changes in the very slow exchange rate group indicate a change of the intramolecular hydrogen bonding.

The peptide 45-58 showed an unexpected result. The reduction decreased the number of very fast exchanging hydrogens by two and increased the number of very slowly exchanging hydrogens by one. This result suggests that the reduction made the active site region more flexible, however, it appears to have made the adjacent region 45-58 more rigid. In the peptides 59-80 and 81-101, there is no direct relationship between native (Oxi- and Red-TRX) and alkylated TRXs (GS- and Cys-TRX) because Oxi- and Red-TRX showed bimodal isotopic mass peaks. Four-component analysis showed little or no difference between Cys- and GS-TRX in the peptides 59-80 and 81-101.

The fragments 59-80 and 81-101 of Oxi- and Red-TRX showed two distinct mass envelopes after a short incubation period in 1% AcOD/D_2O at room temperature (**Figure 2.36**). This is evidence for correlated exchange in the region of these two segments. When correlated exchange prevails, the mass spectra show bimodal isotope patterns and the continuously changing relative intensities of two envelopes of isotope peaks are a direct measure of the population of folded and unfolded forms. The lower mass peak corresponds closely to the ion peak from the nondeuterated protein (0% ref.), and the higher mass peak is very close to the ion peak from the fully deuterated protein (100% ref.).

By measuring conversion rates from the lower to the higher mass peaks, the unfolding rate constant, k_1, could be obtained from the EX1 mechanism (**Figure 2.37**). Different unfolding rate constants are an indication of different lifetimes in an unfolded state. The longer a fragment stays in the unfolded state, i.e. the faster a fragment unfolds, the faster the lower and higher mass peaks change in relative intensities. The intensity of the higher mass peak contains the accumulated H/D exchange information because this peak includes the population of molecules that were unfolded as well as molecules that unfolded then refolded during the incubation time.

The unfolding rate constants, k_1, of each segment were obtained by fitting F/(F+U) to the equation, $F/(F+U) = A\exp(-k_1 t)$, where F and U are the intensities of lower and higher mass peaks in the bimodal isotopic profiles, respectively. By the reduction of the disulfide bond, the unfolding rate constant of peptide 59-80 was doubled, and the unfolding rate constant of peptide 81-101 was tripled. Thus, continuous H/D exchange labeling can be used to identify regions of proteins that unfold at different rates.

These results suggest that even small conformational change in the active site can affect the stability and dynamics of remote regions. Because the H/D

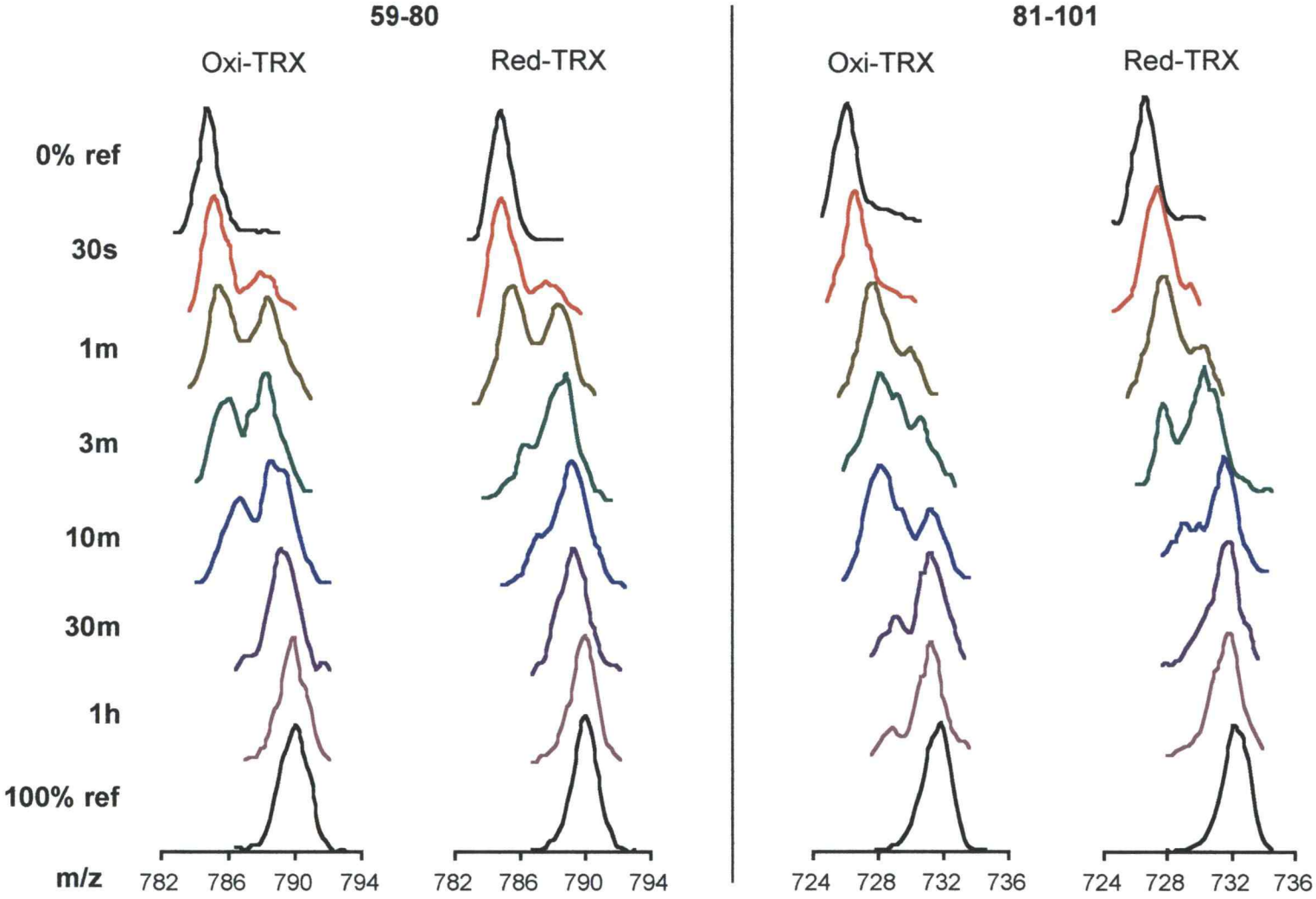

Figure 2.36. Molecular ion peaks of peptic peptides 59-80 and 81-101 of Oxi- and Red-TRX in ESI mass spectra during H/D exchange-in experiments in 1% acetic acid-*d* at 25 °C. Time points refer to H/D exchange-in periods. Top and bottom spectra are for the same fragments of Oxi-TRX that contained no deuterium (0% ref) or Oxi-TRX that was completely exchanged in D_2O (100% ref).

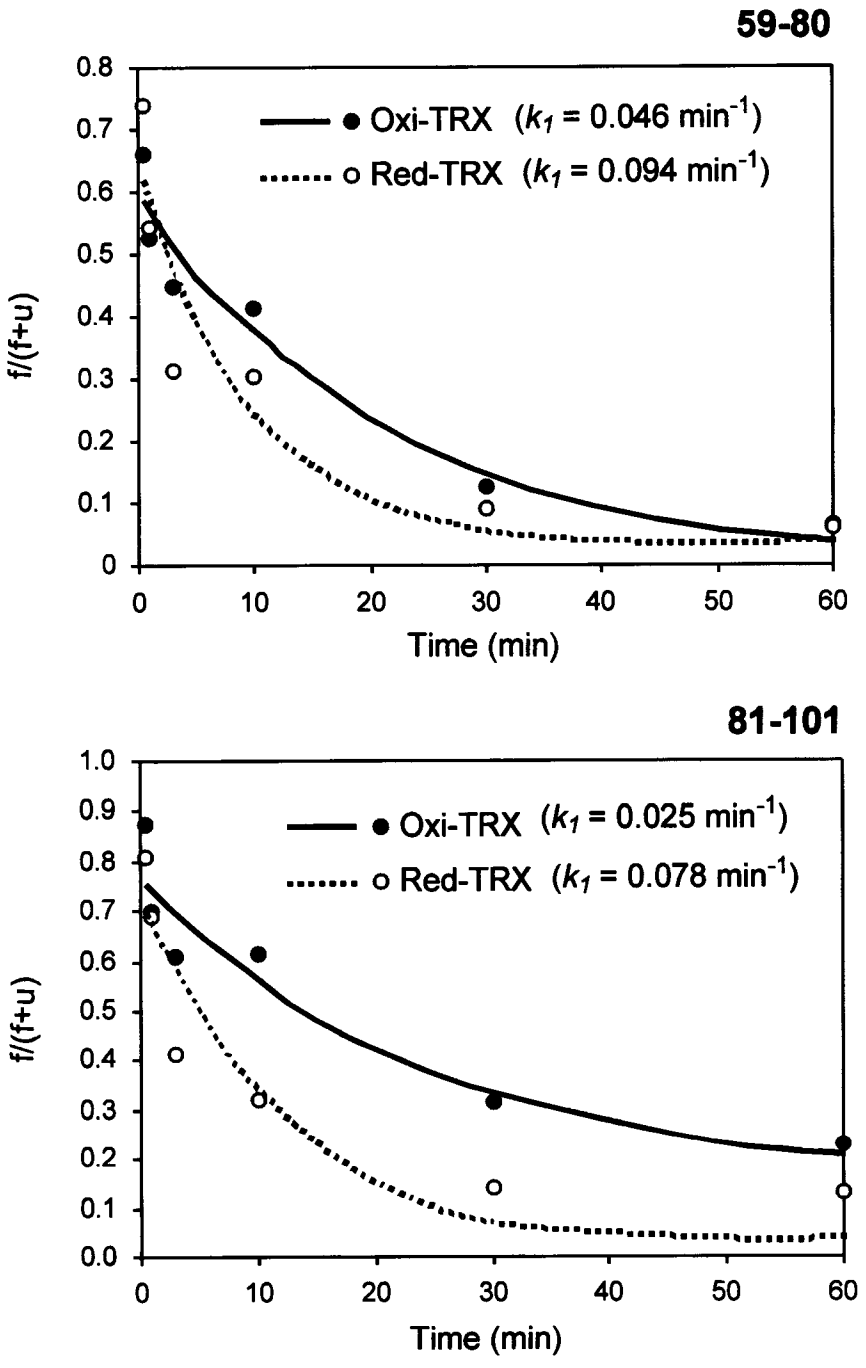

Figure 2.37. Estimation of the rate constant, k_1, of two peptic peptides, 59-80 and 81-101, of Oxi- and Red-TRX. The lines are obtained by curve fitting to f/(f+u) = Aexp(-k_1t) where f and u are the intensities of the lower and higher mass peaks of the bimodal isotopic mass profiles.

exchange time course for the peptic fragments 28-39 already showed significant differences between Oxi- and Red-TRX, the combined results suggest that the reduction of the disulfide linkage triggered conformational changes in the entire protein. These results support previous temperature-dependent global H/D exchange and thermal unfolding behavior that showed a difference in melting temperatures of 15 °C between the Oxi- and Red-TRX.[45]

2.3-3 H/D exchange of TRXs, proteolysis, and tandem mass spectrometry for residue-specific hydrogen exchange

Collision-induced dissociation tandem mass spectrometry (CID MS/MS) was used to measure the extent of H/D exchange at individual amide linkages of TRXs (**Figure 2.38**). Non-deuterated, partially deuterated, and fully deuterated proteins were digested and analyzed by HPLC-MS used for the fragmentation /MS method (**Figure 2.26**). Phosphate buffer solution (10 mM, pH 5.7) was selected for equilibration and exchange-in experiments because previous NMR experiments for hydrogen isotope exchange of Red- and Oxi-TRX were carried out in this particular buffer solution [47] and the intention here was to draw comparisons between NMR and mass data. For deuterium exchange-in experiments, the equilibrated TRXs were exposed to D_2O phosphate buffer solution for 20 sec at room temperature.

After brief exposure to D_2O and quenching, all TRXs except Oxi-TRX were digested by pepsin without prior treatment. As mentioned in chapter 2.3-1, Oxi-TRX was poorly digested under slow exchange conditions and as a result the signals of peptic peptide ions were too weak on which to perform MS/MS experiments. Urea was used to denature Oxi-TRX and to enhance the digestion by pepsin. Pre-cooled concentrated urea solution was added to labeled Oxi-TRX during the mixture being quenched.

The molecular weight of biomolecules can be deduced by deconvolution from a series of peaks of multiply charged variants of the analyte because these multiply charged species differ by a consecutively decreasing number of charges as *m/z* increases. Generally, the molecular weight of a charged ion can be calculated from eq (11).

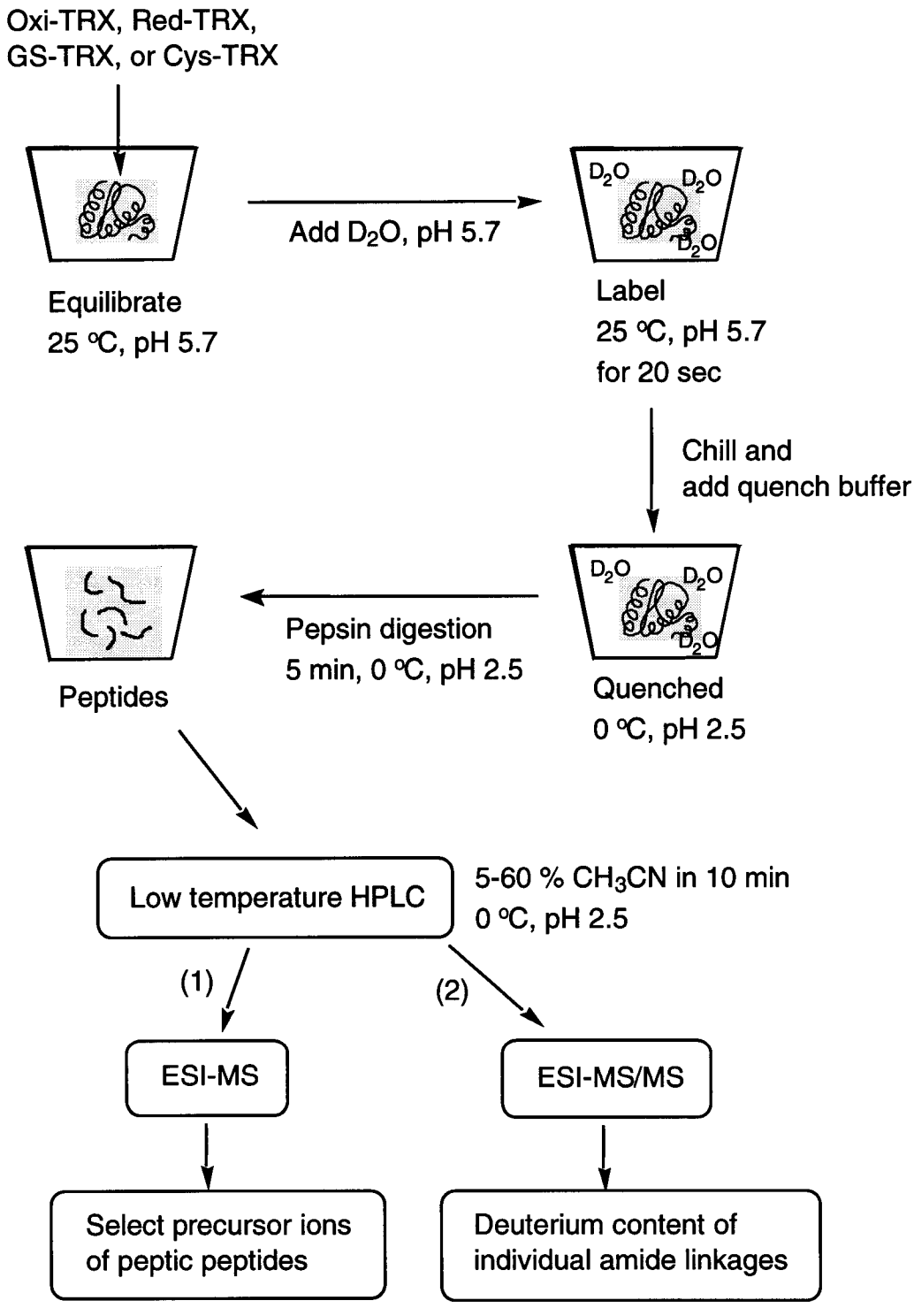

Figure 2.38. Strategy for the determination of deuterium levels at individual peptide amide linkages.

$$m = \frac{M + nX}{n}$$

$$M = mn - nX \qquad (11)$$

The molecular weight of the ion is designated *M*, and the mass of the charge carrier, e.g. H+ or Na+, is designated *X*. The number of charges on a given ion is designated *n*, and the *m/z* value of the peaks in the mass spectrum are represented by *m*.

b ion series

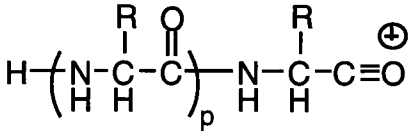

p = 0, 1, ...

for b^{1+} ions, M = m
for b^{2+} ions, M = 2m - 1

y ion series

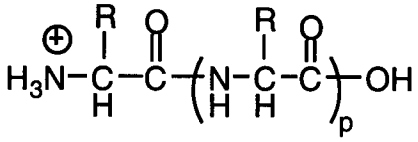

p = 0, 1, ...

for y^{1+} ions, M = m - 1
for y^{2+} ions, M = 2m - 2

Figure 2.39. Molecular weight calculations of *b* and *y* ions

To calculate the molecular weight of ions produced by CID MS/MS of the peptide, a slightly different procedure is used (**Figure 2.39**). For b^{1+} ions, the mass of the charge carrier, *X*, is zero because the first charge site is the carbonyl cation, and M is the *m/z* value itself. For b^{2+} ions, *nX* is one because

the second charge site is generated from protonation of a basic site in the side chain. The molecular weight of b^{2+} ions is 2m-1. For *y* ions, because all charge sites are from protonation of basic sites, *X* is one. The molecular weights of y^{1+} and y^{2+} ions are m-1 and 2m-2, respectively. Even for deuterium exchanged peptides, the mass of charge carrier, *X*, is not two (D^+) but one (H^+) because all charge sites are back-exchanged by H_2O/acetonitrile solvent during HPLC separation.

The ESI ion-trap mass spectrometer, LCQ™, produced CID spectra that showed completely different patterns between singly and doubly charged precursor ions of a peptide 1-12 of Oxi-TRX (**Figure 2.40**). Singly charged precursor ions showed increasing peak intensities as the *m/z* values increased. The *b* ions showed greater intensities in fragment ions from the C-terminal side of a peptide. The *y* ions showed greater intensities in fragment ions from the N-terminal side. Doubly charged precursor ions showed greater intensities in the middle of the spectrum because they are produced by medium-sized *b* and *y* ions. Almost all CID MS/MS experiments of peptic peptides of TRXs were carried out on the doubly charged precursor ions because doubly charged ions usually showed greater peak intensities than singly charged ions. Hence, CID fragment ions possessing extreme *m/z* values, i.e. too high or too low *m/z* values in the MS/MS spectrum, showed very weak signals or no signals at all.

Doubly charged ions of a peptide 1-24 of non-deuterated (0% ref), 20s deuterated, and fully deuterated (100% ref) Oxi-TRX were used as precursor ions for CID MS/MS (**Figure 2.41**). Reference samples, 0% and 100%, were used to adjust for deuterium loss during analysis. Reference samples of the fragment 1-24 of Oxi-TRX indicated that about 15% of the amide deuteriums were lost during digestion and HPLC and MS analysis. Isotope patterns for the CID fragment ion, b_{13}, derived from the MS/MS spectrum of the fragment 1-24

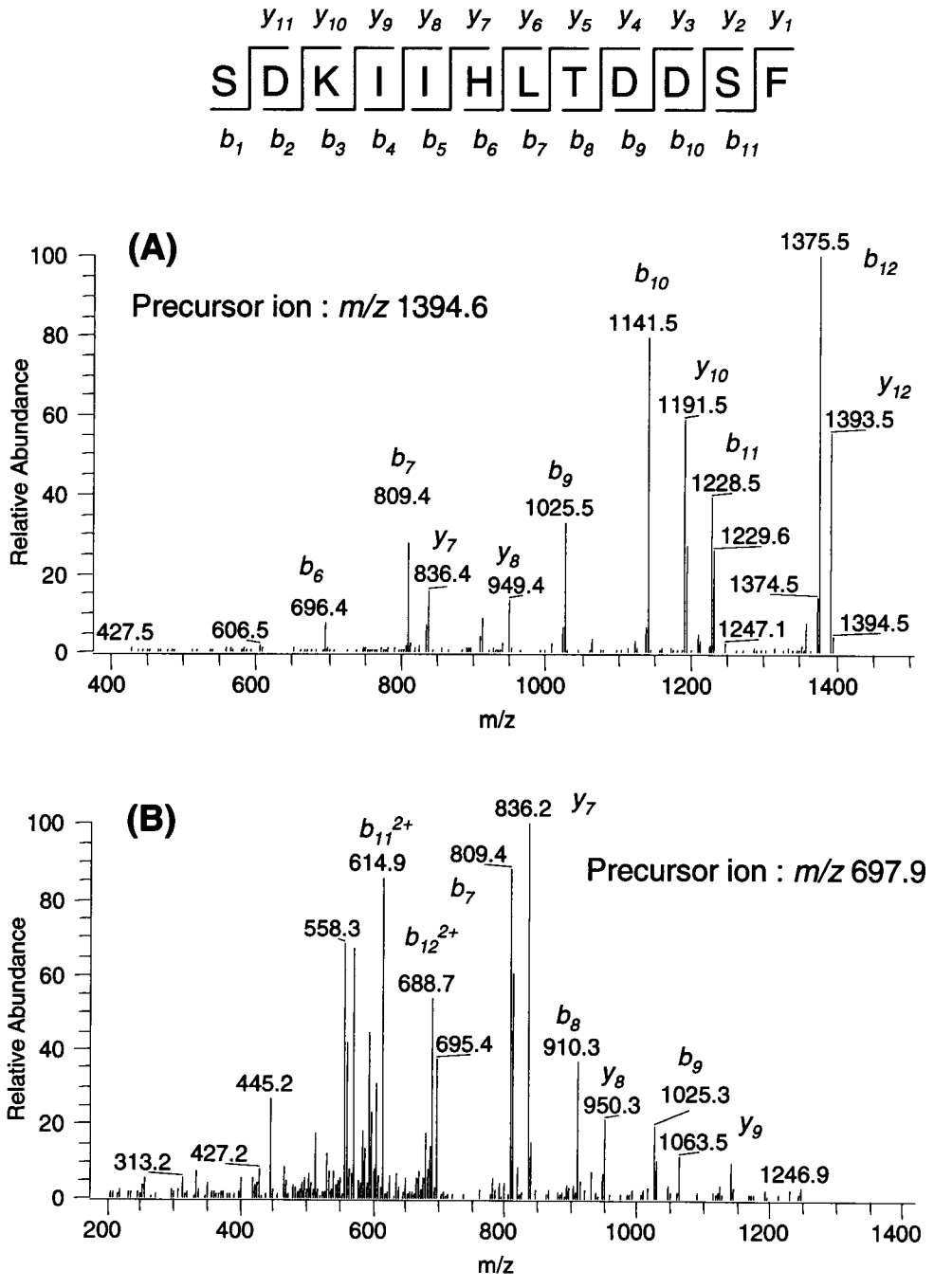

Figure 2.40. Collision-induced dissociation tandem mass spectrometry (CID MS/MS) of singly (A) and doubly (B) charged precursor ions of a peptic peptide 1-12 of 20 s labeled Oxi-TRX.

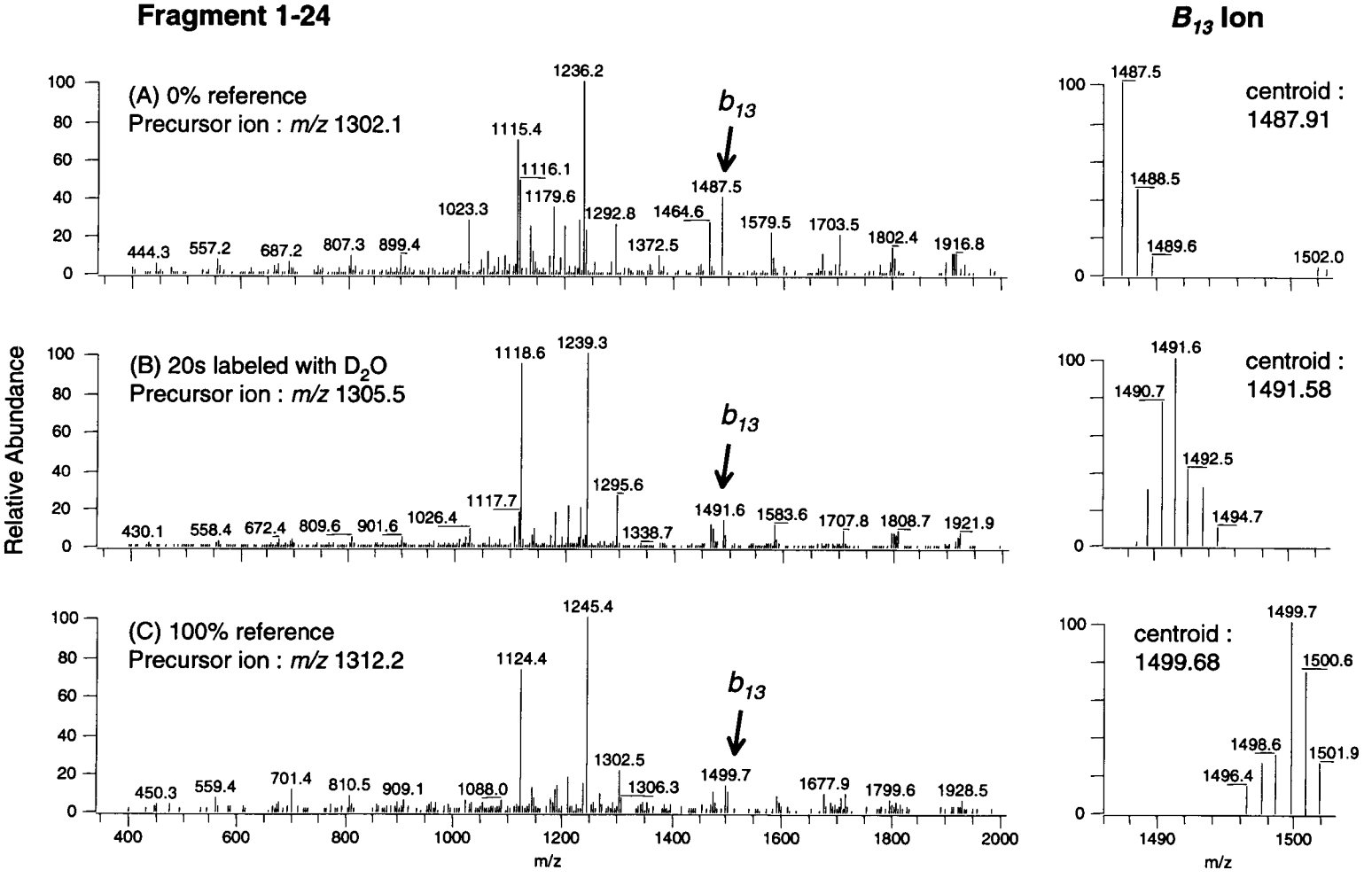

Figure 2.41. CID MS/MS spectra of peptide 1-24 of non-deuterated (A, 0% ref.), 20s labeled (B), fully deuterated (C, 100% ref.) Oxi-TRX. Right panels represent isotope patterns of the CID fragment, b_{13}.

of the 0% reference, 20s deuterated, and 100% reference Oxi-TRX samples are shown in the right side panels. The MS/MS spectra of peptides after H/D exchange normally show a broad distribution of peaks contributed to by the naturally occurring isotopes, ^{13}C and ^{15}N. The centroidal mass values were obtained using MagTran software.[51]

Some isotopic distributions of CID fragments showed overlapped isotopic multiplets (**Figure 2.42**). The b_{12} and y_{13} ions, whose protonated masses were 1372.67 and 1377.73, respectively, overlapped after 20s deuterium labeling. The deconvoluted multiplets indicated by dashed lines were used to determine the centroidal mass values. However, in many cases, the overlapped multiplets could not be resolved when they are very close. This is one of the reasons why the accurate determination of centroidal value is difficult.

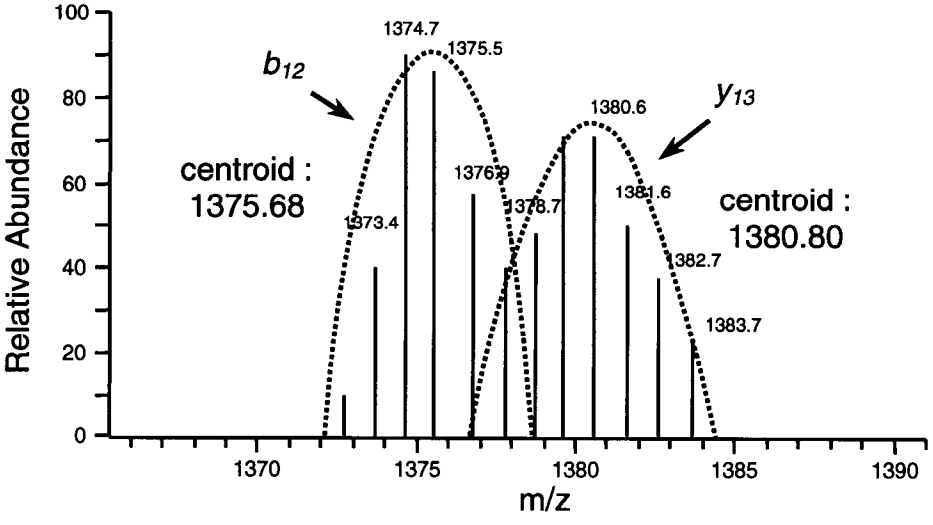

Figure 2.42. Overlapped isotopic multiplets of b_{12} and y_{13} ions derived from CID MS/MS spectra of peptic peptide 1-24 of 20s labeled Oxi-TRX.

Mass values of *b* and *y* ions of peptic peptide 1-24 (**Figure 2.41**) were summarized and calculated for estimating the deuterium levels at individual amide linkages (**Table 2.5**). Calculated *m/z* values for protonated masses were used for 0% reference values because these values showed almost the same *m/z* values as 0% reference sample and they do not have a missing fragment. Fragment ion peaks were not found for b_{11}, b_{14}, b_{16}, b_{21}, y_{12}, *and* y_8.

The molecular weights of CID fragment ions were calculated by the method mentioned above (**Figure 2.39**). The number of deuteriums in a CID fragment ion was calculated by subtracting the protonated mass from the deuterated mass. These numbers were adjusted for deuterium loss during analysis according to eq (12).

$$\text{Adjusted number of deuteriums, } A = D \times (Q/P) \qquad (12)$$

In the equation, the number of deuteriums in a fragment ion is designated as *D*, the number of peptide amide hydrogens is designated as *Q*, and the deuterium number on the peptide from fully deuterated sample (100% ref) is designated as *P*. In the case for peptide 1-24, the *m/z* value of the doubly charged precursor ion from the 100% reference sample was 1312.1, and *P* is 19.51 as obtained from the calculation, (MW of 100% ref sample)-(MW of 0% ref sample)=(1312.2x2-2)-2602.89 where 2602.89 is the calculated average molecular weight of non-deuterated fragment 1-24. The value *Q/P* is 1.18 from 23/19.51. The adjusted numbers of deuteriums in fragment ions were obtained by multiplying the number of deuteriums by *Q/P*. To determine the number of deuteriums on individual peptide amide linkages, the adjusted number of deuteriums in a b_{n-1} ion was subtracted from that in a b_n ion.

Table 2.5. Deuterium levels found at individual amide linkages in peptide 1-24 of Oxi-TRX as determined by CID MS/MS

Ions (charge)		Protonated Mass (calculated)	20s deut. Mass (observed)	Number of D on ions	Adjusted number of D	Number of D on residue	residue	NMR[b] log k_{ex} (s^{-1})	
(1+)	b7	807.47	809.3	1.83	2.18		7Leu	-4	S
	b8	908.52	910.41	1.89	2.25	0.1	8Thr	-5.01	S
	b9	1023.55	1025.6	2.05	2.44	0.2	9Asp	-3.11	S
	b10	1138.57	1141.51	2.94	3.50	1.1	10Asp	-0.21	F
	b11	1225.61	-	-	-	(-0.1)[a]	11Ser	-3.09	S
	b12	1372.67	1375.39	2.72	3.24	(-0.1)[a]	12Phe	-4.18	S
	b13	1487.7	1491.58	3.88	4.62	1.4	13Asp	c	M
	b14	1588.75	-	-	-	(0.4)[a]	14Thr	-3.24	S
	b15	1703.78	1708.33	4.55	5.41	(0.4)[a]	15Asp	-3.51	S
	b16	1816.86	-	-	-	(0.1)[a]	16Leu	-5.4	S
	b17	1915.93	1920.69	4.76	5.66	(0.1)[a]	17Val	-5.93	S
(2+)	b18	1022.52	1025	4.96	5.90	0.2	18Lys	-4.41	S
	b19	1058.03	1060.63	5.2	6.19	0.3	19Ala	-2.75	S
	b20	1115.55	1118.49	5.88	7.00	0.8	20Asp	c	M
	b21	1144.06	-	-	-	(0.4)[a]	21Gly	-0.21	F
	b22	1179.58	1182.83	6.5	7.74	(0.4)[a]	22Ala	c	M
	b23	1236.12	1239.37	6.5	7.74	0.0	23Ile	-7.7	S
	b24	1292.66	1295.78	6.24	7.43	-0.3	24Leu	-7.8	S
(2+)	y22	1200.64	1203.85	6.42	7.64	2.8	3Lys	-0.02	F
	y21	1136.59	1138.62	4.06	4.83	-0.2	4Ile	-2.71	S
	y20	1080.05	1082.18	4.26	5.07	-1.6	5Ile	-4.06	S
	y19	1023.51	1026.3	5.58	6.64	1.5	6His	-2.6	S
(1+)	y18	1908.94	1913.22	4.28	5.09	-0.5	7Leu	-4	S
	y17	1795.86	1800.59	4.73	5.63	1.0	8Thr	-5.01	S
	y16	1694.81	1698.66	3.85	4.58	0.0	9Asp	-3.11	S
	y15	1579.79	1583.62	3.83	4.56	-0.1	10Asp	-0.21	F
	y14	1464.76	1468.64	3.88	4.62	1.0	11Ser	-3.09	S
	y13	1377.73	1380.8	3.07	3.65	(0.0)[a]	12Phe	-4.18	S
	y12	1230.66	-	-	-	(0.0)[a]	13Asp	c	M
	y11	1115.63	1118.65	3.02	3.59	0.1	14Thr	-3.24	S
	y10	1014.58	1017.52	2.94	3.50	0.1	15Asp	-3.51	S
	y9	899.56	902.4	2.84	3.38	(-0.1)[a]	16Leu	-5.4	S
	y8	786.47	-	-	-	(-0.1)[a]	17Val	-5.93	S
	y7	687.4	690.4	3	3.57		18Lys	-4.41	S

[a] For missing fragment ion, the difference in the number of deuterium is equally divided. [b] NMR data were taken from published results.[47] [c] The intermediate exchange rates are designated as M, which is in the range 0.0025-0.25 s^{-1} (log value –2.6 to –0.6).

For instance, the difference of the adjusted number of ions between the b_{10} and b_9 ions was 1.1 corresponding to the number of deuteriums incorporated on peptide amide linkage Asp-10 after 20 s exposure to D_2O. In case of a missing fragment ion, the difference of the adjusted number of deuteriums, $A_{n+2} - A_n$, was equally divided and allotted to the positions n+1 and n+2.

The H/D exchange rate constants of individual peptide amide hydrogens in Oxi-TRX were taken from previously published NMR data.[47] Rapidly exchanging amide hydrogens designated as F have large exchange rate constants ($k_{ex} > 0.25$ s^{-1} or $\log k_{ex} > -0.6$). These rate constants were obtained by saturation-transfer measurements.[52] Very slowly exchanging amide hydrogens are designated as S ($k_{ex} < 0.0025$ s^{-1} or $\log k_{ex} < -2.6$). The amide protons for which the exchange rate was too slow to measure by saturation transfer, but which also exchanged too fast to be observed in the H-D experiments, have intermediate exchange rates and are designated as M, which is in the range 0.0025 to 0.25 s^{-1} (log value –2.6 to –0.6).

The relationship between the deuterium levels of each residue and the exchange rate constants is shown on the graph (**Figure 2.43**). These results indicate that deuterium levels at individual peptide amide linkages can be determined from the *m/z* of the *b* ions, although some of the *b* ion *m/z* values do not show perfect matches. The *y* ions are much less reliable. Some *y* ions showed large fluctuations in deuterium content as, for example, Lys-3 (2.8), His-6 (1.6), and Ile-5 (-1.6) which indicates that deuterium incorporation occurred in the side chain amine sites or deuterium was lost in the peptide amide linkage. Thr-8, Ser-11, Asp-10, and Asp-13 showed too high or too low deuterium levels contrary to what would have been expected on the basis of the NMR data. These results suggest that H/D exchange, i.e. H/D scrambling, randomly occurs at all possible exchangeable sites of the *y* ions.

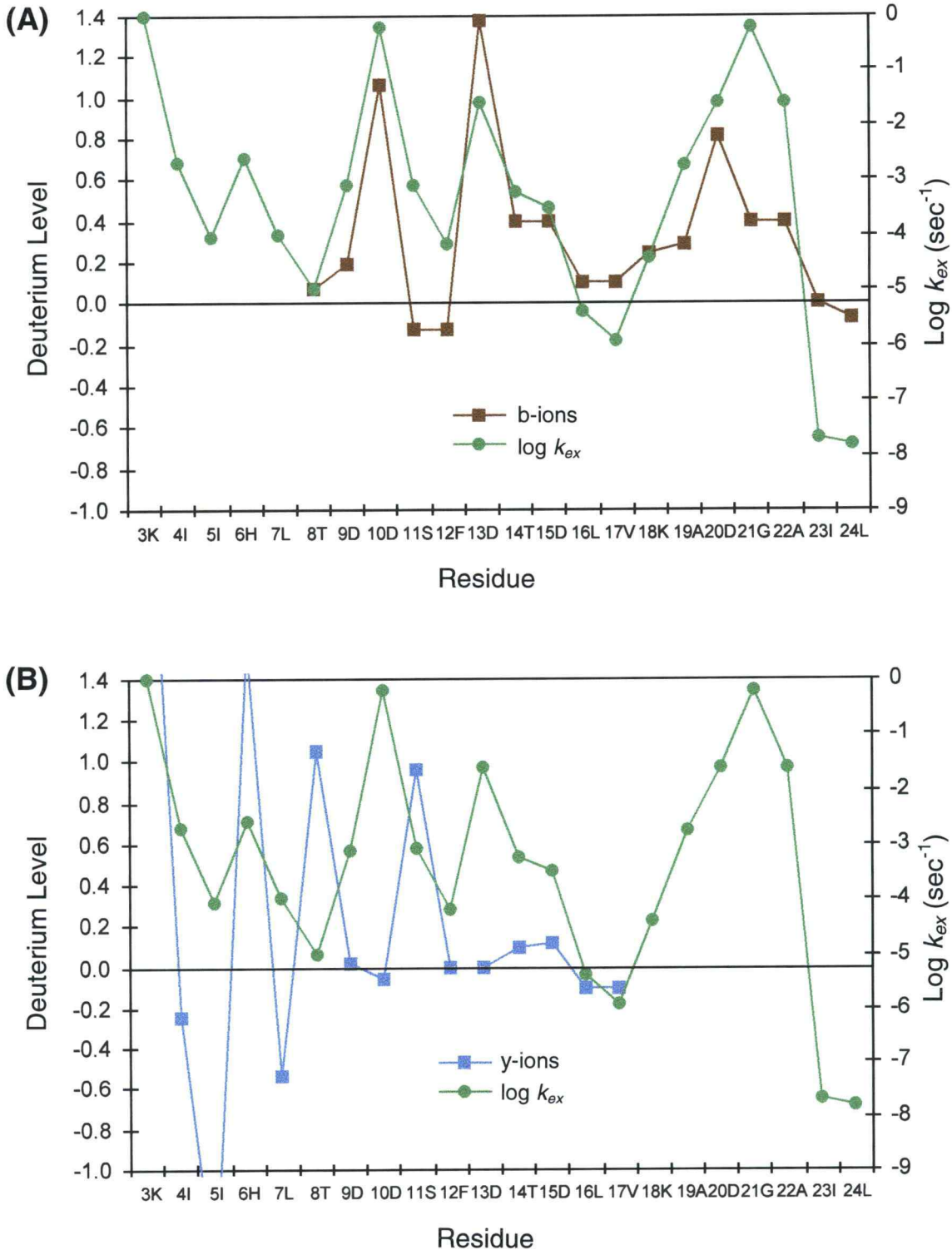

Figure 2.43. Comparison of *b* ions (A) and *y* ions (B) in the deuterium levels on peptide amide linkages in peptide 1-24 of Oxi-TRX. The H/D exchange rate constants (NMR data) for the intermediate range (logk_{ex} –2.6 to –0.6) were designated with the average value, -1.6.

The *b* ions showed relatively good correlation with NMR data. High deuterium levels larger than 0.8 were found at Asp-10, Asp-13, and Asp-20 corresponding to large or medium exchange rate constants. Gly-21 and Ala-22 with fast and medium exchange rates, respectively, also showed significantly higher deuterium levels. However, Thr-14 and Asp-15 have small exchange rate constants, but unexpectedly showed significant deuterium levels of about 0.4. Asp-13 showed an abnormally high deuterium level of 1.4. There are two possible reasons for this result. One is that deuterium is incorporated in the side chain carboxylic acid of Asp-13. The other is that deuterium is lost from the b_{12} ion. The latter is more probable because the b_{12} ion had unusually low deuterium content as shown by the negative deuterium content on Phe-12 and Ser-11. Although *b* ions did not show a perfect match with the NMR data, most of them were in reasonably good agreement with the amount of deuterium incorporated relative to the rate constants.

These results are roughly consistent with CID MS/MS data for cytochrome c, in which *b* ions showed good correlation with the NMR exchange rate data whereas *y* ions produced several discrepancies, suggesting that intramolecular H/D scrambling may occur during CID fragmentation to give the *y* ions.[31] The apparent high probability for scrambling precludes use of the *y* ions for determining deuterium levels at individual amide sites.

The deuterium levels on individual amide sites of fragment 1-24 derived from Oxi-, Red-, and GS-TRX were determined by analysis of the *b* ions and compared with exchange rate constants from NMR data (**Figure 2.44** and **Table 2.6** and **3.18**). Data for Cys-TRX were not available because the precursor ion intensity was too weak to carry out CID-MS/MS experiments. Since only *b* ions were used to determine the deuterium levels, it was inevitable that the H/D exchange information for 5-6 residues at the N-terminal side of this

peptide were lost. At the N-terminal side of a peptide, *b* ions are very weak whereas *y* ions usually are intense. In this peptide, Oxi-, Red-, and GS-TRX showed very similar amounts of deuterium. The reduction of the disulfide linkage in Oxi-TRX had little influence on the exchange rate constants of amide hydrogens obtained by NMR in this fragment except that Asp-13, Asp-20, and Ala-22 showed medium rate constants in Oxi-TRX and large rate constants in Red-TRX. Only one residue, Ala-22, showed the same result by the CID MS/MS data (**Table 2.6**). Although Asp-13 and Asp-20 in Red-TRX showed less deuterium content than Oxi-TRX, those residues still indicated deuterium levels larger than 0.6. The NMR solution structure of TRX indicated that Asp-10, Asp-13, Asp-20, Gly-21, and Ala-22 are in turns or loops.[22b] These five residues showed high levels of deuterium incorporation in the MS/MS data. Red- and GS-TRX generally showed good correlation with NMR data especially in the region that included residues 20-22. They also indicated reasonable data with no deuterium content greater than 1.0 nor the presence of negative deuterium content except in the case of Asp-9 in GS-TRX.

Several amide linkages in fragment 1-24 showed very low deuterium levels for all TRXs. These include Leu-7, Thr-8, Ser-11, Phe-12, Thr-14, Asp-15, Leu-16, Val-17, Lys-18, Ala-19, Ile-23, and Leu-24 (**Figure 2.45**). Residues 7-8 are present in the first β-strand, and residues 23-24 are in the second β-strand. Residues 11-19 are present in the first α-helix. These residues would thus most likely be strongly hydrogen-bonded and well protected from solvent. This protection is especially effective for Ile-23 and Leu-24 which are located in the central strand of the β-sheet. These residues showed persistent amide protons in the ^{15}N-^{1}H HSQC NMR spectrum even after 723 hours (one month) in D_2O.[47]

Table 2.6. Deuterium levels found at individual amide linkages in fragment 1-24 of Oxi-, Red-, and GS-TRX based on the analysis of *b* ions and *y* ions *(in italics)* obtained from CID MS/MS.

Residue	Number of Ds on residue					Log k_{ex} (s^{-1})			
	Oxi-TRX		**Red-TRX**		**GS-TRX**	Oxi-TRX		Red-TRX	
3Lys		*2.8*		*3.9*		-0.02	F	-0.02	F
4Ile		*-0.2*		*-0.5*		-2.71	S	-2.81	S
5Ile		*-1.6*		*-0.7*		-4.06	S	-4.13	S
6His		*1.5*	0.0	*-0.6*		-2.6	S	-2.6	S
7Leu		*-0.5*	0.1	*-0.6*	(0.2)	-4	S	-4.17	S
8Thr	0.1	*1.0*	0.0	*0.5*	(0.2)	-5.01	S	-5.02	S
9Asp	0.2	*0.0*	0.0	*0.0*	-0.1	-3.11	S	-3.28	S
10Asp	1.1	*-0.1*	0.9	*0.8*	0.8	-0.21	F	0.12	F
11Ser	(-0.1)	*1.0*	(0.2)	*(0.2)*	0.0	-3.09	S	-3.22	S
12Phe	(-0.1)	*(0.0)*	(0.2)	*(0.2)*	0.0	-4.18	S	-4.18	S
13Asp	1.4	*(0.0)*	0.9	*(0.1)*	0.7	a	M	-0.4	F
14Thr	(0.4)	*0.1*	0.2	*(0.1)*	0.1	-3.24	S	-3.31	S
15Asp	(0.4)	*0.1*	0.2	*0.6*	0.2	-3.51	S	-3.49	S
16Leu	(0.1)	*(-0.1)*	(0.1)	*(0.2)*	(0.1)	-5.4	S	-5.44	S
17Val	(0.1)	*(-0.1)*	(0.1)	*(0.2)*	(0.1)	-5.93	S	-5.97	S
18Lys	0.2		0.0		(0.3)	-4.41	S	-4.43	S
19Ala	0.3		0.1		(0.3)	-2.75	S	-2.8	S
20Asp	0.8		0.6		0.8	a	M	-0.19	F
21Gly	(0.4)		0.7		(0.9)	-0.21	F	-0.12	F
22Ala	(0.4)		0.8		(0.9)	a	M	-0.34	F
23Ile	0.0		0.2		0.2	-7.7	S	-7.6	S
24Leu	-0.1		0.1		0.0	-7.8	S	-7.8	S

In cases of missing fragment ions, the difference in the number of deuteriums incorporated was equally divided among the residues and these are shown in parentheses. The rate constants were classified as S (slow), M (medium), and F (fast). [a] The intermediate exchange rates are designated as M, which is in the range 0.0025-0.25 s^{-1} (log value –2.6 to –0.6).

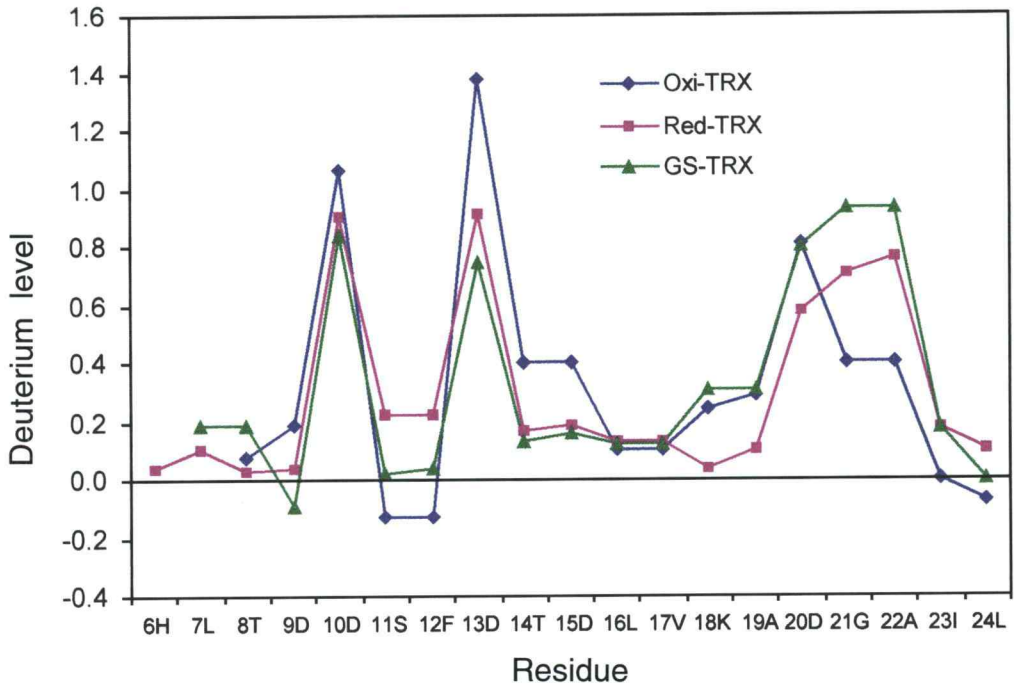

Figure 2.44. Deuterium levels found at peptide amide linkages in fragment 1-24 of Oxi-, Red- and GS-TRX.

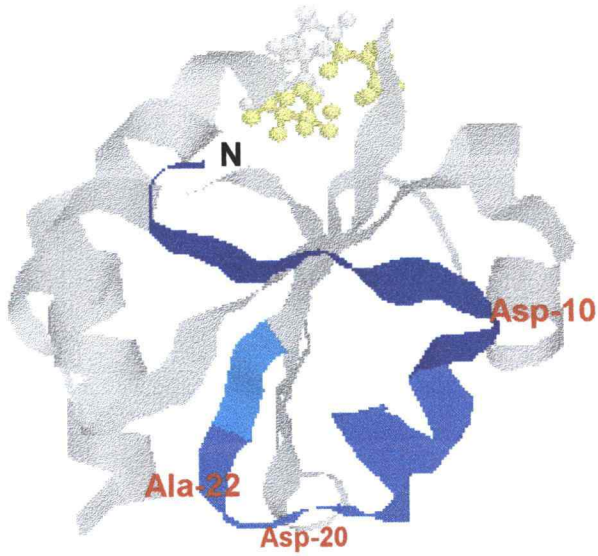

Figure 2.45. NMR solution structure of Oxi-TRX.[22b] A fragment including residues 1-24 is highlighted in blue. The active site is represented in the ball and stick format, and two cysteine residues are colored in yellow.

CID MS/MS spectra of the active site region showed very different patterns between the TRXs (**Figure 2.46** and **Table 2.7** and **3.19**). Singly charged precursor ions were used for Oxi- and Red-TRX, and doubly charged precursor ions were used for GS- and Cys-TRX. In the peptide 28-39 of Oxi-TRX, only the CID fragment ions that included the disulfide loop were found. These are b_8, b_9, b_{10}, b_{11}, and b_{12} ions. CID ions from within the disulfide loop, b_5, b_6, and b_7, were not found. However, in the fragment 28-37 of Red-TRX, b_5 and b_6 ions, which were produced from the dissociation occurring between Cys-32 and Cys-35, were found because the disulfide linkage was reduced. These data indicate that the disulfide loop structure is too stable to be destroyed by CID. This observation supports the results of a previous CID MS/MS experiment in which a peptide that included a cyclic structure was found to be resistant to CID fragmentation.[53] In the fragment 28-37 of GS-TRX, a number of CID ions were obtained by Glu(E) loss from the attached glutathionyl group.

The numbers of deuteriums at individual amide linkages were calculated (**Table 2.8**) using the MS/MS data of 20s labeled TRXs (**Table 2.7**). There is no data from Trp-31 to Cys-35 in Oxi-TRX due to the inability to dissociate the

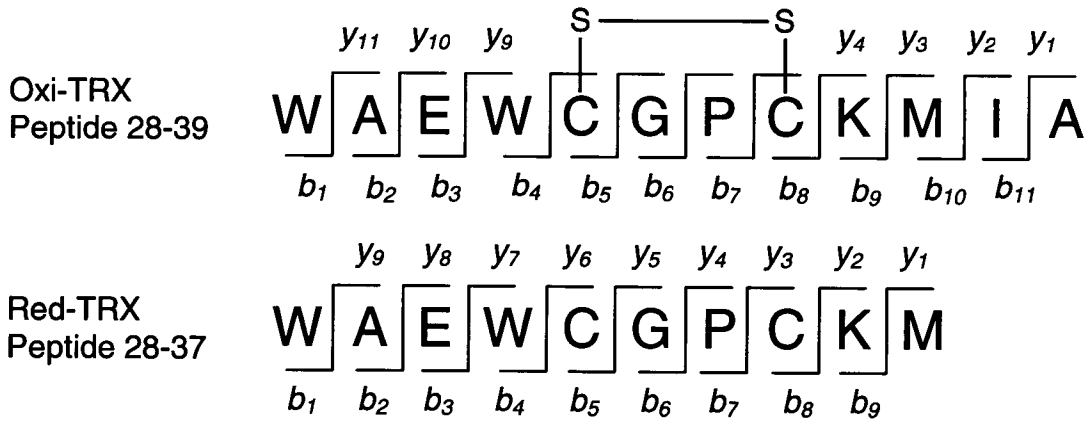

Figure 2.46 (A). Expected CID fragmentation of peptides 28-39 and 28-37.

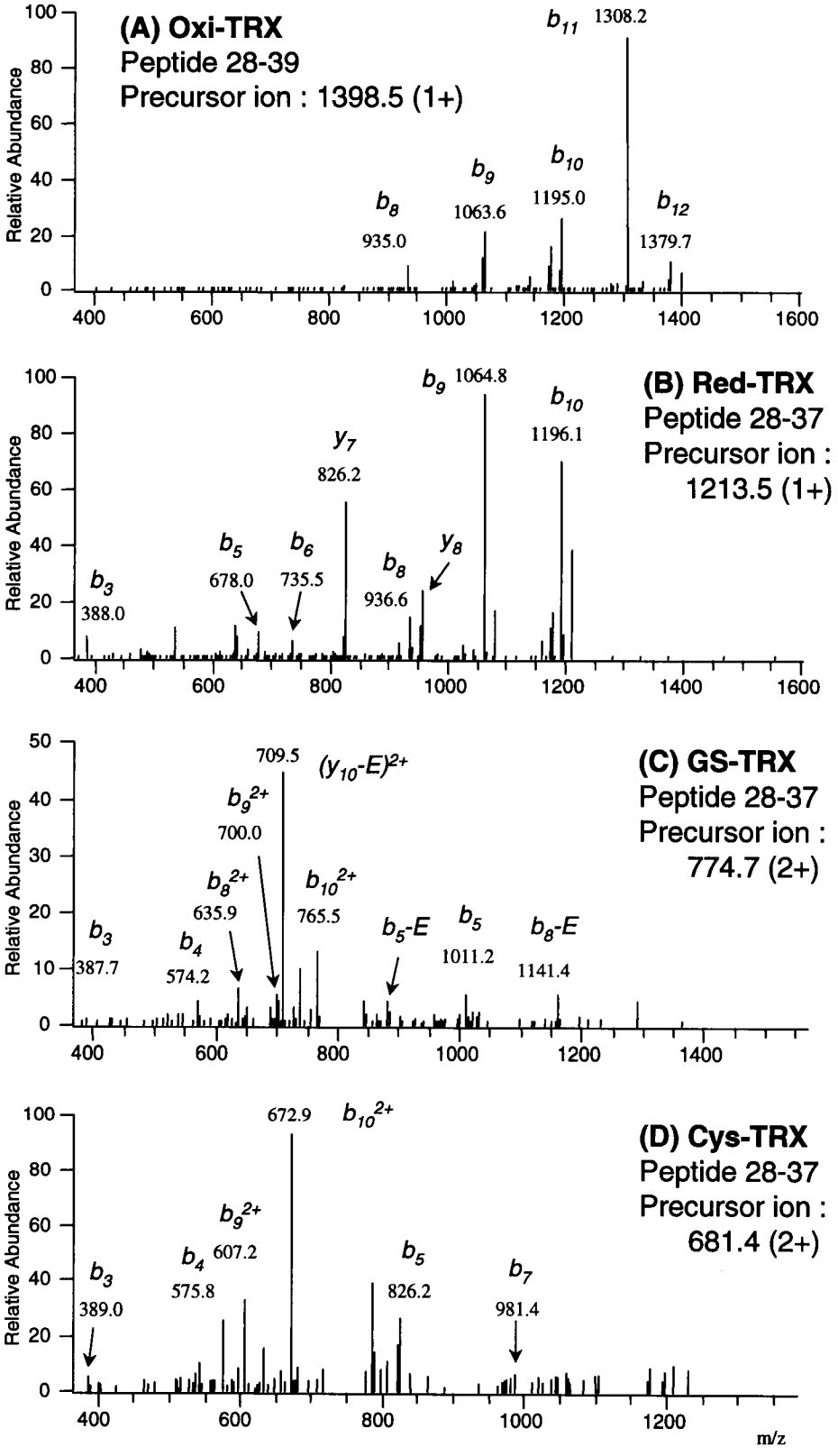

Figure 2.46(B). CID MS/MS spectra of peptide 28-39 (Oxi-TRX) and 28-37 (Red-, GS- and Cys-TRX) of 20s labeled TRXs.

resistant disulfide loop. No deuterium was found for Pro-34 because it does not contain an exchangeable amide hydrogen. NMR data showed a very large difference in rate constants between Oxi- and Red-TRX at Cys-35, a difference of more than 5 orders of magnitude.[47] This disparity is explained on the basis of significant structural differences between Oxi- and Red-TRX. Unfortunately, there is no information forthcoming from MS/MS data to cast further light on the reasons for the differences in NMR exchange rates because no information was obtained for Cys-35 in Oxi-TRX.

Table 2.7. The *m/z* values found in the CID spectra for peptides 28-39 or 28-37 of non-deuterated and 20 sec deuterated TRXs.

Ions (charge)		Protonated Mass (calculated)	20s deut. Mass (observed)
(Oxi-TRX, peptide 28-39)			
(1+)	b3	387.17	-
	b4	573.25	-
	b5	675.25	-
	b6	732.27	-
	b7	829.32	-
	b8	931.32	935.03
	b9	1059.42	1063.64
	b10	1190.46	1195.01
	b11	1303.54	1308.22
	b12	1374.58	1379.72
(Red-TRX, peptide 28-37)			
(1+)	b3	387.17	388.0
	b4	573.25	-
	b5	676.26	678.08
	b6	733.28	735.81
	b7	830.33	-
	b8	933.34	936.56
	b9	1061.43	1064.83
	b10	1192.47	1196.09

Ions (charge)		Protonated Mass (calculated)	20s deut. Mass (observed)
(GS-TRX, peptide 28-37)			
(1+)	b3	387.17	387.71
	b4	573.25	574.22
	b5	1009.35	1011.22
	b6	1066.38	-
	b7	1163.43	-
(2+)	b8	633.72	635.67
	b9	697.77	699.87
	b10	763.29	765.52
(Glutamic acid missing ions)			
(1+)	b5-E	880.35	881.28
	b8-E	1137.44	1141.38
(2+)	y10-E	707.8	709.5
	b9-E	633.27	636.58
	b8-E	569.22	570.78
(Cys-TRX, peptide 28-37)			
(1+)	b3	387.17	388.99
	b4	573.25	575.8
	b5	823.29	826.25
	b6	880.31	-
	b7	977.37	981.35
(2+)	b8	540.69	543.0
	b9	604.74	607.19
	b10	670.26	672.92

Table 2.8. Deuterium levels found at individual amide linkages in peptide 28-39 (Oxi-TRX) and 28-37 (Red-, GS-, and Cys-TRX) of 20s labeled TRXs.

Residue	Number of Ds on residue				Log k_{ex} (s^{-1})	
	Oxi-TRX	Red-TRX	GS-TRX	Cys-TRX	Oxi-TRX	Red-TRX
31Trp	-	(0.5)	0.5	0.7	-0.55 F	-0.34 F
32Cys	-	(0.5)	0.9	0.4	0.37 F	a M
33Gly	-	0.7	(1.0)	1.0	0.14 F	1.16 F
34Pro						
35Cys	-	0.7	(1.0)	0.6	-5.07 S	0.4 F
36Lys	0.6	0.2	0.3	0.3	a M	a M
37Met	0.3	0.2	0.3	0.4	a M	a M
38Ile	0.1	-	-	-	-4.28 S	-2.82 S
39Ala	0.5	-	-	-	-3.08 S	-2.81 S

In cases of missing fragment ions, the difference of deuterium numbers was equally divided into possible sites as shown in parentheses. [a] The intermediate exchange rates are designated as M, which is in the range 0.0025-0.25 s^{-1} (log value –2.6 to –0.6).

The only difference between the Oxi- and Red-TRX observed in the MS/MS data was found at Lys-36. The deuterium level at this residue was found to be decreased from 0.6 to 0.2 when the disulfide linkage was reduced. There is no obvious explanation that can be gleaned from the NMR data because Lys-36 for both Oxi- and Red-TRX showed an intermediate range exchange rate constant. This decrease is comparable in magnitude with the Cys-35 exchange rate results which showed an increase of more than 5 orders of magnitude between Oxi- and Red-TRX.

The alkylation at Cys-32 by glutathionyl and cysteinyl groups generally resulted in increased deuterium levels for a number of residues close to the active site. Gly-33 which has an extremely large exchange rate constant in Red-TRX had even higher deuterium levels in GS- and Cys-TRX when compared to Red-TRX. The deuterium level of Cys-32 in GS-TRX was expected to be larger than 1 because this residue has three amide hydrogens including two in the

glutathionylated side chain. In comparison with Cys-32 in Cys-TRX which has no amide hydrogens in the cysteinylated side chain, the difference in deuterium level is 0.5, which can be attributed to the two amide linkages in the glutathionyl group at Cys-32 of GS-TRX. This level of deuterium, 0.5 (each 0.25 for two amide linkages in the glutathionyl group) is somewhat low, which means that the exchange rate constants for these two amide hydrogens in the glutathionyl group are small. These results suggest that either one or both amide hydrogens in the glutathionylated side chain at Cys-32 participate in intramolecular hydrogen bonding. Because these two glutathionyl group amide hydrogens are located on the surface of the protein, it is assumed that there is no protection from exposure to the solvent.

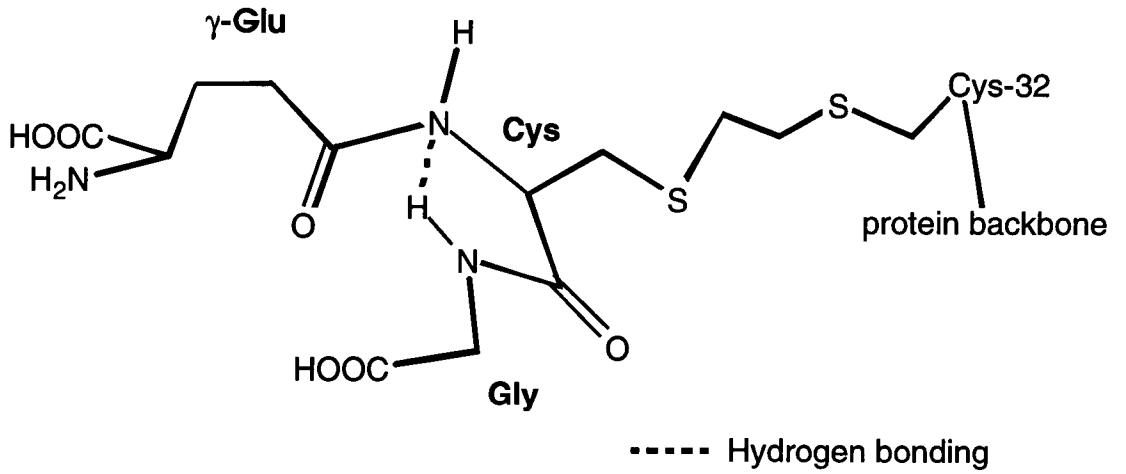

Figure 2.47. Schematic representation of the glutathionyl group in the energy minimized geometry calculated for GS-TRX.

Energy minimized geometries from AMBER force field constant calculations for GS-TRX showed that the Gly NH is hydrogen bonded to the Cys amide nitrogen, and the amide hydrogen of Cys extends towards the outside of the molecule (**Figure 2.47**). From this model, it was assumed that the

deuterium level of 0.5 atom resulted from H/D exchange at the central Cys amide linkage of the glutathionyl group. The exchange rate constant for the Gly amide hydrogen would then be very small.

The deuterium levels found in peptic peptides including residues 45-58 are summarized (**Table 2.9** and **3.20**). MS/MS data for Oxi-TRX for this region were taken from the fragment 45-80 because the precursor ion of fragment 45-58 of Oxi-TRX was so weak that a number of CID fragment ions were not found. Residues 48-50 and 53-58 showed relatively low deuterium levels, while residues 51 and 52 showed high deuterium levels. These results are in fairly good agreement with NMR rate constant data. Residues 48-50 were present in the C-terminal side of the second α-helix, Gly-51 and Lys-52 were found in a turn, and residues 53-58 were found in the third β-strand from the analysis of NMR solution structures of TRX (**Figure 2.48**).[22b] Gly-51 as well as Gly-21 (in **Figure 2.45**) were found in the turn region and showed high deuterium levels and large exchange rate constants. This is consistent with the small size of glycine and with its preference for flexible loop and turn regions in the protein.

Leu-53 and Thr-54 of GS- and Cys-TRX showed somewhat greater levels of deuterium than Oxi- and Red-TRX. This result reflects a marginal distortion or small opening of the core β-strand. However, there is no obvious explanation supporting this result because NMR exchange rate data are not available for the modified TRXs with which to corroborate these results. It is assumed that these results are not directly related to the changes in the acitive site because the active site region and alkylated part are remote from the region that involves residues 45-58 (**Figure 2.48**). At least, it is observed that the alkylation at Cys-32 influences the structure of the nearest part as well as theremote parts of the protein.

Table 2.9. Deuterium levels found at individual amide linkages in peptide 45-58 of 20s labeled TRXs.

Residue	Number of Ds on residue				Log k_{ex} (s^{-1})			
	Oxi-TRX [a]	Red-TRX	GS-TRX	Cys-TRX	Oxi-TRX		Red-TRX	
48Glu	-	0.3	0.1	0.1	-4.31	S	-4.36	S
49Tyr	-	0	-0.2	-0.1	-4.04	S	-4.03	S
50Gln	-	-0.1	0.2	-0.1	-2.85	S	-2.86	S
51Gly	0.8	(0.7) [b]	(0.8) [b]	(0.7) [b]	0.13	F	0.28	F
52Lys	0.5	(0.7) [b]	(0.8) [b]	(0.7) [b]	-0.51	F	-0.19	F
53Leu	0	-0.1	0.4	0.4	-4.62	S	-4.23	S
54Thr	0.1	0	0.3	0.4	-6.54	S	-6.37	S
55Val	-0.1	-0.1	0.2	0	-5.1	S	-5.09	S
56Ala	0	0	0.2	0.1	-8.4	S	-7	S
57Lys	0.2	0.1	0.2	0.2	-5.6	S	-5.66	S
58Leu	0.1	0.2	0.1	0.1	-8.2	S	-7.5	S

[a] Data for Oxi-TRX were taken from a part of the exchange data for peptide 45-80. [b] In cases of missing fragment ions, the difference of deuterium numbers was equally divided into possible sites as shown in parentheses.

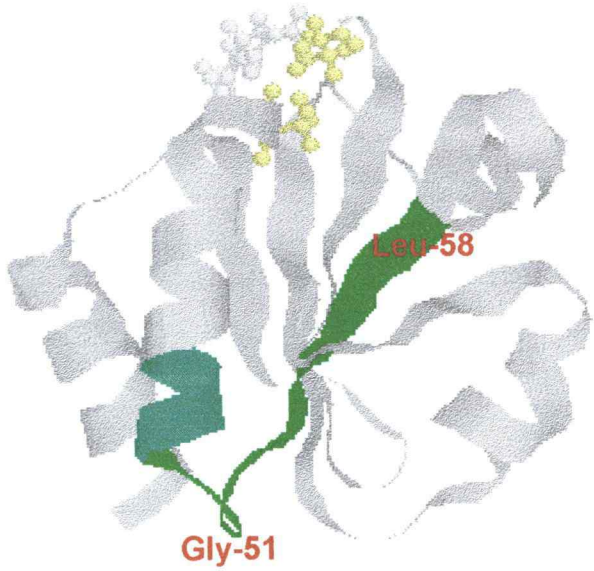

Figure 2.48. NMR solution structure of Oxi-TRX.[12b] A peptide 45-58 is highlighted in green. The active site region is represented as ball and stick, and two cysteine residues are colored in yellow.

Deuterium levels in the regions that include peptides 59-80 for Oxi- and Red-TRX and 59-79 for GS- and Cys-TRX were investigated by CID MS/MS (**Table 2.10** and **3.21**). The *b* ions produced from proline amide linkages were not found because it is very hard to obtain CID fragment ions from this linkage. Ile-75 showed a significant difference in the number of deuteriums incorporated. Only GS-TRX showed low deuterium incorporation on Ile-75 whereas Ile-75 of Red-TRX showed a large exchange rate constant from NMR data and accordingly, the deuterium content at this amino acid in the Red-TRX was high. This residue on GS-TRX can be an important clue to explain the interactions between the glutathionyl group attached at Cys-32 and sites within the protein. In the structure of Oxi-TRX as determined by NMR, Ile-75 is found to be very close to the active site region (**Figure 2.49**). The MS/MS results are very consistent with what one might expect on the basis of the AMBER force field calculations for the structure of GS-TRX (**Figure 2.50** and **2.51**). These calculations indicated that Ile-75 NH is hydrogen bonded to the γ-Glu carbonyl of the glutathionyl group.

Because the b_{13} ion was not observed, the difference in the deuterium content of b_{14} and b_{12} ions were equally divided between Gly-71 and Ile-72 residues. It was assumed that the differences in deuterium numbers between b_{14} and b_{12} ions were derived mainly from Gly-71 because Gly-71 showed medium and large exchange rate constants for Oxi- and Red-TRX, respectively, whereas Ile-72 showed small rate constants for both TRXs. Residues Ile-72 in GS- and Cys-TRX indicated relatively high deuterium levels of about 0.9 deuteriums. This result suggests that there was no protection of the amide hydrogen in Ile-72 from exchange in GS- and Cys-TRX. Similar results were observed at residues Ala-67 and Thr-66 in Cys-TRX and Asn-63 in GS-TRX. These residues had relatively high deuterium levels suggesting there was a loss

of hydrogen bonding. While one can not entirely exclude H/D scrambling, these results suggest there may be more far reaching alterations in the regional conformations of the adducted proteins. The data together in all of these studies (**Table 2.10**) indicate that the deuterium level measured at peptide amide sites is reliable.

Table 2.10. Deuterium levels found at individual amide linkages in fragments 59-79 (GS- and Cys-TRX) and 59-80 (Oxi- and Red-TRX) of 20s labeled TRXs.

Residue	Number of Ds on residue [a]				Log k_{ex} (s^{-1}) [b]			
	Oxi-TRX	Red-TRX	GS-TRX	Cys-TRX	Oxi-TRX		Red-TRX	
62Gln	-	-	0.1	-	-2.72	S	-3.1	S
63Asn	-	0.1	0.5	0.1	-4.8	S	-4.62	S
64Pro	-	-	-	-				
65Gly	0.6	0.9	0.7	0.9	b	M	b	M
66Thr	0.2	0.2	0.1	0.8	-4.36	S	-4.15	S
67Ala	-0.1	0.2	0.2	0.7	-4.66	S	-4.54	S
68Pro	-	-	-	-				
69Lys	0.1	0.1	0.3	0.3	-3.21	S	-3.09	S
70Tyr	0.0	-0.1	0.3	0.2	-5.06	S	-4.91	S
71Gly	(0.3)	(0.4)	(0.9)	(0.9)	b	M	-0.31	F
72Ile	(0.3)	(0.4)	(0.9)	(0.9)	-3.69	S	-3.52	S
73Arg	0.7	0.7	1.0	1.0	-0.14	F	-0.2	F
74Gly	(0.9)	0.8	1.0	1.0	-0.19	F	0.23	F
75Ile	**(0.9)**	**0.8**	**0.1**	**0.9**	b	M	-0.01	F
76Pro	-	-	-	-				
77Thr	0.2	0.3	0.2	0.1	-4.37	S	-3.82	S
78Leu	0.2	0.3	0.1	0.2	-5.74	S	-5.67	S
79Leu	0	0.3	0.2	0.1	-7.6	S	-7.6	S
80Leu	0.1	0.2	-	-	-8	S	-8	S

[a] In cases of missing fragment ions, the difference of deuterium numbers was equally divided into possible sites as shown in parentheses. [b] The intermediate exchange rates are designated as M, which is in the range 0.0025-0.25 s^{-1} (log value –2.6 to –0.6).

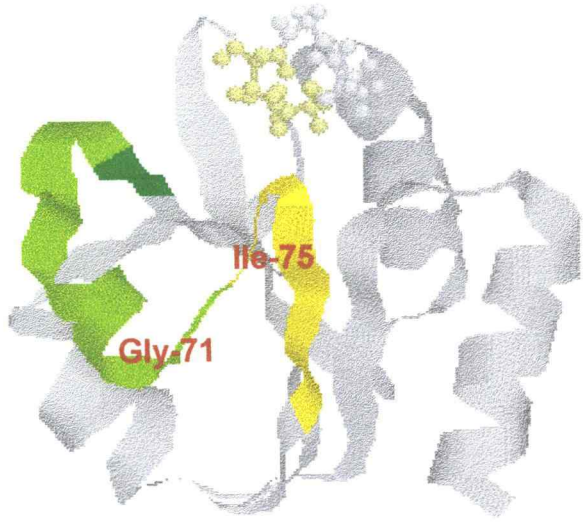

Figure 2.49. The NMR solution structure of Oxi-TRX. A region including residues 59-80 is highlighted in green-yellow. The active site region is represented in ball and stick format, and two cysteine residues are colored in yellow.

Deuterium levels in the C-terminal regions of 20s-labeled TRXs were investigated by CID MS/MS in fragments including peptide 81-108 (**Table 2.11** and **3.22**). For Red-TRX, the peptide 81-101 was used because CID of peptide 81-108 of Red-TRX showed a number of missing ions. NMR data showed that residues 91-98 had medium or large exchange rate constants. Residues 93-98 consist of a long turn region connecting the fifth β-strand to the fourth α-helix (**Figure 2.52**). Although Thr-89 and Val-91 are present in the fifth β-strand of the central β-sheet, they showed very high deuterium levels. The NMR solution structure indicated that amide protons of Thr-89 and Val-91 extend toward the outside of the sheet and are not hydrogen-bonded, so the faster exchange rates

of these residues are not unexpected.[47] Almost all residues showed reasonably good correlation between CID MS/MS data and the NMR rate constant data.

Table 2.11. Deuterium levels found at individual amide linkages in fragments 81-108 (Oxi-, GS- and Cys-TRX) and 81-101 (Red-TRX) of 20s labeled TRXs.

Residue	Number of Ds on residue [a]				Log k_{ex} (s^{-1}) [b]			
	Oxi-TRX	Red-TRX	GS-TRX	Cys-TRX	Oxi-TRX		Red-TRX	
86Val	0	0		-0.2	-2.64	S	-2.57	S
87Ala	-0.1	0	-0.1	0.3	-4.74	S	-4.75	S
88Ala	-0.1	-0.1	(0.3)	0	-4.48	S	-4.48	S
89Thr	0.6	0.4	(0.3)	0.8	-0.6	F	-0.24	F
90Lys	0	-0.1	(0.8)	0	-3.77	S	-3.69	S
91Val	0.6	0.4	(0.8)	0.3	b	M	b	M
92Gly	0.6	0.5	(0.3)	(0.6)	b	M	-0.02	F
93Ala	0.7	(0.7)	(0.3)	(0.6)	-0.59	F	-0.68	F
94Leu	0.9	(0.7)	0.9	0.8	-0.48	F	-0.11	F
95Ser	0.5	0.6	0.7	0.5	b	M	b	M
96Lys	0.8	0.7	0.8	0.9	-0.54	F	-0.6	F
97Gly	(1.0)	(0.8)	0.9	1.0	b	M	-0.08	F
98Gln	(1.0)	(0.8)	(0.5)	1.1	b	M	-0.25	F
99Leu	0.3	0.2	(0.5)	0.1	-3.74	S	-3.84	S
100Lys	(0.2)	-0.1	0.3	(0)	-5.18	S	-5.14	S
101Glu	(0.2)	0	0.2	(0)	-5.62	S	-5.54	S
102Phe	0.1		(0.2)	0.1	-4.26	S	-4.28	S
103Leu	0.2		(0.2)	0.1	-7.51	S	-7.47	S
104Asp	0.2		0.1	0	-6.47	S	-6.41	S
105Ala	0.2		0.2	0.1	-3.94	S	-3.8	S
106Asn	0.1		0.3	0.2	-4.21	S	-4.29	S
107Leu	0.2		0.6	0.2	-3.55	S	-3.35	S
108Ala	0.5		1	0.9	b	M	b	M

[a] In cases of missing fragment ions, the difference of deuterium numbers was equally divided into possible sites as shown in parentheses. [b] The intermediate exchange rates are designated as M, which is in the range 0.0025-0.25 s^{-1} (log value –2.6 to –0.6).

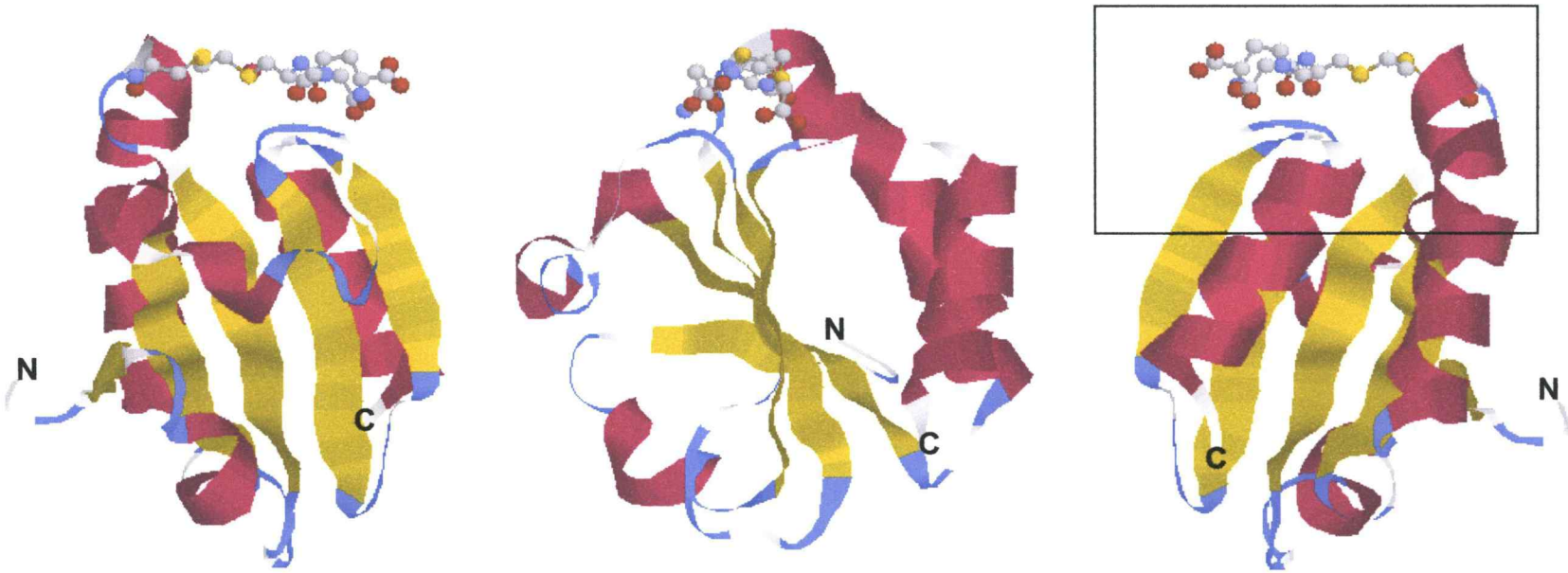

Figure 2.50. Calculated energy-minimized structures of GS-TRX. The glutathionyl group is represented in the ball and stick format (sulfur in yellow, nitrogen in blue, carbon in grey, oxygen in red). The TRX protein is represented as ribbons (α-helices in red, β-sheets in yellow, turns and loops in blue and grey). The structure in the rectangular box in the right view was magnified and is shown in **Figure 2.51**.

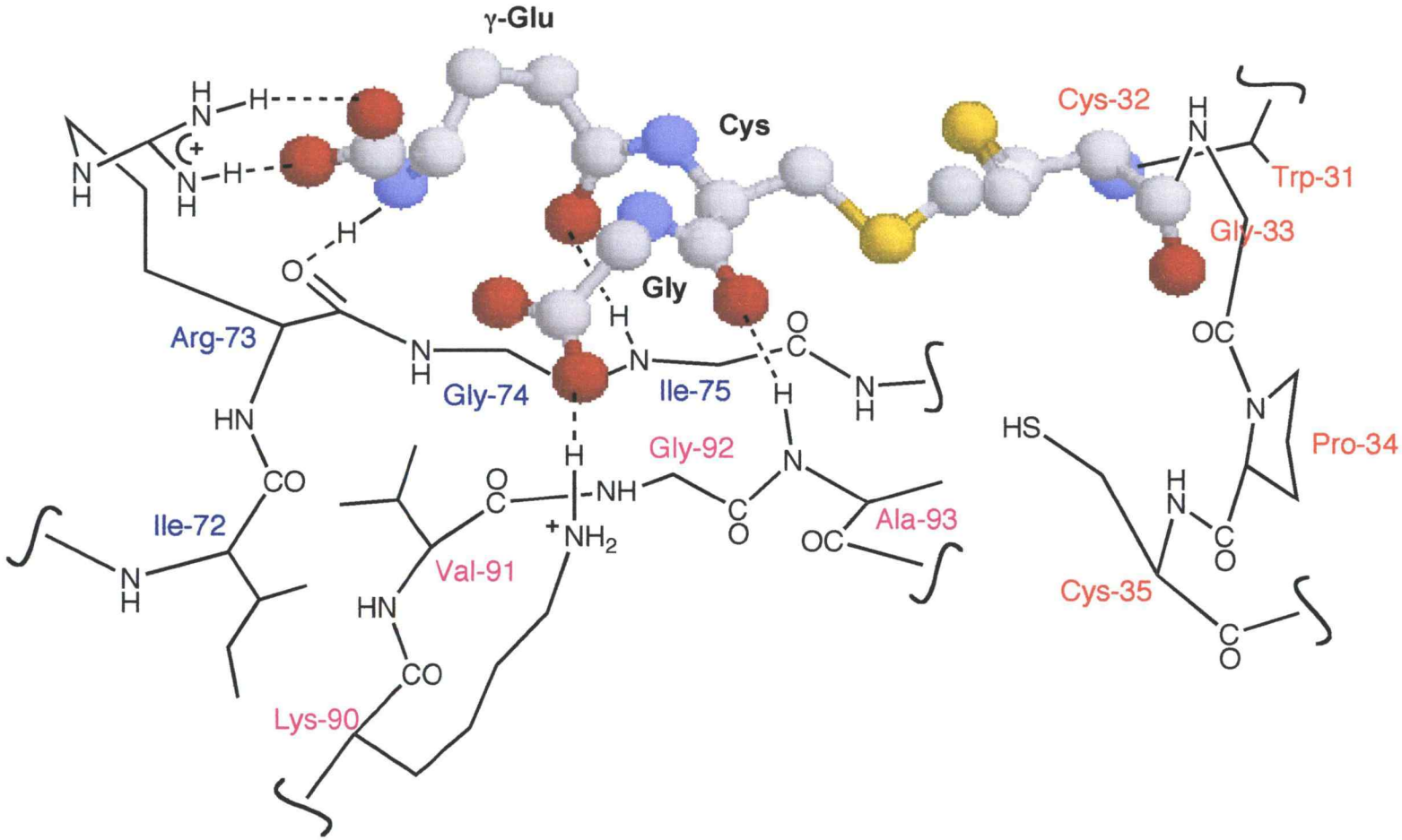

Figure 2.51. Schematic representation showing interactions between the adducted glutathionyl group (ball and stick format; sulfur in yellow, nitrogen in blue, carbon in grey, oxygen in red) and TRX (wire frame). The hydrogen bonds deduced from the calculated structure are illustrated by dashed lines.

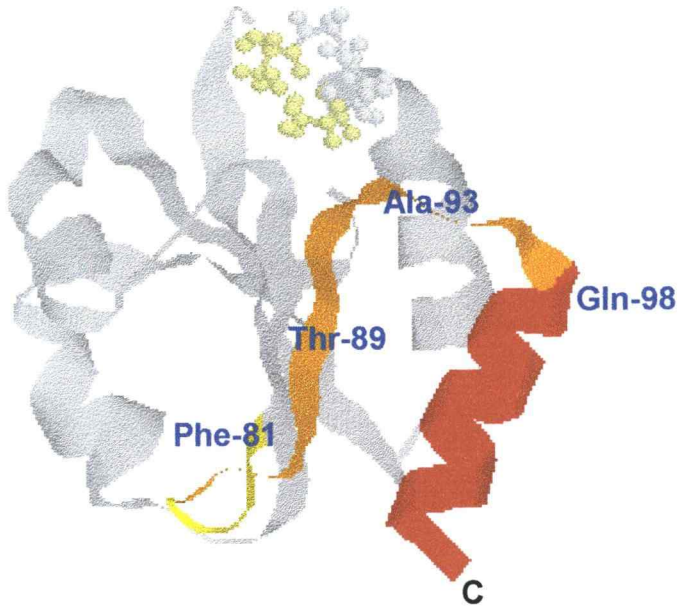

Figure 2.52. The NMR solution structure of Oxi-TRX. A region including residues 81-108 is highlighted in yellow-red. The active site region is represented in ball and stick format, and the two cysteine residues are colored in yellow.

In regions where fast H/D exchange would be expected on the basis of NMR rate constant data, low deuterium content was sometimes observed. The amides where low levels of deuterium were observed could be sites where intramolecular interactions occur between the attached group and the protein. Gly-92 and Ala-93 of GS-TRX and Val-91 of Cys-TRX showed relatively low deuterium levels despite their large exchange rate constants in this region of Red-TRX. Moreover, they are located very close to the active site region where alkylated parts were attached (**Figure 2.51**). Because the b_{12} ion derived from peptide 81-108 of GS-TRX was not found, the difference in the numbers of deuteriums between b_{13} and b_{11} ions, 0.6, was divided equally between Gly-92

and Ala-93, i.e. 0.3 deuteriums each. From the analysis of the calculated energy minimized structure of GS-TRX, it was found that Ala-93 NH is hydrogen bonded to the central Cys carbonyl oxygen of the glutathionyl group attached to Cys-32 (**Figure 2.51**). Thus, it is assumed that the difference in the numbers of deuteriums between b_{13} and b_{11} ions, 0.6, is mainly from Gly-92 which has a large exchange rate constant. In Cys-TRX, Val-91 is responsible for this non-covalent intramolecular interaction because the deuterium level for Val-91 was found to be 0.3 in spite of the medium exchange rate constant. This interaction could result from hydrogen bonding between the carboxylic acid group oxygen of the cysteinyl group attached to Cys-32 and Val-91 NH.

The deuterium levels and peptide amide exchange rate constants of Oxi- and Red-TRX were shown with the primary and secondary structure of TRX (**Figure 2.53**). The *b* ions showed generally good correlations with the exchange rate constants of NMR data. However, this graph shows that CID MS/MS do not always yield complete sequence information for peptides. Usually, intermediate size peptide fragment ions are observed but the smaller ones, i.e., di-, tripeptides, etc., are sometimes missing. As the size of the peptides increase, the completeness of the sequence usually diminishes, and peptides of 30 or more residues almost never yield complete sequence ions. Some information can in principle be obtained for these ions from the reverse direction sequences and possibly from other ion series. The total deuterium content in the stretch of amino acid residues representing the gaps in the sequence, which often involves no more than two or three residues, will, of course, be recorded and the average number of deuteriums per residue can be determined.

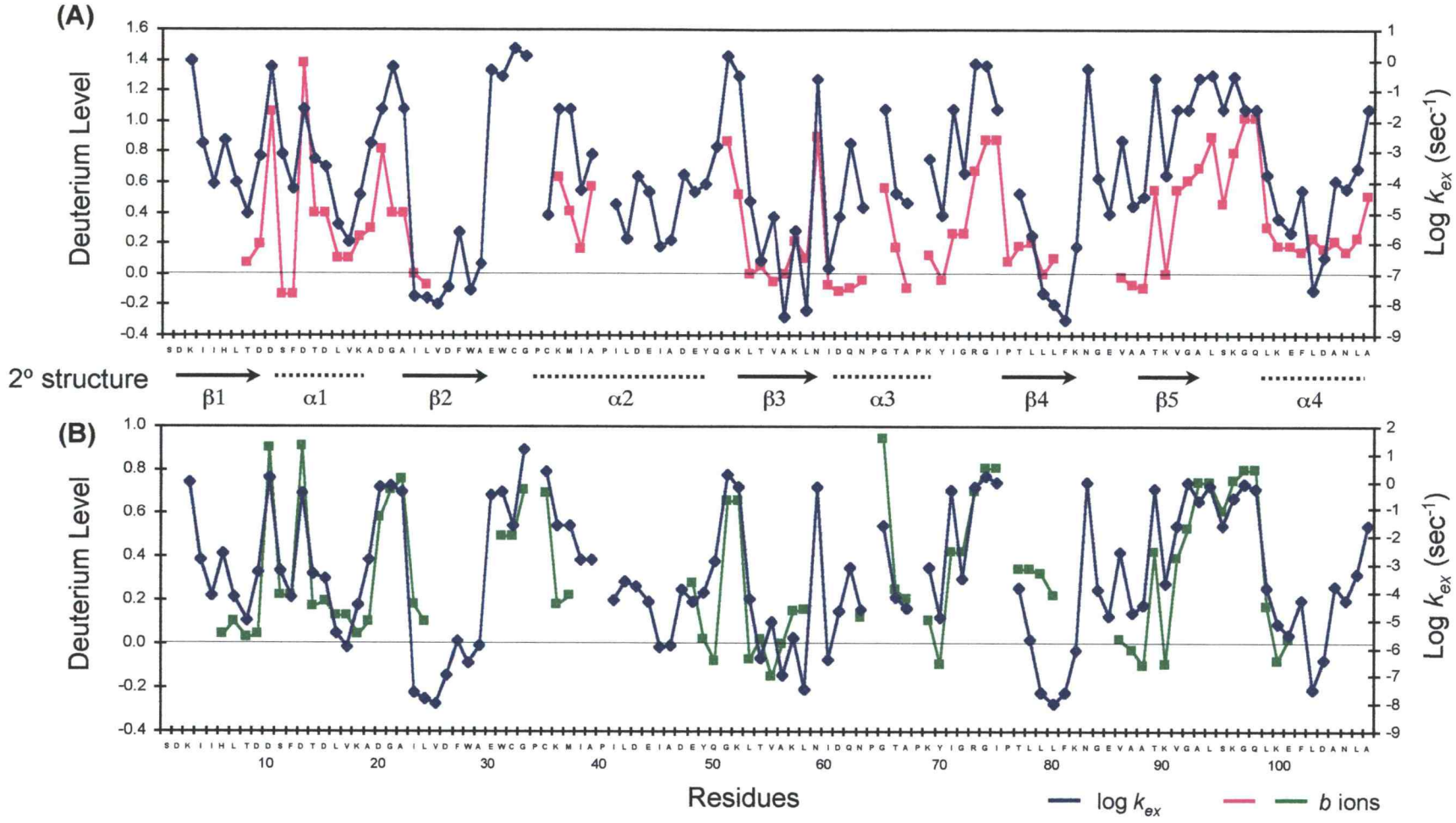

Figure 2.53. The deuterium levels on peptide amide linkages of (A) Oxi-TRX and (B) Red-TRX based on the analysis of *b* ions from CID MS/MS spectra and H/D exchange rate constants from NMR data. H/D exchange rate constants for the intermediate range (logk_{ex} -2.6 to -0.6) were designated with the average value, -1.6.The secondary structures are inserted; β-sheets are designated with arrows and α-helices are shown with dotted lines.

2.3-4 Energy-minimized structure of GS-TRX

The model that was constructed for the GS-TRX places the glutathionyl group on a broad surface formed by two loop structures in the protein (**Figure 2.50** and **2.51**). These loops include the broad turn formed by residues 73-77, and the loop (residues 90 to 93) that connects the fifth β-strand to the fourth α-helix at the C-terminal end of the protein. The effect of the glutathionyl modification on the structure of the protein is minimal between the backbone atoms of the modified and unmodified proteins. The most dramatic conformational change is seen in the rotation of the Arg-73 side chain to form the salt bridge to the γ-Glu of the glutathionyl group.

The resulting model has the two terminal amino acids of the glutathionyl group forming two salt-bridges to basic side-chains of the protein. The carboxylate group of the γ-Glu residue of the glutathionyl group is oriented towards the guanidinium group of Arg-73 in the protein, and the carboxy terminus of the glutathionyl Gly residue towards the amino-side chain of Lys-90 in the protein. This results in a net increase in electrostatic stability of -35 kcal for the modified over the unmodified protein.

In addition, the gluthathionyl group forms three additional hydrogen bonding interactions with the amide nitrogens and amide oxygens of the protein backbone, with the amino terminus of the γ-Glu, the γ-oxygen of γ-Glu, and the keto oxygen of the Cys residues in the glutathionyl group hydogen bonded to the keto oxygen of Arg-73, the amide nitrogen of Ile-75 and the amide nitrogen of Ala-93, respectively, in the peptide backbone of TRX. These hydrogen bonds are estimated to contribute an additional -11.5 kcal of stabilization to the modified protein. Interestingly, the loop that includes Gly 74 and Ile 75 adopt a β-sheet type conformation in the protein (with ϕ and ψ -torsion angles ranging

between -140° and 180°). Thus, the interactions with the γ-Glu of the glutathione extension appear to define a mini-β-sheet at the protein surface. From these interactions, it was predicted that the amide nitrogens of both Ile-75 and Ala-93 would be protected from solvent by the glutathionyl group and, therefore, would show a reduction in their rates of H/D exchange.

2.4 Conclusion

H/D exchange of TRXs in 1% acetic acid was monitored by HPLC-ESIMS. The difference in stability between Oxi- and Red-TRX was clearly demonstrated by thermal denaturation and H/D exchange-in experiments. The rate constants of conversion from folded state to unfolded state were 0.1 and 2.5 min^{-1} for Oxi- and Red-TRX, respectively, at 60 °C. H/D exchange time courses showed 7% difference in deuterium incorporation between Oxi- and Red-TRX. Denaturation curves derived from the charge state distribution showed that Oxi- and Red-TRX have about 15 °C difference in the melting temperature. These results were in close agreement with CD spectral data and comparable to previous NMR data which showed an enhanced flexibility for Red-TRX in the vicinity of the active site. From these global H/D exchange experiments, GS-TRX unambiguously indicated more stabilized structure than Red-TRX. However, Cys-TRX showed almost the same stability with Red-TRX. These results suggest that the intramolecular interactions were induced by the attached glutathionyl group in GS-TRX, and the stabilization by the cysteinyl group attached in Cys-TRX was negligible.

These differences in global H/D exchange were investigated locally by the peptic fragmentation/MS approach. Four component analysis of H/D exchange time courses for each peptide showed dramatic differences in the peptides 28-39 or 28-37. The number of slow exchanging hydrogens changed significantly by the reduction of the disulfide linkage in Oxi-TRX and alkylations, which suggest changes in hydrogen bondings and/or conformations in the active site region. The peptides 59-80 and 81-101 of Oxi- and Red-TRX showed bimodal isotope patterns indicating EX1-type mechanism. This result has very important implications in that even though global H/D exchange showed a stable EX2

mechanism, localized regions may be governed by the EX1 mechanism. However, peptides 59-80 and 81-101 of GS- and Cys-TRX followed the EX2 mechanism. These results suggest that in the region 59-108 there may be some stabilizing effects in the alkylated TRXs. The peptic fragmentation/ESI-MS approach was good for localizing H/D exchange results, but it was still not sufficient to give residue-specific exchange information.

CID MS/MS showed that *b* ions are useful for determining the extent of hydrogen exchange at peptide amide linkages in the protein. MS and NMR data were found to be complementary for determining structural characteristics that involve the exchange of amide hydrogens. The advantages of using MS are that the sensitivity is high (nanomolar or picomolar concentrations of proteins and peptides), large proteins can be analyzed, the time resolution covers a very broad dynamic range, and correlated hydrogen exchange can be detected.

CID MS/MS results for TRXs showed generally excellent correlations with H/D exchange rate constants from NMR data. Strong evidence for noncovalent interactions induced by the glutathionyl group was found at Ile-75 and Ala-93. These residues have unusually low deuterium levels in GS-TRX which is consistent with the expectation from the energy-minimized structure for GS-TRX. Total stabilization energy, -46.5 kcal/mol, calculated from the energy-minimized structure of GS-TRX also supports the increased melting temperature and the reduced rate of conversion of GS-TRX in comparison with Red-TRX.

Although *b* ions are very useful for determining the deuterium levels on individual peptide amide linkages, there were uncertainties in the interpretation of some MS/MS data. First, the missing fragment ions that are attributed to the inability of CID to fragment specific amide linkages poses a unique problem since one cannot determine the level of deuterium at each amide linkage in the intervening sequence. Second, the overlapped multiplets of *b* and *y* ions often

are unresolved so that an accurate calculation of deuterium levels becomes difficult. Third, the intensities of CID fragment ions produced from the C- or N-terminal region in peptides were so weak that it was difficult to obtain well-resolved mass peaks. Accurate measurements of hydrogen exchange rates at individual peptide amide linkages would be possible after the mechanism of CID is better understood.

CHAPTER 3

EXPERIMENTAL

Chemicals. Recombinant *E. coli* thioredoxin (Oxi-TRX) and trypsin were purchased from Promega (Madison, WI). Glutathione, cysteine, pepsin, and iodoacetamide were purchased from Sigma (St. Louis, MO). Trifluoroacetic acid, acetic acid, ammonium bicarbonate, sodium citrate, urea, and formic acid (98%) were purchased from Fluka (Milwaukee, WI). Tris(2-carboxyethyl)phosphine hydrochloride (TCEP.HCl) was purchased from Pierce (Rockford, IL). All deuterated solvents and 1-bromo-2-chloroethane were purchased from Aldrich (Milwaukee, WI). HPLC grade acetonitrile and methanol were purchased from Fisher (Pittsburgh, PA). Water was purified by a Milli-Q reagent water system (Millipore®, Bedford, MA). Protein modification, peptic digestion, and their HPLC fractionation were performed in 1.5 or 0.6 ml Eppendorf tubes. All liquid samples were evaporated on a Savant speed-vac concentrator or freeze-dried on Labconco freeze dry/shell freeze system.

Mass spectrometry. ESI-MS measurements for heat denaturation and global H/D exchange experiments of TRXs were performed on a Perkin-Elmer Sciex API III triple quadrupole mass spectrometer (PE-SCIEX, Thornhill, Ontario, Canada) equipped with a pneumatically assisted electrospray source. Air was used as the nebulizer gas and nitrogen as curtain gas. The collision gas was a mixture of nitrogen and argon in a volume ratio of 9 to 1. A Macintosh Quadra 800 computer was used for instrument control, data acquisition, and processing. MS data for peptide mapping and regiospecific H/D exchange were acquired on a Finnigan LCQ ion-trap mass spectrometer (ThermoQuest, San Jose, CA)

equipped with a Finnigan electrospray source and a home-built microspray source. Xcalibur and MagTran software in IBM PC were used for instrument control, data acquisition, and data processing.

HPLC. Modified TRXs prepared from large-scale syntheses were purified with a Vydac (Hesperia, CA) C4 semi-prep or prep HPLC column. For all HPLC-MS experiments, home-made microbore LC columns were used. For LC separation of peptic peptides at room temperature, a reverse phase column (100 x 0.32 mm) was packed with C18 (Vydac or LUNA) powder with 5 μm pore size. For LC separation of peptic peptides at 0 °C, a longer reverse phase column (200 x 0.32 mm) was packed with larger pore size (15 μm) C18 (LUNA) powder. For HPLC analysis, 0.05% TFA/H_2O was used as eluent A and 0.05% TFA/CH_3CN as eluent B. HPLC instrumentation consisted of a Waters (Milford, MA) automated gradient controller, two Waters 515 HPLC pumps for solvent A and B, and Waters 2487 dual λ absorbance detector. For microbore HPLC analysis, a Waters HPLC system equipped with Rheodyne (Cotati, CA) model 8125 injector and an ABI Spectroflow 783 programmable absorbance detector was used. A Harvard Apparatus (South Natick, MA) syringe pump was used to obtain a flow rate of 0.3-0.5 ml/hr. Fused silica capillary tubing with dimensions of 75 μm i.d. x 145 μm o.d. or 50 μm i.d. x 148 μm o.d. (Polymicro Technologies, Phoenix, AZ) was used to couple the liquid effluent to the ESI mass spectrometer.

UV and CD. UV absorption spectra were recorded with a Cary 15 instrument, purged with nitrogen in the far UV region. CD spectra were recorded on a Jasco J720 spectropolarimeter equipped with a home-built thermoelectrically controlled cell holder. The CD instrument was calibrated with 0.1% *d*-10-camphorsulfonic acid (w/v in deionized water) according to the procedure of Chen and Yang.[54] In UV and CD experiments, a Hellma cylindrical cell with a 0.1 mm or 1 cm path length was used.

3.1 Alkylation of *E. coli* thioredoxin and identification of the adducts

3.1-1 Synthesis of alkylating agents

***S*-(2-Chloroethyl)glutathione (CEG)** was synthesized by dissolving 0.1 g (0.32 mmol) of glutathione in 2.5 ml of methanol to which 0.024 g (1.08 mmol) of sodium was added. The solution was stirred until glutathione was completely dissolved, and then it was added dropwise to a stirred solution of 0.46 g (3.2 mmol) of 1-bromo-2-chloroethane in 2.5 ml of methanol. The reaction mixture was stirred for 1 h and then 0.056 ml of acetic acid was added, and the resulting precipitate was collected by centrifugation. After drying, 95 mg of white solid was recovered and stored at 4 °C in a desiccator. Reverse-phase HPLC analysis showed that 70% of the isolated mass was the desired product. The molecular weight (calc. 369.83) was determined by mass spectrometry, which showed *m/z* values of 369.8 and 371.8 whose ratios were consistent with a molecule containing one chlorine atom. The final product was used for alkylation of the protein without further purification.

***S*-(2-Chloroethyl)cysteine (CEC)** was synthesized by dissolving 0.1 g (0.825 mmol) of L-cysteine in 2.5 ml of methanol to which 0.06 g (2.5 mmol) of sodium was added. After cysteine was completely dissolved, the solution was added dropwise to a stirred solution of 1.2 g (8.3 mmol) of 1-bromo-2-chloroethane in 3 ml of methanol. The reaction was stirred for 1 h, and 0.056 ml of acetic acid was added to the solution. The resulting precipitate was collected by centrifugation. After drying, 80 mg of white product was isolated by the same manner and stored at 4 °C in a desiccator. HPLC analysis showed that 65% of the isolated mass was the desired product.

3.1-2 Reduction and alkylation of *E. coli* thioredoxin by CEG and CEC

Reduction of thioredoxin. The disulfide linkage of *E. coli* thioredoxin (200 μg, 0.02 μmol) was reduced by addition of 17 μl of 8 mM Tris(2-carboxyethyl) phosphine hydrochloride (TCEP.HCl) and incubated for 10 min to yield a 1.2 mM solution of reduced thioredoxin. The reaction was monitored by reverse-phase HPLC.

Modification of thioredoxin by the episulfonium ion of CEG and CEC. Aliquots of reduced thioredoxin (17 μl) were mixed with equal volumes of 0.4 M ammonium bicarbonate buffer (pH 7.7). CEG (265 μg of white solid; actual 184 μg, 0.5 μmol, 25 eq.) was dissolved in 33 μl of 0.4 M ammonium bicarbonate buffer (pH 7.7) and quickly added to the thioredoxin solution. The pH dropped slightly with the addition of CEG so that the pH of the reaction mixture was between 7.0 and 7.4. The reaction was monitored by reverse-phase HPLC. The reaction mixtures were incubated for 90 min at room temperature. More CEG (265 μg x 2) was added until the reduced thioredoxin was completely consumed. (*S*-[2-(Cys^{32})ethyl]glutathione)thioredoxin (GS-TRX) was isolated by preparative reverse-phase HPLC on a C4 column (250 x 10 mm, 5 μm, Vydac, Hesperia, CA). The elution gradient was linear from 20% B to 40% B in 10 min, then to 50% B over 15 min, and finally to 70% B in 10 min; the flow rate was 2.5 ml/min. Solvent A was 0.1% TFA/H_2O, and solvent B was 0.1% TFA/CH_3CN. After freeze-drying the collected eluent, 144 μg (70%) of GS-TRX was obtained. (*S*-[2-(Cys^{32})ethyl]cysteine)thioredoxin (Cys-TRX) was prepared from CEC by the same procedure. After HPLC purification and drying, 160 μg (80%) of Cys-TRX was obtained.

3.1-3 Identification of modified sites in the alkylated TRXs by ESI-MS/MS

Tryptic digestion. The freeze-dried GS-TRX (50 μg) was dissolved in 15 μl of 0.4 M ammonium bicarbonate buffer (pH 7.8) and treated with 5 μl of 8 mM TCEP to minimize dimerization. Free thiols were alkylated by adding 5 μl of 50 mM iodoacetamide and incubating at room temperature for 10 min. To denature the protein, 20 μl of 10 M urea (50mM TRIS buffer, pH 8.5) was added. Sequencing grade trypsin (10 μg) was dissolved in 10 μl of 10 mM HCl, and 2 μg was added to the sample. The concentration of urea was reduced to about 2 M with the addition of 45 μl of H_2O. The mixture was incubated for 5 h at 37 °C and put into the freezer until MS analysis.

Peptic digestion. The freeze-dried GS-TRX or Cys-TRX (30 μg) was dissolved in 30 μl of 0.1 M citrate buffer (pH 3.0). To denature the protein, 22 μl of 10 M urea (0.1 M citrate buffer, pH 3.0) was added to the protein solution, which was incubated for 15 min at room temperature. Pepsin (10 μg) was dissolved in 100 μl of 5% formic acid and 3.3 μg (33 μl) of pepsin was added to the protein solution. Digestion was allowed to proceed for 4 h at 37 °C.

HPLC-tandem mass spectrometry. Peptide mapping of the tryptic and peptic digests was accomplished by reverse phase HPLC on a Vydac C18 column (100 x 1 mm, 5 μm pore size) and Perkin-Elmer Sciex API III plus triple-quadrupole mass spectrometer (Sciex, Thornhill, Canada). The elution gradient was increased linearly at a flow rate of 10 μl/min from 10% B to 40% B in 20 min, then to 60% B over 30 min, and finally to 90% B in 5 min. Solvent A was 0.05% TFA in H_2O, and solvent B was 0.05% TFA in CH_3CN. Small aliquots of digests (5 μl) were introduced via an injector fitted with a 5 μl sample loop. Molecular ions selected by

the first quadrupole of the mass spectrometer were introduced to dissociate by colliding them at an energy of 25 eV with argon (2.5×10^{14} molecules/cm^2) in the second quadrupole, and the resulting fragment ions were mass analyzed in the third quadrupole. The ionspray capillary was maintained at 5300 V, and the orifice voltage was held at 90 V. The doubly charged molecular ion of the peptide 28-37 of GS-TRX had a mass (*m/z*) 772.4. The masses (*m/z*) of the CID fragment ions of precursor ion, *m/z* 772.4, are summarized with their calculated values (**Table 3.1**). CID fragment ions of doubly charged precursor ion, *m/z* 680.0, of peptide 28-37 of Cys-TRX are summarized (**Table 3.2**).

Table 3.1. CID fragment ions of peptic peptide 28-37 of GS-TRX

Ions	Calculated mass	Observed mass
b2	258.12	258.0
b3	387.17	387.2
b5	1009.35	1009.2
y2	278.15	278.4
y3	381.16	381.2
y4	478.22	478.0
y5	535.24	535.2
y6	971.35	971.2
y7	1157.43	1157.6
y8	1286.47	1286.8
y9	1357.5	1358.0
y6-E*	842.25	842.0
y7-E*	1028.33	1028.8
y8-E*	1157.37	1158.8
y9-E*	1228.4	1228.4

* CID fragment ions resulted from Glutamic acid (E) loss from the glutathionyl group attached to Cys-32.

Table 3.2. CID fragment ions of peptic peptide 28-37 of Cys-TRX

Ions	Calculated mass	Observed mass
b2	258.12	258.0
b3	387.17	387.2
y4	478.22	478.0
y5	535.24	534.8
y6	785.28	785.2
y7	971.36	972.4
y8	1100.4	1101.2
y9	1171.44	1172.8

3.1-4 Sample pretreatment of LC-purified modified TRXs

The theoretical basis and experimental details for this section are described under the heading 'analyses of bimodal charge state distributions' (**chap. 2.2-3 and 3.2-3**). Temperature dependent variation of F/(F+U) for GS-TRX before and after 45 °C equilibration has been summarized (**Table 3.3**).

Table 3.3. Temperature dependent variation of F/(F+U) for GS-TRX before and after 45 °C equilibration

Before 45 °C equilibration		After 45 °C equilibration	
Temp.(°C)	F/(F+U)	Temp.(°C)	F/(F+U)
		22	0.81
22	0.465	30	0.825
30	0.505	40	0.815
36	0.55	45	0.8
40	0.66	48	0.745
45	0.73	50	0.69
50	0.63	54	0.58
54	0.49	55	0.51
64	0.41	58	0.45
73	0.385	63	0.42
85	0.37	67	0.39
		76	0.4
		85	0.38

3.2 Thermal denaturation of thioredoxin and its derivatives (TRXs)

3.2-1 Online H/D exchange/ESI-MS experiment

Oxi-TRX, GS-TRX, and Cys-TRX (10 μg/μl, 0.85 mM) were dissolved in 1% AcOH/H_2O (pH 2.6). Red-TRX solution (10 μg/μl, 0.85 mM) was obtained by dissolving Oxi-TRX in 8 mM TCEP/1% AcOH/H_2O. TRX solutions were allowed to equilibrate for 100 min at 25 °C (equilibration solution). The equilibration solutions were diluted 50-fold with 1% AcOD/D_2O (labeling solution) at 0 °C. Immediately, 50 μl of diluted solution was introduced into a Rheodyne injection valve fitted with a 40 μl sample loop by pre-cooled syringe. The sample loop (peek tubing i.d. 0.01 in., o.d. 1/16 in., 65 cm) was used as a reaction capillary. The solvent delivery line, the sample loop, and the injection valve were immersed in a water bath and equilibrated at the desired temperature between 25 and 80 °C (**Figure 2.9**). As soon as the sample was injected into the sample loop, the protein solution in the sample loop was transferred into the ESI source via a fused silica capillary (i.d. 0.075 mm, 100 cm) which was immersed in an ice water bath to quench H/D exchange and to facilitate refolding of thermally unfolded TRX. The solvent flow (0.5 ml/hr) was maintained with a syringe pump and a solvent mixture of 1% AcOD/D_2O. MS data were obtained on a PE-Sciex API III triple quadrupole mass spectrometer. The ionspray voltage was at 4700 V, and the orifice voltage was at 80 V. Data were acquired in the range of *m/z* 1250 to 1800. The time necessary for the transport of the protein from the sample loop to the ESI needle was approximately 60 ± 5 sec. The incubation periods reported represent the time that the protein sample spent in the sample loop. The time-dependent alteration of bimodal 8-fold charged molecular ion peak of TRXs at 50, 55, and 60 °C are summarized (**Table 3.4-3.6**).

Table 3.4. Time-dependent changes of bimodal 8-fold charged molecular ion peak of TRXs in 1% AcOD/D_2O at 50 °C

Time (sec)	Intensity		f/(f+u)
	f	u	
(Red-TRX)			
10	1210300	141730	0.895
40	1029600	248070	0.806
85	947720	375520	0.716
109	801400	388560	0.673
125	584930	402700	0.592
170	573866	470794	0.549
208	510150	565710	0.474
250	356620	587810	0.378
274	306690	508510	0.376
(GS-TRX)			
10	228830	24412	0.904
40	243610	34159	0.877
85	227880	62780	0.784
109	224180	82987	0.730
125	238420	85741	0.735
170	189200	92869	0.671
208	189340	109820	0.633
250	140870	90423	0.609
274	98928	60208	0.622
307	52677	40191	0.567
(Cys-TRX)			
10	79821	10435	0.884
40	78808	18863	0.807
85	55031	23297	0.703
109	76703	38367	0.667
125	47252	36955	0.561
170	50803	68150	0.427
208	48166	58738	0.451
250	22182	30457	0.421
274	15381	24944	0.381

Table 3.5. Time-dependent changes of bimodal 8-fold charged molecular ion peak of TRXs in 1% AcOD/D_2O at 55 °C

time (sec)	Intensity		f/(f+u)
	f	u	
(Red-TRX)			
10	736470	126620	0.853
22	662630	227700	0.744
34	403170	294070	0.578
46	346850	460330	0.430
58	211640	368990	0.365
70	157140	539760	0.225
82	156500	629570	0.199
94	140720	641430	0.180
106	68527	764830	0.082
118	109740	776080	0.124
(GS-TRX)			
10	181850	20981	0.897
34	149930	45743	0.766
58	121770	77015	0.613
82	99161	105630	0.484
106	92246	150880	0.379
130	41061	184570	0.182
154	70853	233760	0.233
178	79140	243140	0.246
202	41476	265660	0.135
226	56045	270240	0.172
250	40253	213420	0.159
(Cys-TRX)			
10	91362	18744	0.830
22	88977	30682	0.744
34	58809	37760	0.609
46	71775	90715	0.442
61	39715	109260	0.267
70	38957	84301	0.316
82	26688	94627	0.220
94	17542	100940	0.148
106	22461	116230	0.162
118	14700	131100	0.101

Table 3.6. Time-dependent changes of bimodal 8-fold charged molecular ion peak of TRXs in 1% AcOD/D_2O at 60 °C

Time (sec)	Intensity		f/(f+u)
	f	u	
(Oxi-TRX)			
43	1538700	196060	0.887
76	1378300	384730	0.782
109	1554800	294770	0.841
142	1375600	614940	0.691
175	1344000	720550	0.651
208	1275100	760220	0.626
241	1081800	598500	0.644
274	778960	457810	0.630
307	473820	403040	0.540
(Red-TRX)			
10	350930	66500	0.841
19	543530	227480	0.705
28	352770	410850	0.462
37	107260	512560	0.173
46	83228	592040	0.123
55	78522	588030	0.118
64	96483	633480	0.132
(GS-TRX)			
10	149970	26094	0.852
19	129160	41198	0.758
28	100450	64819	0.608
37	71546	83124	0.463
46	53705	88664	0.377
55	36157	137910	0.208
64	23122	164020	0.124

3.2-2 Offline H/D exchange/ESI-MS experiments

Oxi-TRX, GS-TRX, and Cys-TRX (10 μg/μl, 0.85 mM) were dissolved in 1% AcOH/H_2O (pH 2.6). Red-TRX solution (10 μg/μl, 0.85 mM) was obtained by dissolving Oxi-TRX in 8 mM TCEP/1% AcOH/H_2O. TRX solutions were allowed to equilibrate for 100 min at 25 °C (equilibration solution). H/D exchange was initiated by diluting the equilibration solution 50-fold with 1% AcOD/D_2O at 25 °C (labeling solution). At each time point, 5 μl (0.43 nmol) of labeling solution was introduced into an injection valve fitted with a 5 μl sample loop by a precooled syringe. The sovent delivery line, the sample loop, and the injection valve were immersed in an ice-water bath to minimize H/D exchange of all exchangeable hydrogens during infusion into the mass spectrometer. The solvent flow (0.3 ml/hr) was maintained with a syringe pump and a solvent mixture of 1% AcOD/D_2O. The molecular weight of deuterium labeled TRXs was calculated from the 7-, 8-, and 9-fold charged molecular ions by using eq (11). The percentage of deuterium incorporation for Oxi-, Red-, GS-, and Cys-TRX was calculated by eq (7) (**Table 3.7-3.10**).

Table 3.7. Percent deuterium incorporated onto Oxi-TRX after exchange-in in 1% AcOD/D_2O at 25 °C

Time (sec)	Molecular ions			Average MW	% of D incorporation*
	7+ ion	8+ ion	9+ ion		
0.5	1674.6	1465.7	1303.3	11709.8	20.92
2.5	1675.8	1466.9	1304.3	11718.8	26.09
4	1676.5	1467.4	1304.8	11723.3	28.64
4.5	1676.8	1467.6	1305.0	11725.2	29.74
6	1676.8	1467.8	1305.2	11726.2	30.32
6.5	1677.3	1468.1	1305.4	11728.7	31.75
8.5	1677.7	1468.4	1305.6	11731.3	33.23
9.5	1677.4	1468.3	1305.6	11730.2	32.62
11	1677.8	1468.7	1305.8	11732.5	33.94
12	1677.8	1468.5	1305.7	11732.1	33.71
13	1678.1	1468.7	1306.1	11734.3	34.98
14	1678.1	1468.7	1306.1	11734.5	35.07
15	1678.3	1468.9	1306.1	11735.5	35.65
16	1678.5	1469.1	1306.4	11737.2	36.67
18	1678.3	1468.9	1306.3	11736.0	35.96
33	1679.0	1469.6	1306.8	11740.9	38.78
35	1678.8	1469.4	1306.7	11739.5	37.96
40	1678.9	1469.5	1306.6	11740.0	38.25
60	1679.7	1470.1	1307.3	11745.3	41.27
68	1679.8	1470.2	1307.5	11746.5	41.99
82	1679.8	1470.4	1307.5	11747.0	42.25
98	1680.1	1470.7	1307.8	11749.5	43.71
125	1680.5	1470.9	1307.9	11751.3	44.76
143	1680.7	1471.0	1308.1	11752.6	45.49
175	1681.1	1471.8	1308.1	11755.8	47.35
188	1681.3	1471.8	1308.5	11757.3	48.2
254	1681.6	1472.0	1308.9	11759.5	49.46

* The molecular weight of undeuterated Oxi-TRX is 11,673.4.

Table 3.8. Percent deuterium incorporated onto Red-TRX after exchange-in in 1% AcOD/D_2O at 25 °C

Time (sec)	Molecular ions			Average MW	% of D incorporation*
	7+ ion	8+ ion	9+ ion		
0.5	1675.9	1466.5	1303.9	11716.8	23.45
2	1677.4	1467.9	1305.2	11727.8	29.72
3.5	1678.1	1468.9	1305.6	11733.2	32.79
6	1678.6	1469.0	1306.3	11736.7	34.77
8	1678.9	1469.2	1306.4	11738.4	35.72
10	1679.1	1469.6	1306.8	11741.0	37.22
14	1679.7	1470.0	1307.0	11744.5	39.19
18	1680.3	1470.3	1307.0	11746.6	40.36
25	1680.7	1470.7	1307.4	11749.7	42.13
28	1680.5	1470.6	1307.3	11748.7	41.59
31	1680.9	1470.9	1307.6	11750.9	42.83
40	1681.0	1471.0	1308.0	11752.8	43.91
53	1681.2	1471.5	1308.4	11755.9	45.64
65	1681.4	1471.6	1308.9	11758.2	46.97
76	1681.5	1471.7	1309.0	11758.8	47.29
82	1681.9	1472.3	1309.0	11761.4	48.78
98	1682.2	1472.3	1309.2	11762.9	49.66
125	1682.3	1472.6	1309.5	11765.0	50.81
138	1682.8	1472.5	1309.4	11765.3	51.00
155	1682.9	1472.7	1309.7	11767.1	52.00
178	1683.3	1472.9	1309.7	11768.6	52.84
194	1682.8	1473.3	1309.9	11769.2	53.21
250	1683.0	1474.0	1310.0	11771.4	54.45

* The molecular weight of undeuterated Red-TRX is 11,675.5.

Table 3.9. Percent deuterium incorporated onto GS-TRX after exchange-in in 1% AcOD/D_2O at 25 °C

Time (sec)	Molecular ions			Average MW	% of D incorporation*
	7+ ion	8+ ion	9+ ion		
0.5	1722.6	1507.9	1340.8	12046.9	21.04
2	1724.0	1509.1	1342.0	12056.8	26.47
4	1724.8	1509.7	1342.4	12061.6	29.12
6	1725.4	1510.1	1342.9	12065.5	31.31
8	1725.7	1510.6	1343.2	12068.5	32.95
12	1726.4	1511.1	1343.6	12072.4	35.12
14	1726.7	1511.0	1343.8	12073.7	35.81
16	1726.9	1511.3	1344.0	12075.7	36.90
18	1727.2	1511.4	1344.2	12077.0	37.63
23	1727.2	1511.8	1344.4	12078.9	38.68
35	1727.6	1511.8	1344.7	12080.4	39.52
45	1728.3	1511.8	1345.1	12083.3	41.12
52	1728.3	1512.0	1345.2	12084.1	41.54
69	1728.5	1512.3	1345.4	12085.9	42.57
76	1728.8	1512.9	1345.8	12089.4	44.52
92	1728.9	1512.9	1345.8	12089.9	44.77
105	1729.2	1513.4	1345.6	12091.0	45.37
115	1729.1	1513.5	1345.7	12091.7	45.77
134	1729.3	1513.6	1345.9	12092.9	46.42
152	1729.6	1513.9	1345.9	12094.7	47.40
172	1730.0	1514.0	1346.0	12096.0	48.14
203	1730.2	1514.2	1346.5	12098.5	49.52
251	1730.3	1514.5	1346.5	12099.4	50.02

* The molecular weight of undeuterated GS-TRX is 12,008.8.

Table 3.10. Percent deuterium incorporated onto Cys-TRX after exchange-in in 1% AcOD/D_2O at 25 °C

Time (sec)	Molecular ions			Average MW	% of D incorporation*
	7+ ion	8+ ion	9+ ion		
0.5	1696.1	1484.4	1320.0	11860.2	21.06
2	1697.2	1485.5	1320.9	11868.2	25.58
4	1698.3	1486.2	1321.4	11874.2	28.92
6	1698.7	1486.6	1321.9	11877.6	30.87
8	1698.8	1486.8	1322.3	11879.7	32.03
10	1699.3	1487.3	1322.5	11882.6	33.68
14	1699.6	1487.6	1322.7	11884.9	34.94
18	1700.3	1488.0	1323.2	11889.0	37.24
23	1700.8	1488.4	1323.6	11892.2	39.04
29	1700.9	1488.8	1323.6	11893.8	39.95
45	1701.3	1489.2	1324.3	11897.5	42.04
52	1701.1	1489.3	1324.1	11896.9	41.71
58	1701.2	1489.2	1324.3	11897.4	41.96
75	1701.8	1489.5	1324.8	11901.1	44.03
86	1702.1	1489.4	1324.7	11901.2	44.08
100	1702.9	1489.7	1324.0	11902.0	44.53
105	1702.3	1489.7	1325.0	11903.6	45.48
115	1702.5	1489.9	1325.5	11906.2	46.91
123	1702.8	1490.2	1325.2	11906.5	47.08
144	1702.8	1490.3	1325.3	11907.3	47.53
175	1703.5	1490.6	1325.5	11910.4	49.26
244	1703.7	1490.8	1325.9	11912.5	50.42

* The molecular weight of undeuterated Cys-TRX is 11,822.7.

3.2-3 Analyses of bimodal charge state distributions

Oxi-TRX, GS-TRX, and Cys-TRX (0.2 μg/μl, 0.017 mM) were dissolved in 1% AcOH/H_2O (pH 2.6). Red-TRX solution (0.2 μg/μl, 0.017 mM) was obtained by diluting Red-TRX stock solution (0.85 mM in 8 mM TCEP/1% AcOH/H_2O) 50-fold with 1% AcOH/H_2O. Protein solutions (50 μl) were introduced into a Rheodyne injection valve fitted with a 40 μl sample loop. The solvent delivery line, the sample loop, and the injection valve were immersed in a water bath and equilibrated at the desired temperature between 25 and 80 °C. After the protein solutions were incubated for 2 min in the sample loop, they were transferred into the ESI source. The solvent flow (0.5 ml/hr) was maintained with a syringe pump and a solvent mixture of 1% AcOH/H_2O. F/(F+U) was determined as a function of temperature.

Table 3.11. Temperature dependent variation of F/(F+U) of TRXs in 1% AcOH/H_2O

Temp (°C)	F/(F+U)			
	Oxi-TRX	Red-TRX	GS-TRX	Cys-TRX
30	0.889	0.662	0.815	0.685
40	0.892	0.65	0.831	0.692
45	0.89	0.652	0.812	0.675
50	0.9	0.582	0.79	0.64
53	0.895	0.511	0.728	0.57
56	0.886	0.393	0.619	0.468
60	0.868	0.351	0.46	0.403
65	0.757	0.33	0.395	0.38
68	0.604	0.328	0.4	0.385
72	0.515	0.334	0.39	0.375
76	0.49	0.325	0.405	0.372
80	0.504	0.319	0.41	0.389

3.2-4 Spectroscopic experiments : UV absorption and circular dichroism

UV spectra of TRXs (34.1 μM, 1% AcOH/H_2O) were measured in the near-UV range (240-350 nm) at 25 °C. Protein solutions were placed in square 1 cm path length quartz cuvettes. The TRX solution concentration was determined by using a molar extinction coefficient of 13,700 $M^{-1}cm^{-1}$ at 280 nm.

Far-UV CD spectra of TRXs (34.1 μM, 10 mM TRIS.HCl, pH 2.5) were measured in the far-UV range (184-260 nm) in cylindrical 0.1 mm path length quartz cuvettes and with a bandwidth of 2 nm and a scan speed of 10 nm/min.

Near-UV CD spectra of TRXs (34.1 μM, 1% AcOH/H_2O) were measured in the near-UV range (250-360 nm) in cylindrical 1 cm path length quartz cuvettes. The temperature control of the sample cell was maintained by circulating water from a thermostatically controlled water bath through a built-in water jacket sleeve that is mounted around the CD cell. Temperature readings were measured online with a thermocouple element glued to the outside of the cuvette wall. Cuvettes were allowed a 5-min equilibration period after reaching the desired operating temperature before scanning. The temperature was manually increased from 25 to 80 °C. Equilibrium thermal denaturation of TRXs was monitored at 280 nm. All spectra were smoothed with software provided with the instrument and base line-corrected for the CD signal in the absence of protein.

The mean residue molar ellipticity $[\theta]_\lambda$ at a given wavelength was calculated according to eq (13):

$$[\theta]_\lambda = \frac{(MW/n)\theta_\lambda}{100[P]l} \qquad (13)$$

where θ_λ is the observed ellipticity in degrees, *MW* is the molecular weight of TRXs, n is the number of residues (n = 108), [P] is the protein concentration in mol dm^{-3}, and l is the path length in centimeters. The thermal denaturation of TRXs was observed by near UV-CD experiments (**Table 3.12**).

Table 3.12. Temperature dependent variation of the mean residue molar ellipticity at 280 nm, $[\theta]_{280}$, of TRXs in 1% AcOH/H_2O

Temp. (°C)	$[\theta]_{280} \times 10^{-2}$			
	Oxi-TRX	Red-TRX	GS-TRX	Cys-TRX
25	2.158	1.733	1.158	1.059
30	2.054	1.574	1.076	0.950
34	-	1.402	1.001	0.869
38	1.767	1.183	0.932	0.821
43	1.701	0.604	0.854	0.728
48	1.621	0.169	0.677	0.422
53	1.446	0.032	0.232	-0.064
57	1.144	-0.038	-	-0.200
61	0.544	-0.143	-0.239	-0.309
65	-0.022	-	-0.278	-
68	-0.235	-	-0.340	-0.348
72	-0.369	-	-0.334	-
76	-0.397	-	-	-

3.3 Structural features of TRXs analyzed by H/D exchange

3.3-1 Peptide mapping and sequencing of TRXs

Oxi-TRX, GS-TRX, and Cys-TRX (1 μg/μl, 85 μM) were dissolved in 1% AcOH/H_2O (pH 2.6). Red-TRX solution (1 μg/μl, 85 μM) was obtained by dissolving Oxi-TRX in 8 mM TCEP/1% AcOH/H_2O. Pepsin solution was prepared by dissolving pepsin (3 μg/μl) in 5% formic acid. The solution was stored at 0 °C until used. TRX was digested by mixing 5 μl (5 μg) of protein solution with 1 μl (3 μg) of pepsin solution and incubating for 5 min at 0 °C. For the peptic digests, 5 μl of digest was loaded onto a C18 column (Vydac, 100 x 0.32 mm, 5 μm). The Rheodyne injector, column, and transfer line were immersed in an ice bath (0 °C) for low-temperature separation. The resulting peptides were separated in 10 min with a 25-70% acetonitrile/water gradient system. MS and MS/MS data were obtained with a Finnigan LCQ mass spectrometer. CID MS/MS data were used for identifying the peptic peptides. The observed CID fragment ions for eight major peptic peptides of TRXs are shown below (**Table 3.13**)

Table 3.13. Observed fragment ions in CID MS/MS spectra of peptic peptides from the digestions of TRXs

Peptide (residues)	Observed Fragment Ions
P6 (1-12)	1372.6 (b12), 1225.5 (b11), 1188.6 (y10), 1138.5 (b10), 1060.6 (y9), 1023.5 (b9), 947.4 (y8), 908.5 (b8), 834.3 (y7), 807.4 (b7), 694.5 (b6)

Table 3.13 (Continued)

P15 (1-24)	1916.8 (b17), 1908.9 (y18), 1703.5 (b15), 1579.5 (y15), 1487.5 (b13), 1464.6 (y14), 1372.5 (b12), 1292.8 ($b24^{+2}$) 1236.2 ($b23^{+2}$), 1179.6 ($b22^{+2}$), 1115.4 ($b20^{+2}$), 1058.1 ($b19^{+2}$) 1023.3 (b9), 899.4 ($y17^{+2}$), 807.3 (b7), 687.2 (b12+2) 557.2 (b5), 444.3 (b4)
P17 (28-39) Oxi-TRX	1374.5 (b12), 1303.4 (b11), 1190.4 (b10), 1172.4 (b10-H_2O) 1135.4 (y10), 1059.4 (b9), 1006.4 (y9)
P18 (28-37) GS-TRX	1286.5 (y8), 1157.6 (y7), 1137.6 (b8-E), 1028.4 (y7-E), 1009.7 (b5), 842.5 (y6-E), 763.3 ($b10^{+2}$), 707.8 ($y10^{+2}$-E), 699.0 ($b10^{+2}$-E), 697.5 ($b9^{+2}$), 633.9 ($b8^{+2}$)
P18 (28-37) Cys-TRX	977.6 (b7), 823.3 (b5), 670.3 ($b10^{+2}$), 604. 7 ($b9^{+2}$), 574.0 (b4), 540.8 ($b8^{+2}$), 387.7 (b3)
P5 (45-58)	1530.7 (b14), 1417.6 (b13), 1364.7 (y12), 1289.6 (b12), 1249.7 (y11), 1218.6 (b11), 1120.6 (y10), 1119.6 (b10), 1018.5 (b9), 957.6 (y9), 905.4 (b8), 829.5 (y8), 777.4 (b7), 720.3 (b6), 592.2 (b5)
P16 (59-80)	1881.0 (y18), 1797.9 (b17), 1767.8 (y17), 1626.9 (b15), 1613.9 (y15), 1512.9 (y14), 1470.0 (b14), 1412.5 (b13), 1441.9 (a14), 1440.8 (y13), 1215.7 (y11), 1168.4 ($b22^{+2}$), 1120.0 ($y21^{+2}$), 1111.3 ($b21^{+2}$), 1063.4 ($y20^{+2}$), 1054.8 ($b20^{+2}$), 1005.8 ($y19^{+2}$), 997.6 ($b19^{+2}$), 947.8 ($b18^{+2}$), 941.5 ($y18^{+2}$), 911.5 (b9), 882.6 (y8),740.4 (b7), 585.3 (b5), 556.2 (y5), 359.4 (y3)
P13 (81-108)	1899.8 (b19), 1874.7 (y18), 1774.6 (y17), 1786.7 (b18), 1758.7 (a18), 1717.6 (y16), 1716.0 (y16), 1658.8 (b17), 1647.7 (y15), 1601.5 (b16), 1533.6 (y14), 1473.7 (b15), 1452.2 ($b28^{+2}$), 1446.6 (y13), 1416.5 ($b27^{+2}$), 1407.5 ($b26^{+2}$), 1386.6 (b14), 1318.4 (y12), 1302.7 ($b25^{+2}$), 1273.5 (b13), 1266.9 ($b24^{+2}$), 1262.4 (y11), 1209.9 ($b23^{+2}$), 1203.0 (b12), 1152.9 ($b22^{+2}$), 1145.6 (b11), 1133.6 (y10), 1079.2 ($b21^{+2}$), 1046.3 (b10), 1020.8 (y9), 918.4 (b9), 817.4 (b8), 746.3 (b7), 675.4 (b6)

3.3-2 H/D exchange of TRXs, proteolysis, and the determination of the deuterium content of peptide segments

Oxi-TRX, GS-TRX, and Cys-TRX (10 μg/μl, 0.85 mM) were dissolved in 1% AcOH/H_2O (pH 2.6). Red-TRX solution (10 μg/μl, 0.85 mM) was obtained by dissolving Oxi-TRX in 8 mM TCEP/1% AcOH/H_2O. Deuterium exchange was initiated by diluting the protein solution 20-fold with 1% AcOD/D_2O. Solutions were maintained at room temperature and allowed to exchange for various lengths of time. At appropriate intervals, aliquots (10 μl, 430 pmole) of diluted solution were taken and cooled to 0 °C. Immediately after quenching, exchanged TRXs in aliquots were digested by adding 1 μl of pepsin solution (3 μg/μl in 5% formic acid) for 5 min. Aliquots (5 μl) were taken from the digest and loaded onto a microbore HPLC column in an ice bath. The peptic peptides were separated in 10 min with a 25-70% acetonitrile/water gradient containing 0.05% trifluoroacetic acid. The column effluent (10 μl/min) was delivered directly to the PE-Sciex API III triple quadrupole mass spectrometer. The deuterium levels of peptic peptides of TRXs are summarized (**Table 3.14.- 3.17**). When there are two molecular ions with different charge states, an average deuterium level was calculated.

A quantitative interpretation of these results was obtained by conversion of time course data into rate data. Nonlinear curve fitting was performed by using a program of Microcal Origin (Microcal software, Northampton, MA).

Table 3.14. Deuterium levels of peptic peptides of Oxi-TRX in H/D exchange-in experiments in 1% AcOD/D_2O

Peptide	Time (min)	*m/z*	D level	Peptide	Time (min)	*m/z*	D level
1-12	0	696.0(+2)		**13-24**	0	616.0(+2)	
	0.5	698.8	5.6		0.5	616.6	1.2
	1	699.1	6.2		1	618.4	4.8
	3	699.4	6.8		3	618.4	4.8
	10	699.4	6.8		10	617.5	5.6
	30	700.0	7.5		30	619.9	7.2
	60	699.7	7.4		60	619.1	7.5
	120	700.0	8		120	620.5	8.5
	180	699.7	8		180	619.6	8.4
28-39	0	697.0(+2)		**45-58**	0	775.3(+2)	
	0.5	697.6	1.2		0.5	777.7	4.8
	1	698.2	2.4		1	778.0	5.4
	3	699.1	4.2		3	778.9	7.2
	10	699.4	4.8		10	780.1	9.2
	30	700.9	6.2		30	780.7	10.2
	60	700.6	7.2		60	780.4	10.8
	120	700.6	7.2		120	781.0	11.4
	180	700.9	7.8		180	780.7	11.2

Table 3.15. Deuterium levels of peptic peptides of Red-TRX in H/D exchange-in experiments in 1% AcOD/D_2O

Peptide	Time (min)	*m/z*	D level
1-12	0	696.0(+2)	
	0.5	698.5	5
	1	699.5	7
	3	699.7	7.4
	10	700	8
	30	700.1	8.2
	60	700.3	8.6
	120	700	8.4
	180	700	8.8
28-39	0	698.2(+2)	
	0.5	698.8	2.5
	1	699.5	3.6
	3	699.9	4.4
	10	700.5	5.6
	30	700.9	7.8
	60	701.2	8.2
	120	701.5	8
	180	701.6	8.4

Peptide	Time (min)	*m/z*	D level
13-24	0	616.0(+2)	
	0.5	617.2	2.4
	1	617.6	3.2
	3	618.1	4.2
	10	619.1	6.2
	30	619.4	6.8
	60	619.7	7.4
	120	620.1	8.2
	180	620	8

Peptide	Time (min)	*m/z*	D level	*m/z*	D level	Average D level
45-58	0	775.3(+2)		517.0(+3)		
	0.5	776.5	2.4	518.2	3.6	**3**
	1	776.9	3.2	518.5	4.5	**3.85**
	3	778.3	6	518.8	5.4	**5.7**
	10	779.5	8.4	519.1	6.3	**7.35**
	30	780.8	11	520	9	**10**
	60	780.7	10.8	520.5	10.5	**10.65**
	120	780.7	10.8	520.6	10.8	**10.8**
	180	781	11.4	521.2	12.6	**12**

Table 3.16. Deuterium levels of peptic peptides of GS-TRX in H/D exchange-in experiments in 1% AcOD/D_2O

Peptide	Time (min)	*m/z*	D level
28-37	0	772.4 (2+)	
	0.5	773.3	1.8
	1	774.2	3.6
	3	774.2	3.6
	10	774.5	4.2
	30	775	5.2
	60	775.1	5.4
	120	775.5	6.2
	180	775.4	6

Peptide	Time (min)	*m/z*	D level	*m/z*	D level	Average D level
1-12	0	695.9 (2+)		1390.7 (1+)		
	0.5	698.6	5.4	1397	6.3	**5.85**
	1	698.9	6	1397	6.3	**6.15**
	3	699.8	7.8	1397.9	7.2	**7.5**
	10	699.8	7.8	1398.8	8.1	**7.95**
	30	700.1	8.4	1399.1	8.4	**8.4**
	60	700.1	8.4	1399.4	8.7	**8.55**
	120	700.1	8.4	1399.1	8.4	**8.4**
	180	700.1	8.4	1400	9.3	**8.85**
13-24	0	615.8 (2+)		1230.8 (1+)		
	0.5	617	2.4	1233.2	2.4	**2.4**
	1	617.3	3	1233.8	3	**3**
	3	617.6	3.6	1234.4	3.6	**3.6**
	10	618.2	4.8	1235.6	4.8	**4.8**
	30	618.8	6	1237.1	6.3	**6.15**
	60	618.8	6	1237.7	6.9	**6.45**
	120	619.4	7.2	1238	7.2	**7.2**
	180	619.4	7.2	1238	7.2	**7.2**
45-58	0	517.1 (3+)		775.1 (2+)		
	0.5	518.6	4.5	776.9	3.6	**4.05**
	1	518.3	3.6	777.2	4.2	**3.9**
	3	519.5	7.2	779.3	8.4	**7.8**
	10	520.4	9.9	780.2	10.2	**10.05**
	30	520.7	10.8	780.5	10.8	**10.8**
	60	521	11.7	780.8	11.4	**11.55**
	120	520.7	10.8	780.8	11.4	**11.1**
	180	521.3	12.6	781.1	12	**12.3**

Table 3.16 (Continued)

Peptide	Time (min)	*m/z*	D level	*m/z*	D level	D level (Ave.)
59-80	0	784.7 (3+)		1176.5 (2+)		
	0.5	786.8	6.3	1179.8	6.6	**6.45**
	1	787.1	7.2	1180.4	7.8	**7.5**
	3	788.3	10.8	1182.6	12.2	**11.5**
	10	789.2	13.5	1183.7	14.4	**13.95**
	30	789.8	15.3	1184.6	16.2	**15.75**
	60	789.8	15.3	1184.3	15.6	**15.45**
	120	789.8	15.3	1184.3	15.6	**15.45**
	180	790.1	16.2	1184.6	16.2	**16.2**
81-101	0	725.9 (3+)		1088.6 (2+)		
	0.5	727.8	5.7	1091.3	5.4	**5.55**
	1	728.6	8.1	1092.5	7.8	**7.95**
	3	730.7	14.4	1095.2	13.2	**13.8**
	10	731.3	16.2	1096.4	15.6	**15.9**
	30	731.9	18	1097	16.8	**17.4**
	60	731.9	18	1097.3	17.4	**17.7**
	120	731.6	17.1	1097.3	17.4	**17.25**
	180	731.6	17.1	1097.3	17.4	**17.25**

Table 3.17. Deuterium levels of peptic peptides of Cys-TRX in H/D exchange-in experiments in 1% AcOD/D_2O

Peptide	Time (min)	*m/z*	D level
28-37		679.4 (2+)	
	0.5	680.3	1.8
	1	680.9	3
	3	681	3.2
	10	681.2	3.6
	30	681.2	3.6
	60	681.6	4.4
	120	681.6	4.4
	180	681.8	4.8

Peptide	Time (min)	*m/z*	D level	*m/z*	D level	D level (Ave.)
1-12		695.9 (2+)		1391 (1+)		
	0.5	698.3	4.8	1395.8	4.8	**4.8**
	1	699.2	6.6	1397.6	6.6	**6.6**
	3	699.8	7.8	1398.8	7.8	**7.8**
	10	700.1	8.4	1398.8	7.8	**8.1**
	30	700.1	8.4	1399.1	8.1	**8.25**
	60	700.1	8.4	1399.4	8.4	**8.4**
	120	700.1	8.4	1399.4	8.4	**8.4**
	180	700.2	8.6	1400	9	**8.8**

Table 3.17 (Continued)

Peptide	Time (min)	*m/z*	D level	*m/z*	D level	Average D level
13-24		616.1(2+)		1230.8(1+)		
	0.5	616.7	1.2	1232.9	2.1	**1.65**
	1	617.2	2.2	1232.9	2.1	**2.15**
	3	617.6	3	1233.8	3	**3**
	10	618.2	4.2	1235.6	4.8	**4.5**
	30	618.5	4.8	1236.8	6	**5.4**
	60	619.4	6.6	1237.1	6.3	**6.45**
	120	619.4	6.6	1237.7	6.9	**6.75**
	180	619.4	6.6	1238.3	7.5	**7.05**
45-58		517.1(3+)		775.1(2+)		
	0.5	518	2.7	776.6	3	**2.85**
	1	518.6	4.5	777.2	4.2	**4.35**
	3	519.6	7.5	778.7	7.2	**7.35**
	10	520.2	9.3	779.8	9.4	**9.35**
	30	520.5	10.2	780.5	10.8	**10.5**
	60	520.7	10.8	780.8	11.4	**11.1**
	120	520.7	10.8	780.8	11.4	**11.1**
	180	520.9	11.4	780.8	11.4	**11.4**
59-80		784.7(3+)		1176.5(2+)		
	0.5	786.2	4.5	1179.5	6	**5.25**
	1	787.1	7.2	1180.7	8.4	**7.8**
	3	788.6	11.7	1182.1	11.2	**11.45**
	10	789.2	13.5	1183.7	14.4	**13.95**
	30	789.8	15.3	1184.6	16.2	**15.75**
	60	789.8	15.3	1184.6	16.2	**15.75**
	120	789.8	15.3	1184.3	15.6	**15.45**
	180	789.8	15.3	1184.7	16.4	**15.85**
81-101		725.9(3+)		1088.6(2+)		
	0.5	727.4	4.5	1091.3	5.4	**4.95**
	1	728.9	9	1093.1	9	**9**
	3	729.8	11.7	1094.9	12.6	**12.15**
	10	731	15.3	1096.4	15.6	**15.45**
	30	731.6	17.1	1097.3	17.4	**17.25**
	60	731.9	18	1097.3	17.4	**17.7**
	120	731.9	18	1097.3	17.4	**17.7**
	180	731.6	17.1	1097.3	17.4	**17.25**

3.3-3 H/D exchange of TRXs, proteolysis, and tandem mass spectrometry for residue-specific hydrogen exchange

Oxi-TRX, GS-TRX, and Cys-TRX (10 μg/μl, 0.85 mM) were dissolved in phosphate buffer (10 mM, pH 5.7). Red-TRX solution (10 μg/μl, 0.85 mM) was obtained by dissolving Oxi-TRX in 8 mM TCEP/phosphate buffer (10 mM, pH 5.7). Deuterium exchange was initiated by diluting 1 μl of protein solution with 20 μl of 10 mM phosphate buffer (D_2O). Solutions were maintained at room temperature and allowed to exchange for 20 sec. Aliquots (5 μl, 200 pmole) of diluted solution were adjusted to pH 2.5 by the addition of 0.1M HCl and cooled to 0 °C. Immediately after quenching, exchanged TRX aliquots were digested by adding 1 μl of pepsin solution (3 μg/μl in 5% formic acid) for 5 min. Aliquots (5 μl) were taken from the digest and loaded onto a microbore HPLC column in an ice bath. The peptic peptides were separated over a 10 min period with a 25-70% acetonitrile/water gradient containing 0.05% trifluoroacetic acid. The column effluent (30 μl/min) was delivered directly to a Finnigan LCQ ion-trap mass spectrometer for ESI-MS and ESI-MS/MS experiments. The observed CID fragment ions for major peptic peptides of 20 sec deuterium labeled TRXs are summarized below (**Table 3.18-3.22**). The TRX protein models (**Figure 2.45, 2.48, 2.49,** and **2.52**) were constructed by the software RasMol (v. 2.7.1) [55] based on the structure downloaded from the Protein Data Bank (PDB code : 1XOA).

3.3-4 Structural calculations of GS-TRX

The construction of a model for the GS-TRX was started with the 2.2 Å resolution single-crystal structure of *E. coli* thioredoxin which was downloaded from the Protein Data Bank (PDB code : 1TXX).[56] The disulfide bond between

the β-sulfurs of Cys A32 and Cys A35 was broken, and a hydrogen added to the A35 residue. All subsequent molecular mechanical simulations were performed using the AMBER force-field as implemented in the Discover module of the program Insight II (Biosym/MSI, San Diego, CA). The entire protein structure was subjected to energy minimization to relieve strain in the starting model. The glutathionyl group was constructed with the amino acids in their extended conformations off the sulfur of Cys-32 using the Biopolymer module of the Insight II program. With the atoms of the protein fixed, the glutathionyl chain was subjected to a systematic set of rigid rotations about the four bonds of the ethylene link between Cys-32 and the Cys residue of the glutathionyl modification. This search resulted in four classes of rotamer conformations with no major collisions near the site of attachment. The glutathionyl-chain in each of these four rotamers were then subjected to a series of molecular dynamics simulations and energy minimizations, again with the atoms of the protein fixed, to adapt each rotamer of the glutathionyl-chain to the protein structure. Finally, the overall structure of the glutathionyl-modified proteins were subjected to molecular dynamics at low temperature (300K), and energy minimized. The structure having the lowest overall potential energy was defined as the GS-TRX model.

Table 3.18. CID fragment ions of peptic peptide 1-24 of TRXs after an incubation in 10 mM phosphate buffer (D_2O) for 20 sec

CID ion (charge state)		Protonated Mass (cal.)	Observed mass (*m/z*)		
			Oxi-TRX	Red-TRX	GS-TRX
(1+)	b5	557.33	-	558.34	-
	b6	694.39	-	695.43	696.94
	b7	807.47	809.3	808.59	-
	b8	908.52	910.41	909.66	911.45
	b9	1023.55	1025.6	1024.72	1026.39
	b10	1138.57	1141.51	1140.45	1142.25
	b11	1225.61	-	-	1229.31
	b12	1372.67	1375.39	1374.9	1376.41
	b13	1487.7	1491.58	1490.65	1492.18
	b14	1588.75	-	1591.83	1593.36
	b15	1703.78	1708.33	1707.01	1708.55
	b16	1816.86	-	-	-
	b17	1915.93	1920.69	1919.36	1920.94
(2+)	b18	1022.52	1025	1024.25	-
	b19	1058.03	1060.63	1059.8	1060.85
	b20	1115.55	1118.49	1117.55	1118.77
	b21	1144.06	-	1146.34	-
	b22	1179.58	1182.83	1182.16	1183.73
	b23	1236.12	1239.37	1238.77	1240.36
	b24	1292.66	1295.88	1295.35	1296.9

Table 3.19. CID fragment ions of peptides 28-39 or 28-37 of TRXs after an incubation in 10 mM phosphate buffer (D_2O) for 20 sec

Ion	Oxi-TRX		Red-TRX		GS-TRX		Cys-TRX	
	Calc.	Observed	Calc.	Observed	Calc.	Observed	Calc.	Observed
b3	387.17	-	387.17	388.0	387.17	387.71	387.17	388.99
b4	573.25	-	573.25	-	573.25	574.22	573.25	575.8
b5	675.25	-	676.26	678.08	1009.4	1011.2	823.29	826.25
b6	732.27	-	733.28	735.81	1066.4	-	880.31	-
b7	829.32	-	830.33	-	1163.4	-	977.37	981.35
b8	931.32	935.03	933.34	936.56	633.72	635.67	540.69	543
b9	1059.42	1063.64	1061.43	1064.83	697.77	699.87	604.74	607.19
b10	1190.46	1195.01	1192.47	1196.09	763.29	765.52	670.26	672.92
b11	1303.54	1308.22	-	-	-	-	-	-
b12	1374.58	1379.72	-	-	-	-	-	-

Table 3.20. CID fragment ions of peptic peptide 45-58 of TRXs after an incubation in 10 mM phosphate buffer (D_2O) for 20 sec.

CID Ion		Oxi-TRX		CID Ion		Protonated Mass (calc)	Observed mass (*m/z*)		
		Calc.	Observed				Red-TRX	GS-TRX	Cys-TRX
				(1+)	b3	300.16	301.8	300.94	301.37
					b4	429.2	429.73	430.04	430.5
					b5	592.26	592.78	592.96	593.5
(1+)	b6	720.32	721.42		b6	720.32	721.19	721.17	721.48
	b7	777.34	779.27		b7	777.34	-	-	-
	b8	905.44	907.87		b8	905.44	907.08	907.67	907.86
	b9	1018.52	1020.95		b9	1018.52	1020.07	1021.1	1021.31
	b10	1119.57	1122.05		b10	1119.57	1122.34	1122.4	1122.72
	b11	1218.64	1221.07		b11	1218.64	1221.02	1221.68	1221.83
	b12	1289.67	1292.1		b12	1289.67	1291.97	1292.91	1292.95
	b13	1417.77	1420.4	(2+)	b13	709.39	710.64	711.08	711.1
	b14	1530.85	1533.58		b14	765.93	767.55	767.68	767.7

Table 3.21. CID fragment ions of peptic peptide 59-79 or 59-80 of TRXs after an incubation in 10 mM phosphate buffer (D_2O) for 20 sec.

CID ion		Protonated Mass (calc)	Observed mass (*m/z*)			
			Oxi-TRX	Red-TRX	GS-TRX	Cys-TRX
(1+)	b4	471.22	-	473.02	475.27	474.37
	b5	585.26	587.5	587.18	589.83	588.5
	b6	682.32	-	-	687	685.62
	b7	739.34	742.14	742.2	744.72	743.52
	b8	840.39	843.36	843.5	845.83	845.4
	b9	911.42	914.3	914.74	917.05	-
	b10	1008.48	-	-	-	1014.15
	b11	1136.57	1139.57	1140	-	1142.57
	b12	1299.63	1302.59	1302.97	1305.92	1305.81
	b13	1412.72	-	-	-	-
	b14	1469.74	1473.23	1473.92	1477.89	1477.79
	b15	1625.84	1630	1630.72	1635.01	1634.93
	b16	1682.86	-	1688.55	1693.02	1692.98
	b17	1795.95	1801.87	1802.45	-	-
(2+)	b17	898.48	-	-	903.61	904
	b18	947	950	-	-	952.55
	b19	997.53	1000.62	1000.95	1002.75	1003.15
	b20	1054.07	1057.26	1057.66	1059.36	1059.8
	b21	1110.61	1113.8	1114.36	1116.02	1116.4
	b22	1167.15	1170.39	1171.01	-	-

Table 3.22. CID fragment ions of peptic peptide 81-101 or 81-108 of TRXs after an incubation in 10 mM phosphate buffer (D_2O) for 20 sec.

CID ion		Protonated Mass (calc)	Observed mass (*m/z*)			
			Oxi-TRX	Red-TRX	GS-TRX	Cys-TRX
(1+)	b5	576.28	577.8	579.22	-	577.99
	b6	675.35	676.85	678.31	676.58	676.9
	b7	746.38	747.82	749.31	747.5	748.2
	b8	817.42	818.78	820.25	-	819.2
	b9	918.47	920.31	921.7	920.22	920.96
	b10	1046.56	1048.4	1049.7	-	1049.05
	b11	1145.63	1147.95	1149.14	1148.8	1148.45
	b12	1202.65	1205.5	1206.66	-	-
	b13	1273.69	1277.14	-	1277.39	1277.7
	b14	1386.77	1391	1392.18	1391.3	1391.49
	b15	1473.81	1478.44	1479.8	1479	1479
	b16	1601.9	1607.22	1608.6	1607.83	1607.98
	b17	1658.92	-	-	1665.66	1665.94
	b18	1786.98	1794.08	-	-	1795
(2+)	b18	893.99	-	898.1	-	-
(2+)	b19	950.54	-	954.73	-	-
(1+)	b19	1900.07	1907.43	-	1907.71	1908.21
(2+)	b20	1014.58	-	1018.73	1018.54	-
	b21	1079.11	1082.95	1083.27	1083.15	1083.2
	b22	1152.64	1156.54		-	1156.77
	b23	1209.18	1213.18		1213.38	1213.35
	b24	1266.7	**1270.77**		**1270.96**	**1270.88**
	b25	1302.21	1306.37		1306.58	1306.42
	b26	1359.24	1363.46		1363.76	1363.53
	b27	1415.78	1420.1		1420.6	1420.18
	b28	1451.3	1455.84		1456.58	1456.12

References

1. Kuwajima, K. *Proteins: Struct. Funct. Genet.* **1989**, *6*, 87-103.

2. (a) Johnson, W. C., Jr. *Proteins: Struct. Func. Genect.* **1990**, *7*, 205-214. (b) Johnson, W. C., Jr. *Ann. Rev. Biophys. Biophys. Chem.* **1988**, *17*, 145-166. (c) Fasman G. D. *Circular Dichroism and the Conformational Analysis of Biomolecules* ; Plenum Press: New York, 1996.

3. Wyckoff, B. H. W. *Methods Enzymol.* **1985**, *114 and 115*.

4. Havel, H. A. *Spectroscopic Methods for Determining Protein Structure in Solution* **1996**, VCH Publishers Inc., New York.

5. (a) Braun, W. *Quart. Rev. Biophys.* **1987**, *19*, 115-157. (b) Wüthrich, K. *Acc. Chem. Res.* **1989**, *22*, 36-44. (c) Clore, G. M.; Gronenborn, A. M. *Ann. Rev. Biophys. Biophys. Chem.* **1991**, *20*, 29-63.

6. Cole, R. B. *Electrospray Ionization Mass Spectrometry*; John Wiley & Sons, Inc., New York, 1997.

7. Hillenkamp, F.; Karas, M.; Ingendoh, A.; Stahl, B. In *Biological Mass Spectrometry*; Burlingame, A. L., McCloskey, J. A., Ed.; Elsevier, Amsterdam,1990; p 24.

8. (a) Englander, S. W.; Kallenbach, N. R. *Q. Rev. Biophys.* **1984**, *16*, 521-655. (b) Woodward, C.; Simon, I.; Tüchsen, E. *Mol. Cell. Biochem.* **1982**, *48*, 135-160.

9. (a) Kaminsky, S. M.; Richards, F. M. *Protein Sci.* **1992**, *1*, 10-21. (b) Marmorino, J. L.; Auld, D. S.; Betz, S. F.; Doyle, D. F.; Young, G. B.; Pielak, G. J. *Protein Sci.* **1993**, *2*, 1966-1974.

10. (a) Bai, Y.; Sosnick, R. R.; Mayne, L.; Englander, S. W. *Science* **1995**, *269*, 192-197.
(b) Jones, B. E.; Matthews, C. R. *Protein Sci.* **1995**, *4*, 167-177.
(c) Miranker, A.; Robinson, C. V.; Radford, S. E.; Aplin, R. T.; Dobson, C. M. *Science* **1993**, *262*, 896-900. (d) Baldwin, R. L. *Curr. Opin. Struct. Biol.* **1993**, *3*, 84-91.

11. (a) Loh, S. N.; Prehoda, K. E.; Wang, J.; Markley, J. L. *Biochemistry* **1993**, *32*, 11022-11028. (b) Benjamin, D. C.; Williams, D. C., Jr.; Smith-Gill, S. J.; Rule, G. S. *Biochemistry* **1992**, *31*, 9539-9545. (c) Mayne, L.; Paterson, Y.; Cerasoli, D.; Englander, S. W. *Biochemistry* **1992**, *31*, 10678-10685.

12. (a) Rosa, J. J.; Richards, F. M. *J. Mol. Biol.* **1979**, *133*, 399-416.

(b) Englander, J. J.; Rogero, J. R.; Englander, S. W. *Anal. Biochem.* **1985**, *147*, 234-244.
(b) Zhang, Z.; Smith, D. L. *Protein Sci.* **1993**, *2*, 522-531.
(c) Zhang, Z.; Post, C. B.; Smith, D. L. *Biochemistry* **1996**, *35*, 779-791.

13. (a) Molday, R. S.; Englander, S. W.; Kallen, R. G. *Biochemistry* **1972**, *11*, 150-158. (b) Bai, Y.; Milne, J. S.; Mayne, L.; Englander, S. W. *Proteins: Struct. Funct. Genet.* **1993**, *17*, 75-86.

14. Creighton, T. E. *Proteins: Structures and Molecular Properties*; Freeman, W.H. and Co.: New York, 1993; p282.

15. (a) Englander, S. W.; Sosnick, T. R.; Englander, J. J.; Mayne, L. *Curr. Opin. Struct. Biol.* **1996**, *6*, 18-23.
(b) Yi, Q.; Baker, D. *Protein Sci.* **1996**, *5*, 1060-1066.

16. (a) Bai, Y. W.; Milne, J. S.; Mayne, L.; Englander, S. W. *Proteins: Struct. Funct. Genet.* **1994**, *20*, 4-14. (b) Itzhaki, L. S.; Neira, J. L.; Fersht, A. R. *J. Mol. Biol.* **1997**, *270*, 89-98. (c) Chamberlain, A. K.; Marqusee, S. *Biochemistry* **1998**, *37*, 1736-1742.

17. Engen, J. R.; Gmeiner, W. H.; Smithgall, T. E.; Smith, D. L. *Biochemistry* **1999**, *38*, 8926-8935.

18. Deng, Y.; Zhang, Z.; Smith, D. L. *J. Am. Soc. Mass Spectrom.* **1999**, *10*, 675-684.

19. Holmgren, A.; Björnstedt, M. *Methods in Enzymology Vol. 252*; Academic Press: San Diego, 1995; p199.

20. (a) Adler, S.; Modrich, P. *J. Biol. Chem.* **1983**, *258*, 6956-6962.
(b) Russel, M.; Model, P. *Proc. Natl. Acad. Sci. U.S.A.* **1985**, *82*, 29-33.
(c) Russel, M.; Model, P. *J. Biol. Chem.* **1986**, *261*, 14997-15005.

21. (a) Holmgren, A.; Soderberg, B. O.; Eklund, H.; Branden, C. I. *Proc. Natl. Acad. Sci. USA* **1975**, *72*, 2305-2309. (b) Katti, S. K.; LeMaster, D. M.; Eklund, H. *J. Mol. Biol.* **1990**, *212*, 167-184.

22. (a) Dyson, H. J.; Gippert, G. P.; Case, D. A.; Holmgren, A.; Wright, P. E. *Biochemistry* **1990**, *29*, 4129-4136. (b) Jeng, M.-F.; Campbell, A. P.; Begley, T.; Holmgren, A.; Case, D. A.; Wright, P. E.; Dyson, H. J. *Structure* **1994**, *2*, 853-868.

23. Loo, J. A.; Ogorzalek Loo, R. R.; Udseth, H. R.; Edmonds, C. G.; Smith, R. D. *Rapid Commun. Mass Spectrom.* **1991**, *5*, 101.

24. Mirza, U. A.; Cohen, S. L.; Chait, B. T. *Anal. Chem.* **1993**, *65*, 1.

25. (a) Covey, T. R.; Douglas, D. J. *J. Am. Soc. Mass Spectrom.* **1993**, *4*, 616. (b) Hudgins, R. R.; Woenckhaus, J.; Jarrold, M. F. *Int. J. Mass Spectrom. Ion Processes* **1997**, *165/166*, 497. (c) Suckau, D.; Shi, Y.; Beu, S. C.; Senko, M. W.; Quinn, J. P.; Wampler, F. M.; McLafferty, F. W. *Proc. Natl. Acad. Sci. U.S.A.* **1993**, *90*, 790.

26. (a) Johnson, R. S.; Krylov, D.; Walsh, K. A. *J. Mass Spectrom.* **1995**, *30*, 386-387. (b) McLafferty, F. W.; Guan, Z.; Haupts, U.; Wood, T. D.; Kelleher, N. L. *J. Am. Chem. Soc.* **1998**, *120*, 4732-4740.

27. Biemann, K. *Biomed. Environ. Mass Spectrom.* **1988**, *16*, 99-111.

28. Anderegg, R. J.; Wagner, D. S.; Stevenson, C. L.; Borchardt, R. T. *J. Am. Soc. Mass Spectrom.* **1994**, *5*, 425-433.

29. Kenny, P. T. M.; Nomoto, K.; Orlando, R. *Rapid Commun. Mass Spectrom.* **1992**, *6*, 95-97.

30. Zubarev, R. A.; Kelleher, N. L.; McLafferty, F. W. *J. Am. Chem. Soc.* **1998**, *120*, 3265-3266.

31. Deng, Y.; Pan, H.; Smith, D. L. *J. Am. Chem. Soc.* **1999**, *121*, 1966-1967.

32. Holmgren, A.; Björnstedt, M. *Methods in Enzymology Vol. 252*; Academic Press: San Diego, 1995; p3.

33. (a) van Bladeren, P. J.; Breimer, D. D.; van Huijevoort, J. A. T. C. M.; Vermeulen, N. P. E.; van der Gen, A. *Biochem. Pharmacol.* **1981**, *30*, 2499-2502. (b) Guengerich, F. P.; Crawford, W. M.; Domoradzki, J. Y.; MacDonald, T. L.; Watanabe, P. G. *Toxicol. Appl. Pharmacol.* **1980**, *55*, 303-317.

34. (a) Humphreys, W. G.; Kim, D.-H.; Cmarik, J. L.; Shimada, T.; Guengerich, F. P. *Biochemistry* **1990**, *29*, 10342-10350. (b) Ozawa, N.; Guengerich, F. P. *Proc. Natl. Acad. Sci. U.S.A.* **1983**, *80*, 5266-5270. (c) Erve, J. C. L.; Barofsky, E.; Barofsky, D. F.; Deinzer, M. L.; Reed, D. J. *Chem. Res. Toxicol.* **1995**, *8*, 934-941.

35. (a) Reed, D. J.; Foureman, G. L. *Biological reactive intermediates III*; Plenum Press: New York, 1986; pp469-475. (b) Peterson, L. A.; Harris, T. M.; Guengerich, F. P. *J. Am. Chem. Soc.* **1988**, *110*, 3284-3291.

36. Han, J. C.; Han, G. Y. *Anal. Biochem.* **1994**, 220, *5-10.*

37. Kortemme, T.; Creighton, T. E. *J. Mol. Biol.* **1995**, *253*, 799-812.

38. Dillet, V.; Dyson, H. J.; Bashford, D. *Biochemistry* **1998**, *37*, 10298-10306.

39. Snyder, L. R.; Kirkland, J. J.; Glajah, J. L. *Practical HPLC Method Development*; John Wiley & Sons: New York, 1997; pp479-536.

40. Vis, H.; Heinemann, U.; Dobson, C. M.; Robinson, C. V. *J. Am. Chem. Soc.* **1998**, *120*, 6427-6428.

41. (a) Chan, H. S.; Dill, K. A. *Proteins: Struct. Funct. Genet.* **1998**, *30*, 2-33. (b) Dobson, C. M.; Sali, A.; Karplus, M. *Angew. Chem. Int. Ed. Engl.* **1998**, *37*, 868-893. (c) Onuchic, J. N.; Wolynes, P. G.; Luthey-Schulten, Z.; Socci, N. D. *Proc. Natl. Acad. Sci. U.S.A.* **1995**, *92*, 3626-3630.

42. (a) Ladbury, J. E.; Wynn, R.; Hellinga, H. W.; Sturtevant, J. M. *Biochemistry* **1993**, *32*, 7526-7530. (b) Ladbury, J. E.; Wynn, R.; Thomson, J. A.; Sturtevant, J. M. *Biochemistry* **1995**, *24*, 2148-2152.

43. (a) Zhang, Z.; Smith, D. L. *Protein Sci.* **1996**, *5*, 1282-1289. (b) Kim, K. S.; Fuchs, J. A.; Woodward, C. K. *Biochemistry* **1993**, *32*, 9600-9608. (c) Robertson, A. D.; Baldwin, R. L. *Biochemistry* **1991**, *30*, 9907-9914. (d) Roder, H.; Wagner, G.; Wüthrich, K. *Biochemistry* **1985**, *24*, 7396-7407. (e) Roder, H.; Wagner, G.; Wüthrich, K. *Biochemistry* **1985**, *24*, 7407-7411.

44. (a) Katta, V.; Chait, B. T. *J. Am. Chem. Soc.* **1993**, *115*, 6317-6321. (b) Vis, H.; Heinemann, U.; Dobson, C. M.; Robinson, C. V. *J. Am. Chem. Soc.* **1998**, *120*, 6427-6428.

45. Hiraoki, T.; Brown, S. B.; Stevenson, K. J.; Vogel, H. J. *Biochemistry* **1988**, *27*, 5000-5008.

46. Maier, C. S.; Shimerlik, M. I.; Deinzer, M. L. *Biochemistry* **1999**, *38*, 1136-1143.

47. Jeng, M.-F.; Dyson, H. J. *Biochemistry* **1995**, *34*, 611-619.

48. Van Holde, K. E.; Johnson, W. C., Jr.; Ho, P. S. *Principles of Physical Biochemistry*; Prentice Hall: New York, 1998; pp418-451.

49. Reutimann, H.; Straub, B.; Luisi, P. L.; Holmgren, A. *J. Biol. Chem.* **1981**, *256*, 6796-6803.

50. Englander, S. W.; Poulsen, A. *Biopolymers* **1969**, *7*, 379-393.

51. Zhang, Z.; Marshall, A. G. *J. Am. Soc. Mass. Spectrom.* **1998**, *9*, 225-233.

52. Hoffman, R. A.; Forsen, S. *Prog. NMR Spectrosc.* **1966**, *1*, 15-204.

53. Loo, J. A.; He, J. X.; Cody, W. L. *J. Am. Chem. Soc.* **1998**, *120*, 4542-4543.

54. Chen, G. C.; Yang, J. T. *Anal. Lett.* **1977**, *10*, 1195-1207.

55. http://www.bernstein-plus-sons.com/software/rasmol

56. Schultz, L. W.; Chivers, P. T.; Raines, R. T. *Acta Crystallogr.* **1999**, 55, 1533.